Manganese and Iron Coordination Complexes for Biological Imaging and Oxidative Catalysis

by

Qiao Zhang

A dissertation submitted to the Graduate Faculty of
Auburn University
in partial fulfillment of the
requirements for the Degree of
Doctor of Philosophy

Auburn, Alabama
May 4, 2014

Keywords: Manganese, Iron, MRI Contrast Agent,
Homogenous Catalysis, Epoxidation, Regioselectivity, C-H Activation

Approved by

Christian R. Goldsmith, Chair, Associate Professor, Chemistry and Biochemistry
Douglas C. Goodwin, Associate Professor, Chemistry and Biochemistry
Michael L. McKee, Alumni Professor, Chemistry and Biochemistry
David M. Stanbury, J. Milton Harris Professor, Chemistry and Biochemistry

Abstract

The ligand *N*,*N*'-bis(2-pyridylmethyl)-bis(ethylacetate)-1,2-ethanediamine (debpn) coordinates divalent transition metal ions in either a pentadentate or hexadentate fashion. The coordination number correlates with the ionic radius of the metal ion, with larger cations being heptacoordinate as assessed by solid-state analysis. With Mn(II), the debpn ligand is hexadentate and remains bound to the oxophilic metal ion, even when dissolved in water. The ligand's incomplete coordination of the manganous ion allows water molecules to coordinate to the metal center. These two properties, coupled with the high paramagnetism associated with the $S = 5/2$ metal center, enable $[Mn(debpn)(H_2O)](ClO_4)_2$ to serve as a stable and effective magnetic resonance imaging contrast agent despite the ligand's lack of both a macrocyclic component and an anionic charge.

The Mn(II) and Fe(II) complexes of debpn are capable of catalyzing alkene epoxidation and aliphatic C-H activation reactions, although these activities are inferior to those of related complexes with less coordinating ligands. The hydrocarbon oxidation catalyzed by iron is more severely disrupted. Cyclic voltammetry indicates that the +2 oxidation states for both debpn complexes' metal ions are stabilized by the two additional chelate arms. Product analysis of the C–H activation and olefin epoxidation chemistries suggest that ligand-substrate steric interactions may exert additional inhibitory effects on the reactivity for the manganese catalysts.

The compound *N*,*N*'-bis(2-pyridylmethyl)-*N*,*N*'-bis(neopentyl)-1,2-ethanediamine (dnbpn) and its ferrous complex $[Fe(dnbpn)(OTf)_2]$ were synthesized. The Fe(II) complex was

used to catalyze the oxidation of hydrocarbons by both H_2O_2 and O_2. Although the catalyzed alkane oxidation by H_2O_2 displays a higher preference for secondary over tertiary carbons than those associated with previously reported non-heme iron catalysts, the catalytic activity is markedly inferior. In addition to directing the catalyzed oxidation towards the less sterically congested C-H bonds of the substrates, the neopentyl groups destabilize the metal-based oxidants generated from H_2O_2 and the Fe(II) complex. The oxidant generated from O_2 reacts with allylic and benzylic C-H bonds in the absence of a sacrificial reductant; less dehydrogenation activity is observed than with related previously described systems that use O_2 as a terminal oxidant.

The formation of a ferric hydroperoxide species from $[Fe(bbpc)(MeCN)_2]^{2+}$ (bbpc = *N*,*N*'-di(phenylmethyl)-*N*,*N*'-bis(2-pyridinylmethyl)-1,2-cyclohexanediamine) and its subsequent decomposition were analyzed with stopped-flow kinetics. The rate of decay does not scale linearly with the concentrations of either water or substrate, suggesting that the ferric hydroperoxide degrades through homolysis of the O-O bond and is not the relevant metal-based oxidant in aliphatic C-H activation. The rate law corresponding to the complex's formation from O_2 is consistent with the intermediacy of a mononuclear ferric superoxo species.

Acknowledgments

First, I would like to thank my advisor Prof. Christian Goldsmith. He spent a lot of time discussing experimental details, data analysis, writing, etc., and I learned a lot from him. I also want to thank my committee members: Prof. Douglas Goodwin, Prof. Michael McKee, Prof. David Stanbury, and outside reader Prof. Xinyu Zhang. Their suggestions for my dissertation are very valuable.

I got a lot of help from my colleagues during the course of my graduate studies. I would like to thank Prof. John Gorden and Mr. Jian Lin (University of Notre Dame) for crystallography research, Dr. Ronald Beyers (Auburn University MRI Research Center) for the analysis of my MRI contrast agent, Prof. David Stanbury and his group members Dr. Nootan Bhattarai, and Dr. Changwei Pan for their assistance with the stopped-flow experiments, Prof. Eduardus Duin and his group members Mr. Divya Prakash, Ms. Xiao Xiao, and Ms. Selamawit Ghebreamlak for their help with EPR experiments, Dr. Michael Meadows for NMR experiments, Dr. Yonnie Wu for LC-MS and GC-MS experiments, Dr. Tae Bum Lee for computational chemistry work, Dr. Yajiao Yu, Dr. Axline Sanghapi, and Mr. Sanjun Fan for Raman spectroscopy studies.

I also want to thank my lab-mates, Prof. Cristina Coates, Dr. Yu He, Dr. Wenchan Jiang, Mr. Meng Yu, and all of the undergraduate students who have worked in Prof. Goldsmith's lab. Without their help, much of this research would not have been done.

Auburn University Department of Chemistry and Biochemistry provided much of the facilities and financial support. Other financial support came from the American Chemical Society

- Petroleum Research Fund, and a fellowship from Auburn University Cellular and Molecular Biosciences Program (supported by National Science Foundation).

Finally, I would like to thank my family and my friends who have provided me with knowledge, power, and love. I hope this dissertation is a wonderful gift for them.

Table of Contents

Abstract ii

Acknowledgments iv

List of Tables ix

List of Figures xi

List of Schemes xv

Chapter 1 The Application of Manganese and Iron Compounds to Magnetic Resonance Imaging and Oxidative Catalysis 1

1.1 Mn Based MRI Contrast Agent 2

1.2 Alkene Epoxidation Catalyzed by Mn or Fe Coordination Complex 10

1.3 Alkane C-H Activation Catalyzed by Fe Coordination Complex 19

Appendix 23

References 26

Chapter 2 Manganese(II)-Containing MRI Contrast Agent Employing a Neutral and Non-Macrocyclic Ligand 29

2.1 Introduction 30

2.2 Experimental Section 32

2.3 Results 42

2.4 Discussion 51

2.5 Conclusions 56

Appendix 58

References 62

Chapter 3 Hydrocarbon Oxidation Catalyzed by Manganese and Iron Complexes with the Hexadentate Ligand *N*,*N*'-Di(ethylacetate)-*N*,*N*'-bis(2-pyridylmethyl)-1,2-ethanediamine 66

3.1 Introduction 67

3.2 Experimental Section 69

3.3 Results 71

3.4 Discussion 78

3.5 Conclusions 82

Appendix 83

References 87

Chapter 4 C-H Oxidation by H_2O_2 and O_2 Catalyzed by a Non-Heme Iron Complex with a Sterically Encumbered Tetradentate N-Donor Ligand 90

4.1 Introduction 91

4.2 Experimental Section 92

4.3 Results 97

4.4 Discussion 108

4.5 Conclusions 114

Appendix 115

References 125

Chapter 5 Kinetic Analysis of the Formation and Decay of a Non-Heme Ferric Hydroperoxide Species Susceptible to O-O Bond Homolysis 129

5.1 Introduction 130

5.2 Experimental Section 131

5.3 Results and Discussion 133

5.4 Conclusions 143

Appendix 144

References 146

Appendix Crystal Structure of the Perchloric Acid Salt of the Macrocyclic Ligand 1,8-Bis(2-pyridylmethyl)-1,4,8,11-tetraazacyclotetradecane 148

List of Tables

Table 1.1 Asymmetric Epoxidation of Representative Olefins by Mn(III)-Salen Catalyst 12

Table 1.2 Epoxidations Catalyzed by [Mn(*R*,*R*-mcp)$(OTf)_2$] with CH_3CO_3H 15

Table 1.3 Epoxidation Reactivity of [Mn(II)(L)$(OTf)_2$] Complexes 16

Table 1.4 Epoxidations catalyzed by $[Fe(mep)(MeCN)_2]^{2+}$ 17

Table 1.5 Ratios of Tertiary (3°) to Secondary (2°) Carbon Oxidation Observed with Non-Heme Iron Catalysts 22

Table 2.1 Selected Crystallographic Data for Coordination Complexes 40

Table 2.2 Comparison of the Bond Lengths and Bond Angles for the Heptacoordinate Complexes $[Mn(debpn)(H_2O)]^{2+}$ and $[Fe(debpn)(H_2O)]^{2+}$ 44

Table 2.3 Comparison of the Bond Lengths and Bond Angles for the Heptacoordinate Complexes $[Co(debpn)(MeCN)]^{2+}$ and $[Ni(debpn)(MeCN)]^{2+}$ 45

Table 2.4 Bond Lengths and Bond Angles for the Heptacoordinate Complexes $[Zn(debpn)]^{2+}$ 46

Table 2.5 Carbonyl Stretching Frequencies for Debpn Species 48

Table 3.1 Epoxidation of 1-Octene Catalyzed by $[Mn(debpn)(H_2O)]^{2+}$ and [Mn(bpmen)$(OTf)_2$] 72

Table 3.2 Epoxidation of Alkenes by 7.5% Peracetic Acid Catalyzed by $[Mn(debpn)(H_2O)]^{2+}$ 73

Table 3.3 Epoxidation of Alkenes by Hydrogen Peroxide Catalyzed by $[Fe(debpn)(H_2O)]^{2+}$ and [Fe(bpmen)$(MeCN)_2$]$(SbF_6)_2$ 75

Table 3.4 Oxidation of Alkanes by Hydrogen Peroxide Catalyzed by $[Fe(debpn)(H_2O)]^{2+}$ 77

Table 4.1 Selected Crystallographic Data for [Fe(dnbpn)$(OTf)_2$] 100

Table 4.2 Selected Bond Lengths for the Three [Fe(dnbpn)$(OTf)_2$] Molecules 101

Table 4.3 Catalytic Oxidation of Hydrocarbons by H_2O_2 102

Table 4.4 Regioselectivity of Hydrocarbon Oxidation Catalyzed by [Fe(dnbpn)$(OTf)_2$] 103

Table 4.5 Catalytic Oxidation of Hydrocarbons by O_2 105

Table 4.6 Ratios of Tertiary to Secondary Carbon Oxidation Observed with Non-Heme Iron Catalysts 110

Table A1 Hydrogen Bond Geometry 152

List of Figures

Figure 1.1 The brain MR image of Prof. Peter Caravan 2

Figure 1.2 Relationship between rotational diffusion and water exchange at a given field strength (1.5 T) for a q = 1 compound with a long (>10 ns) T_{1e} 6

Figure 1.3 Commercial Gd(III) MRI contrast agents 7

Figure 1.4 Non-macrocyclic ligands for Mn(II) MRI contrast agents 9

Figure 1.5 Macrocyclic ligands for Mn(II) MRI contrast agents 10

Figure 1.6 Crystal structure of [Mn(*R*,*R*-mcp)$(OTf)_2$] 14

Figure 1.7 Crystal structure of $[Fe(mep)(MeCN)_2]^{2+}$ 17

Figure 1.8 Crystal structure of $[Fe_2(\mu\text{-}O)(\mu\text{-}CH_3CO_2)(mep)_2]$ 18

Figure 1.9 (A) Chemical properties of aliphatic C-H bonds. (B) Synergistic effects on site selectivity. Steric, stereoelectronic (influence of orientation of electron orbitals in space on reactivity), and electronic influences on reactivity with catalyst Fe(*S*,*S*)-pdp have an additive effect in complex molecule settings, which can lead to highly predictable and selective outcomes. (C) Electrophilic, bulky catalyst Fe(*S*,*S*)-pdp for predictably selective aliphatic C-H oxidation 21

Figure 1.10 Crystal structure of $[Fe(bbpc)(MeCN_2)]^{2+}$ 21

Figure 2.1 ORTEP representations of the dications (A) $[Mn(debpn)(H_2O)]^{2+}$, (B) $[Fe(debpn)(H_2O)]^{2+}$, (C) $[Co(debpn)(MeCN)]^{2+}$, (D) $[Ni(debpn)(MeCN)]^{2+}$ and (E) $[Zn(debpn)]^{2+}$ 39

Figure 2.2 X-Band electron paramagnetic resonance spectra of $[Mn(H_2O)_6](ClO_4)_2$ and $[Mn(debpn)(H_2O)](ClO_4)_2$ in H_2O at 77 K 47

Figure 2.3 Inversion recovery magnetic resonance images of samples at initial time of inversion, exemplifying the different T_1 relaxation rates by the contrast change 49

Figure 2.4 Plots of ($1/T_1$) as functions of Mn(II) concentration for $[Mn(H_2O)_6](ClO_4)_2$, $Na_2[Mn(EDTA)(H_2O)]$, and $[Mn(debpn)(H_2O)](ClO_4)_2$ 50

Figure 2.A1 ^1H NMR spectrum of $[Zn(debpn)](ClO_4)_2$ in CD_3CN at 298 K and 338 K 58

Figure 2.A2 ^1H NMR spectrum of $[Ni(debpn)(MeCN)](ClO_4)_2$ in CD_3CN at 298 K and 338 K..... 59

Figure 2.A3 ^1H NMR spectrum of $[Fe(debpn)(H_2O)](ClO_4)_2$ in CD_3CN at 294 K..... 60

Figure 2.A4 ^1H NMR spectrum of $[Co(debpn)(MeCN)](ClO_4)_2$ in CD_3CN at 294 K 60

Figure 2.A5 Comparative UV/vis spectra of $[Fe(debpn)(H_2O)]^{2+}$, $[Co(debpn)(MeCN)]^{2+}$, and $[Ni(debpn)(MeCN)]^{2+}$ in MeCN at 294 K 61

Figure 2.A6 Reaction between 1.0 mM $[Mn(debpn)(H_2O)](ClO_4)_2$ and 1.0 mM $Fe(ClO_4)_2$ in MeCN at 294 K..... 61

Figure 3.A1 Cyclic voltammogram for $[Mn(debpn)(H_2O)]^{2+}$ in a 0.10 M solution of tetrabutylammonium perchlorate in MeCN..... 83

Figure 3.A2 Cyclic voltammogram for $[Fe(debpn)(H_2O)]^{2+}$ in a 0.10 M solution of tetrabutylammonium perchlorate in MeCN..... 83

Figure 3.A3 Cyclic voltammogram for $[Mn(bpmen)(OTf)_2]$ in a 0.10 M solution of tetrabutylammonium perchlorate in MeCN..... 84

Figure 3.A4 Cyclic voltammogram for $[Fe(bpmen)(MeCN)_2]^{2+}$ in a 0.10 M solution of tetrabutylammonium perchlorate in MeCN..... 84

Figure 3.A5 Mass spectrum (ESI) of aliquot from reaction between 1.0 mM $[Mn(debpn)(H_2O)](ClO_4)_2$ and 5.0 mM PAA_R in 294 K MeCN..... 85

Figure 3.A6 Mass spectrum (ESI) of aliquot from reaction between 1.0 mM $[Fe(debpn)(H_2O)](OTf)_2$, 5.0 mM acetic acid, and 5.0 mM H_2O_2 in 294 K. 87

Figure 4.1 ORTEP representation of $[Fe(dnbpn)(OTf)_2]$ (subunit A)..... 99

Figure 4.2 Oxidation of cyclohexene by O_2 catalyzed by $[Fe(dnbpn)(OTf)_2]$ 105

Figure 4.3 Comparative UV/vis plots of 1.0 mM **3**, 1.0 mM **3** plus 10 mM H_2O_2, and 1.0 mM **3** plus 10 mM H_2O_2 plus 100 mM cumene 107

Figure 4.4 X-Band EPR spectrum of a 77 K solution of 1.0 mM **3**, 2 mM H_2O_2, and 50 mM cumene in MeCN..... 107

Figure 4.5 Resonance Raman spectroscopy of the intermediate generated from the reaction between 2.0 mM **3**, 10 mM H_2O_2, and 100 mM ethylbenzene in MeCN 108

Figure 4.A1 HR-MS of reaction between 1.0 mM **3** and 10 mM H_2O_2 in MeCN at 294 K..... 118

Figure 4.A2 ^{1}H NMR spectrum of compound **1** 119

Figure 4.A3 ^{13}C NMR spectrum of compound **1** 119

Figure 4.A4 ^{1}H NMR spectrum of compound **2** 120

Figure 4.A5 ^{13}C NMR spectrum of compound **2** 120

Figure 4.A6 ^{1}H NMR spectrum of compound **A1** 121

Figure 4.A7 ^{13}C NMR spectrum of compound **A1** 121

Figure 4.A8 ^{1}H NMR spectrum of compound **4** 122

Figure 4.A9 ^{13}C NMR spectrum of compound **4** 122

Figure 4.A10 ^{1}H NMR spectrum of compound **5** 123

Figure 4.A11 ^{13}C NMR spectrum of compound **5** 123

Figure 4.A12 Resonance Raman spectroscopy of the intermediate generated from the reaction between 2.0 mM **3**, 10 mM H_2O_2, and 100 mM cumene in MeCN..... 124

Figure 5.1 Initial rate analysis for the formation of **2** from **1** and H_2O_2: dependence on [**1**] ... 134

Figure 5.2 Relationship between the k_{obs} for the formation of **2** from **1** and H_2O_2 and the initial concentration of H_2O_2 135

Figure 5.3 Eyring plot for the formation of **2** from a reaction between 0.50 mM **1** and 5.0 mM H_2O_2 in MeCN at temperatures ranging from 294 K to 324 K 136

Figure 5.4 Influence of additives on the k_{obs} for the formation of **2** from 0.50 mM **1** and 5.0 mM H_2O_2 137

Figure 5.5 Relationship between the k_{obs} for the decomposition of **2** and the concentration of H_2O_2 originally present in solution 138

Figure 5.6 Influence of additives on the k_{obs} for the decomposition of **2** formed from 0.50 mM **1** and 5.0 mM H_2O_2 139

Figure 5.7 Eyring plot for the decomposition of **2** from a reaction between 0.50 mM **1** and 5.0 mM H_2O_2 in MeCN at temperatures ranging from 294 K to 324 K 140

Figure 5.8 Initial rate analysis for the formation of **2** from **1** and O_2: dependence on [**1**]..... 142

Figure 5.9 Initial rate analysis for the formation of **2** from **1** and various [O_2]..... 142

Figure 5.A1 Sample kinetic trace for a reaction between 0.50 mM **1** and 5.0 mM H_2O_2 in MeCN at 298 K 144

Figure 5.A2 Sample kinetic trace for a reaction between 0.50 mM **1** and 8.1 mM O_2, and 100 mM cyclohexene in MeCN at 298 K 145

Figure 5.A3 Absorbance measured at 690 nm at 600 s for the reaction between 0.50 mM **1** and 5.0 mM H_2O_2 in MeCN at 298 K with various concentrations of $HClO_4$ 145

Figure A1 ORTEP representation of the **1**H_2^{2+} dication showing the numbering scheme 149

Figure A2 ORTEP representation of a portion of the **1**H_2^{2+} dication, highlighting the hydrogen bond interaction between the pyridine ring and the secondary amine.... 152

List of Schemes

Scheme 1.1 Energy splitting in magnetic field 3

Scheme 1.2 Inner-sphere and outer sphere relaxivity 4

Scheme 1.3 Gd-HOPO complexes 5

Scheme 1.4 Structure of the ligand of Teslascan 9

Scheme 1.5 The application of epoxides 11

Scheme 1.6 The structure of Mn-Salen catalyst 11

Scheme 1.7 Mechanisms of Mn-Salen catalyzed epoxidation 13

Scheme 1.8 Mechanisms of Mn-Salen catalyzed epoxidation 13

Scheme 1.9 Ligand *R*,*R*-mcp 14

Scheme 1.10 Epoxidation catalyzed by [Mn(*R*,*R*-mcp)$(OTf)_2$] 14

Scheme 1.11 Epoxidation catalyzed by $[Fe(mep)(MeCN)_2]^{2+}$ 17

Scheme 1.12 Proposed mechanisms for non-heme iron catalyzed olefin epoxidation 18

Scheme 1.13 Proposed mechanisms of catalytic cycle of Cytochrome P450 and TauD 19

Scheme 2.1 The structure of ligand debpn 31

Scheme 3.1 The structures of ligands debpn and bpmen 68

Scheme 3.2 Inner-sphere coordination of $[Mn(debpn)(H_2O)]^{2+}$ and $[Fe(debpn)(H_2O)]^{2+}$ 69

Scheme 4.1 Synthetic route for [Fe(dnbpn)$(OTf)_2$] 92

Scheme 5.1 Conversion of $[Fe(bbpc)(MeCN)_2]^{2+}$ to $[Fe(bbpc)(OOH)]^{2+}$ 131

Scheme 5.2 Homolytic O-O bond cleavage of $[Fe(bbpc)(OOH)]^{2+}$ 140

Chapter 1

The Application of Manganese and Iron Compounds to Magnetic Resonance Imaging and Oxidative Catalysis

1.1 Magnetic Resonance Imaging (MRI)

Magnetic resonance imaging, also known as MRI, has played an important role in science for more than thirty years.[1] Its ability to non-invasively acquire high resolution, three-dimensional images of soft tissues make MRI a powerful diagnostic tool in medicine.[2]

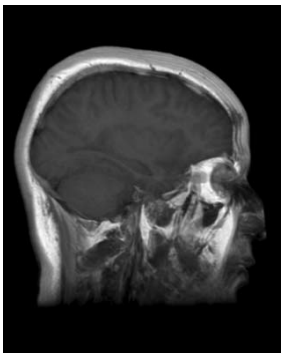

Figure 1.1. The brain MR image of Prof. Peter Caravan (Harvard Medical School).[3]

Physical principles of MRI

Nuclei that contain odd numbers of nucleons or odd numbers of atomic mass such as ^{1}H and ^{13}C have a magnetic moment and are capable of being imaged by nuclear magnetic resonance (NMR). For ^{1}H, there are two spin states: $m_I = -1/2$ and $m_I = +1/2$ (Scheme 1.1). These normally have the same energy but become non-degenerate when a magnetic field is applied. The energetic gap between the spin-states under such circumstances normally corresponds to a radio frequency (RF) photon. RF excitation can therefore induce a spin-flip.[4] After a certain amount of time, the excited nucleus relaxes back to its original spin-state. There are two kinds of relaxations: longitudinal magnetic relaxation (also known as spin-lattice relaxation) and transverse relaxation (also known as spin-spin relaxation).

The former process refers to a nucleus returning to the ground state in the magnet. The latter refers to two nuclei falling out of alignment with each other. T_1 and T_2 are the mean times of

the two kinds of relaxations. Their inverses, r_1 and r_2, refer to the rates of T_1 and T_2 relaxation, respectively.[5,6]

At the present time, approximately 30% of all MRI exams use a paramagnetic contrast agent. MRI contrast agents improve the resolution of MR imaging by reducing T_1 and T_2. The association of a paramagnetic complex with water molecules introduces new and more efficient pathways for nuclear relaxation. The effectiveness of an MRI contrast agent depends upon its interaction with nearby water molecules that provide the protons for the MRI signal. Many contrast agents directly coordinate water molecules; this leads to the most effective contrast enhancement. Outer-sphere interactions can also make significant contributions.[7,8]

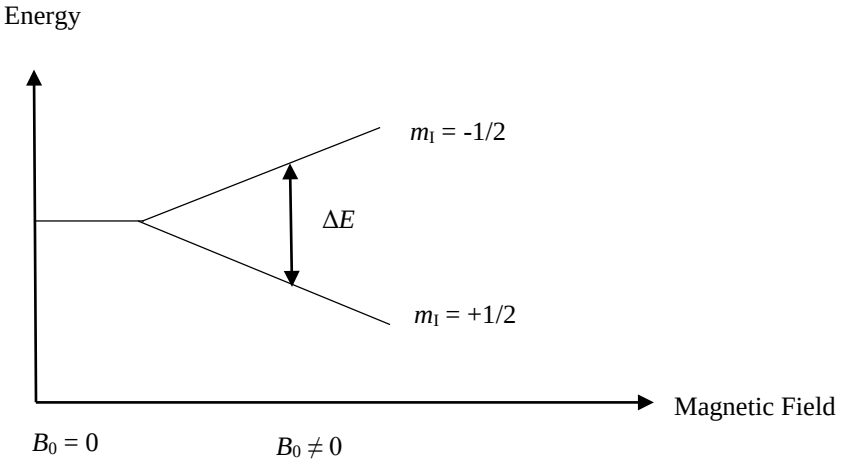

Scheme 1.1. Energy splitting in magnetic field

Most mononuclear MRI contrast agents contain Gd(III). The valence electron configuration of Gd(III) is f^7, and the half-filled *f* orbitals yield 7 unpaired electrons. Consequently, Gd(III) complexes are highly paramagnetic, making them useful for MR imaging. Clinically, gram quantities of a Gd(III) complex are often needed to obtain sufficiently clear images.[2,9]

All contrast agents shorten T_1 and T_2, increasing r_1 and r_2. Most contrast agents impact one relaxation process to a greater degree than the other and are therefore classified as either T_1 or T_2

contrast agents. T_1 contrast agents alter T_1 more than T_2 due to the fast endogenous transverse relaxation. If T_1 decreases, the signal enhancement increases, so they are positive contrast agents. Mononuclear Gd(III), Fe(III), and Mn(II) contrast agents are usually T_1 contrast agents. T_2 contrast agents, conversely, influence T_2 more than T_1. Also, they often reduce signal intensity and are consequently referred to as negative contrast agents. Iron oxide particles are the best known examples.

Relaxivity and its determinants

Relaxivity, which refers to the relaxation enhancement of solvent water protons promoted by a given complex per 1 mM of concentration is the most common measure of a contrast agent's efficiency. Larger r_1 values lower the required doses for contrast enhancement; contrast agents with higher relaxivities are therefore more valuable for clinical use. There are two kinds of relaxivities: inner-sphere relaxivity and outer-sphere relaxivity (including second-sphere relaxivity). The former process relies on water molecules directly binding to the metal center. The latter refers to water molecules binding to the ligands of the complex rather than the metal center.[6] Scheme 1.2 illustrates the pathways and the three major factors that contribute to a contrast agent's relaxivity:[10]

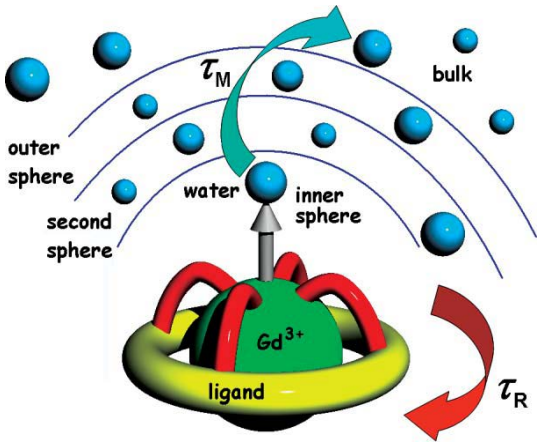

Scheme 1.2. Inner-sphere and outer sphere relaxivity.[10]

(1) The hydration number (q) refers to the number of water molecules that could bind to the metal ion. The contrast improves as more water molecules are able to coordinate to the paramagnetic ion. With most contrast agents, only one coordination site of the metal ion is accessible to water molecules, resulting in a $q = 1$. This low value is a consequence of the highly coordinating ligands needed for the contrast agent's aqueous stability. With some MRI contrast agents, q can reach 2 (Scheme 1.3). The hydration number q generally scales linearly with relaxivity.[2] In some cases, $q = 0$, and outer-sphere interactions with water are solely responsible for the contrast agent's relaxivity.

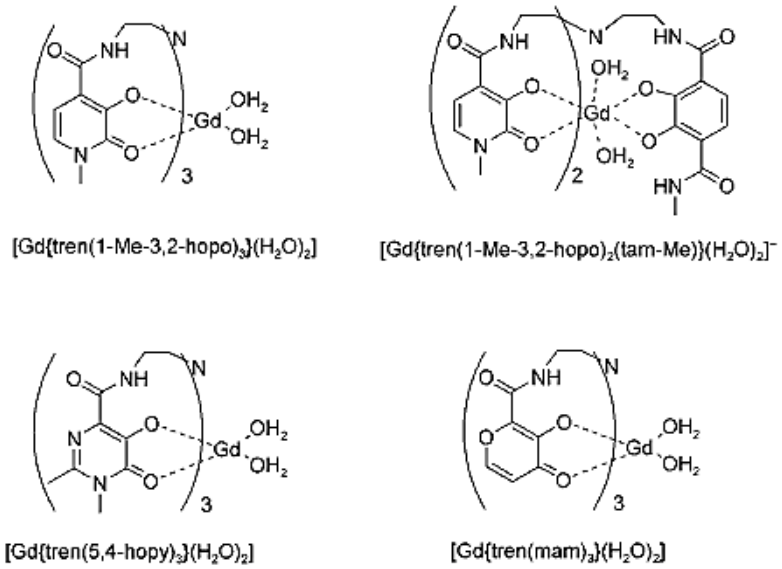

Scheme 1.3. Gd-HOPO complexes,[2] $q = 2$.

(2) In a magnetic field, the molecular rotational correlation time (τ_R) plays an important role in determining relaxivity. That the complex tumbles slowly in solution results in high relaxivity. If the molecular volume is large, the rotational correlation time will be long, increasing the rate of relaxation.[3,6]

(3) The mean time of water exchange (τ_M) also impacts the relaxivity. In order to get a high relaxivity, it is necessary to have an appropriate rate of water exchange. Obviously, relaxivity will be limited if the rate of water exchange is too slow. However, if the rate is too fast, it also limits relaxivity by not providing water molecules with enough time to interact with the paramagnetic center for the alternative relaxation pathways to be operable.[3] The optimal rate of water exchange depends on τ_R (Figure 1.2).[3] If τ_R = 0.1 ns, the relaxivity has little dependence on τ_M. However, if τ_R = 10 ns, the ideal residency time is 2 ~ 30 ns.

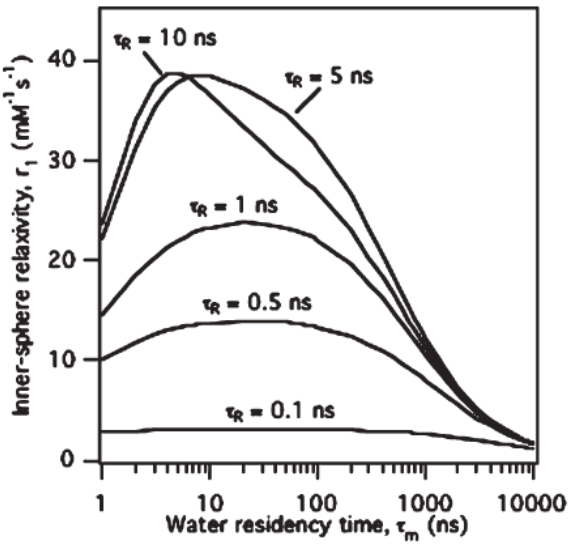

Figure 1.2. Relationship between rotational diffusion and water exchange at a given field strength (1.5 T) for a q = 1 compound with a long (>10 ns) T_{1e}.[3]

Inner-sphere relaxivity can be described by the following equation:[6]

$$R = \frac{Cq}{55.6}\frac{1}{T_{1M} + \tau_M}$$

C is the concentration of the contrast agent; q is the hydration number; T_{1M} is the longitudinal relaxation time of the water protons, which is influenced by the rotational correlation time (τ_R); τ_M is the mean residence time for water coordination.

Mononuclear transition metal complexes as contrast agents

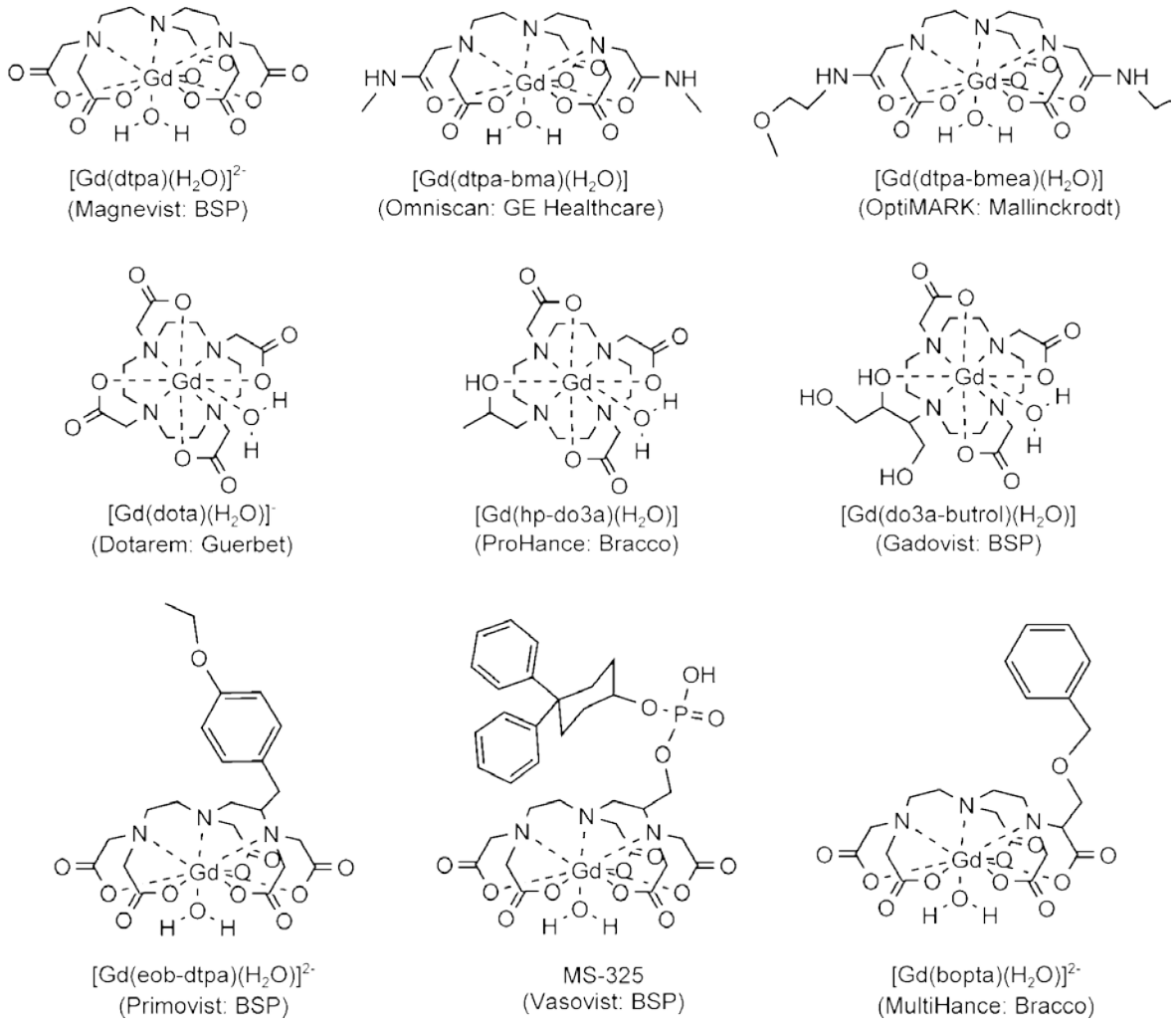

Figure 1.3. Commercial Gd(III) MRI contrast agents.[2]

Gd(III) complexes are most commonly used as MRI contrast agents. Figure 1.3 shows commercially used Gd(III) MRI contrast agents with aminocarboxylate ligands. All of the ligands have N and O donors, and all the complexes have inner-sphere water molecules (q = 1). Note that the first six complexes are general contrast agents. The last three complexes however have specific biological targets: Vasovist interacts with human serum albumin that increase the *in vivo* retention

time;[11,12,13] MultiHance and Primovist are specific for liver imaging and they are taken up by hepatocytes.[1,2,14,15]

Although Gd MRI contrast agents are widely used clinically, free Gd^{3+} ions are toxic due to interfering with calcium-ion channel dependent processes. This necessitates the highly coordinating ligands. Macrocycles, which present a high kinetic barrier of metal dissociation, are also common in FDA-approved contrast agents. Although the complexes pass through the body intact, there exist concerns about subsequent complex degradation introducing Gd^{3+} into ground water.

Manganese has been explored as an alternative paramagnetic reporter. High-spin Mn(II) is highly paramagnetic with an *S* equal to 5/2. Furthermore, manganese is an element that has many known biological roles.[16,17] Organisms have therefore evolved to manage manganese and regulate its traffic and distribution with the body. The cheap price of Mn salt is another attractive quality. The price per mole of $GdCl_3$ is six-fold higher than that of $MnCl_2$ ($6021 vs. $976). The given costs are from Sigma-Aldrich.

$MnCl_2$ was the first manganese-containing MRI contrast agent.[17] Although $MnCl_2 \cdot 4H_2O$ was approved by FDA in 1997 for clinical use, the neurotoxicity of free Mn^{2+} limits its application.[18,19]

Teslascan is a clinically approved manganese contrast agent that is commonly used to image the liver (Scheme 1.4).[20] The negatively charged ligand DPDP (*N*,*N*'-dipyridoxylethylenediamine-*N*,*N*'-diacetate-5,5'-bisphosphate) stabilizes the Mn(II) complex and lowers the toxicity of the contrast agent: the LD_{50} for Gd-DTPA is 60 ~ 100 mmol/kg but it is 540 mmol/kg for Teslascan.[21] However, this complex does not have inner-sphere water exchange mechanisms for increasing r_1, and the large enhancement is attributed to the slow release of Mn^{2+}

ions.[16,17,21] In addition to Teslascan, most non-macrocyclic ligands designed for Mn MRI contrast agents are anionic in pH = 7 water; examples include EDTA, DTPA, and their derivatives.[16] The ligands are also highly coordinating and are usually hexadentate. All of the complexes have a coordination number of 7. Mn(II) chelates with macrocyclic ligands have also been explored as MRI contrast agents. The macrocyclic effects increase the complexes' kinetic and thermodynamic stability, and hinder the release of toxic free metal ions.[16] Prior to the work in Chapter 2 of this dissertation, Mn-containing contrast agents were thought to require either a macrocycle or a negatively charged ligand for adequate water stability.

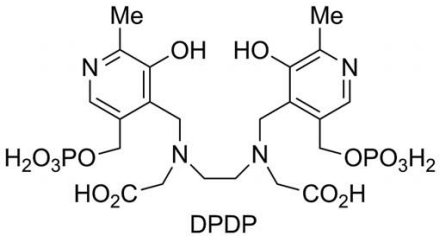

Scheme 1.4. Structure of the ligand of Teslascan.[16] Mn binds to 2 nitrogens in the ethylenediamine backbone, and 4 oxygens in phenols and carboxylates.

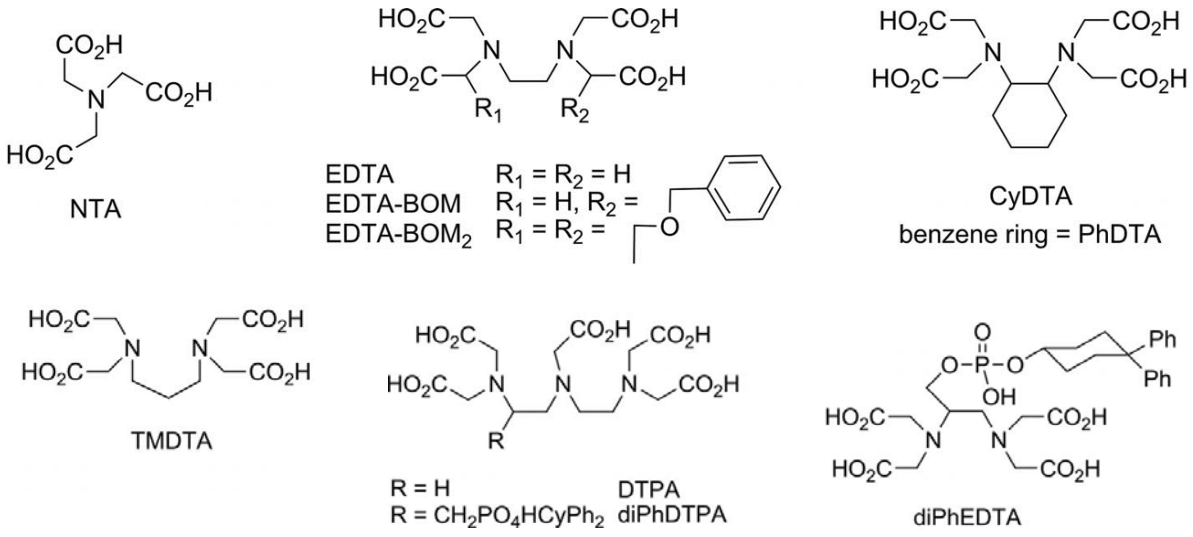

Figure 1.4. Non-macrocyclic ligands for Mn(II) MRI contrast agents.[16]

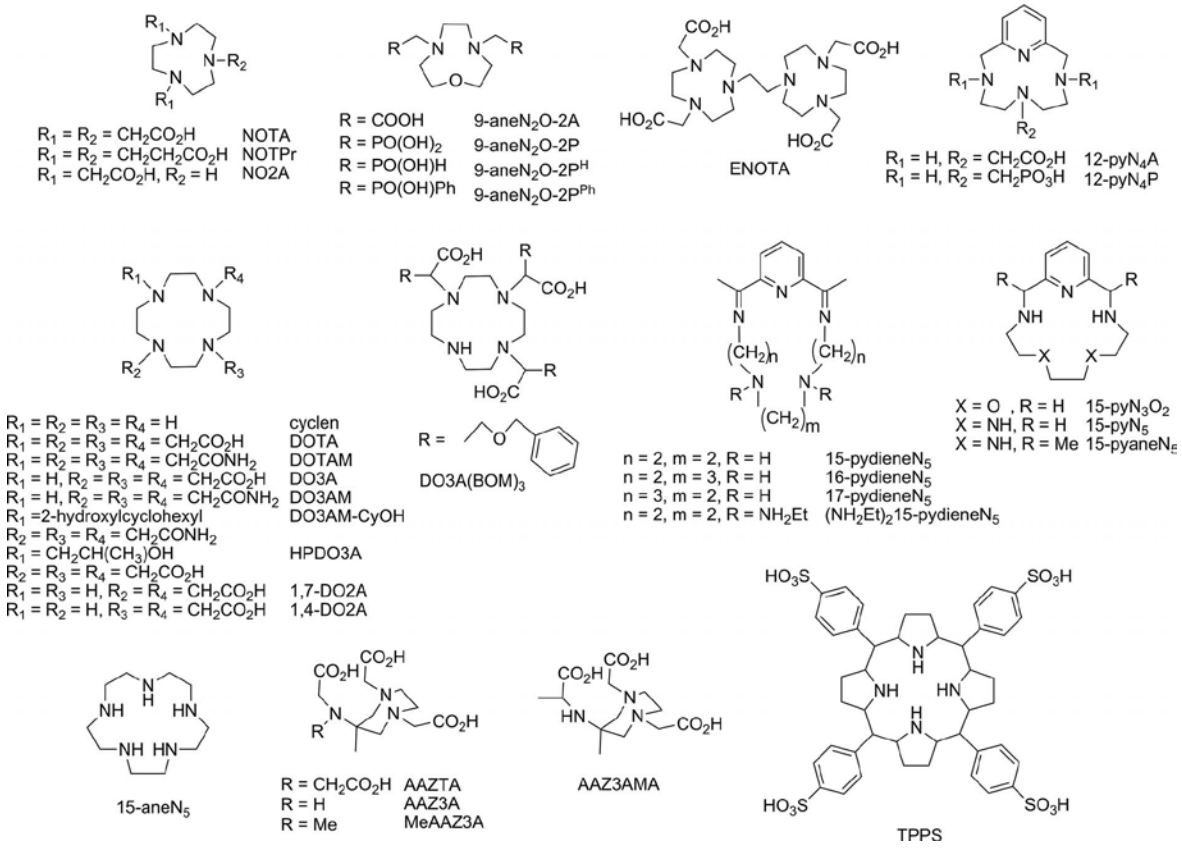

Figure 1.5. Macrocyclic ligands for Mn(II) MRI contrast agents.[16]

1.2 Alkene epoxidation catalyzed by Mn and Fe coordination complexes

Epoxides are cyclic ethers with three-membered rings. Due to their highly strained structures, epoxides are reactive and can be converted to a wide array of functional groups.[22,23] They are common intermediates in the syntheses of pharmaceuticals and petroleum industry. For example, the precursor of HIV Protease Inhibitor L-735,524 and the precursor of anti-diabetic agent CL 316,243 are epoxides (Scheme 1.5).[24]

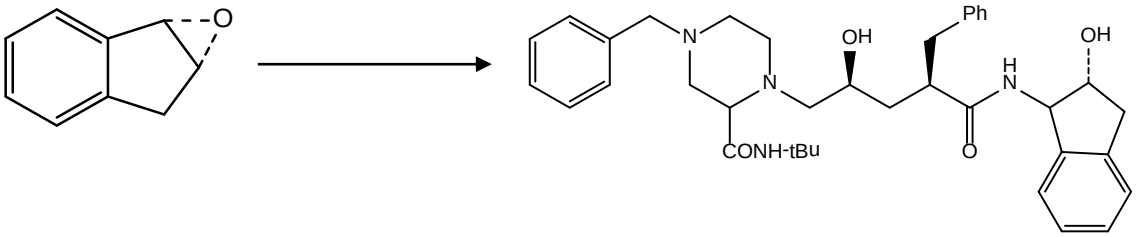

HIV Protease Inhibitor L-735,524

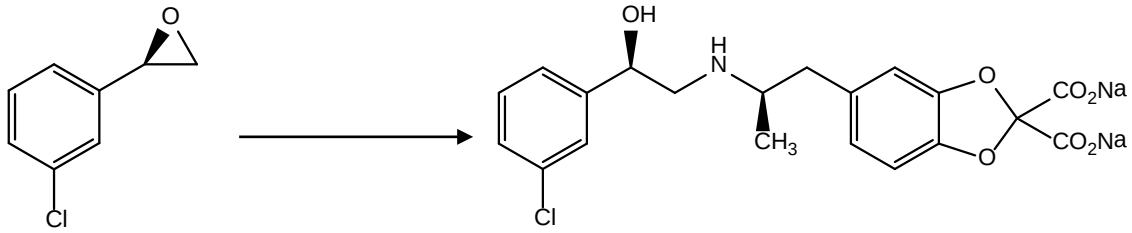

Anti-diabetic agent CL 316,243

Scheme 1.5 [24]

The most common way of synthesizing epoxides is olefin peroxidation. Manganese and iron coordination complexes have been explored extensively as homogenous catalysts for these reactions. A brief introduction to the catalysts most relevant to this dissertation follows.

[Mn(Salen)X]

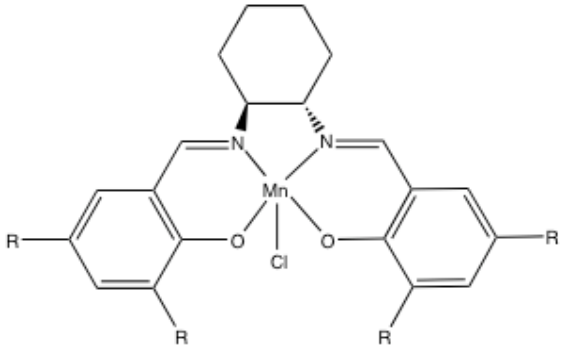

Scheme 1.6

Scheme 1.6 shows the core structure of the Mn(III)-Salen catalyst (R = alkyl, O-alkyl, and *tert*-butyl) developed by Jacobsen and coworkers.[25-28] With a low loading of this chiral catalyst, NaOCl oxidizes olefins to epoxides with high yields and high enantiomeric excesses (ee%) within 6 h.[27] (Table 1.1)

Table 1.1. Asymmetric Epoxidation of Representative Olefins by Mn(III)-Salen Catalyst[27] (R = *t*-Bu).[a]

entry	olefin substrate	yield (%)[b]	ee (%)[c]	equiv of catalyst required for complete reaction
1	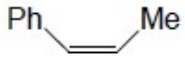	84	92	0.04
2	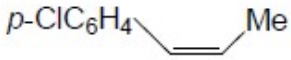	67	92	0.04
3	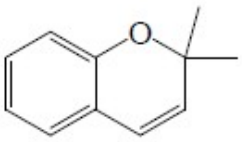	72	98	0.02
4	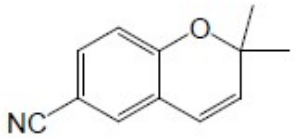	96	97	0.03
5	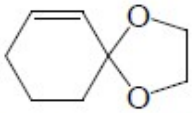	63	94	0.15
6[d]	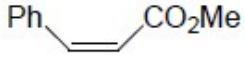	65[e]	89	0.10

[a]Reactions were run at 4 °C in CH_2Cl_2 with 0.25 mmol catalyst and 12.5 mmol substrate. [b]Isolated yield based on olefin. [c]Enantiomeric excess. [d]Reaction carried out in the presence of 0.4 equiv of 4-phenylpyridine *N*-oxide. [e]Yield determined by GC. All data are from reference 27.

The mechanism of how Mn(III)-Salen catalyzed olefin epoxidation proceeds is not fully understood. Linker proposed a Mn(V)=O intermediate as the oxidant; this intermediate was suggested to transfer the oxo group to the alkene in a single, concerted step (concerted pathway **A**, Scheme 1.7).[29]

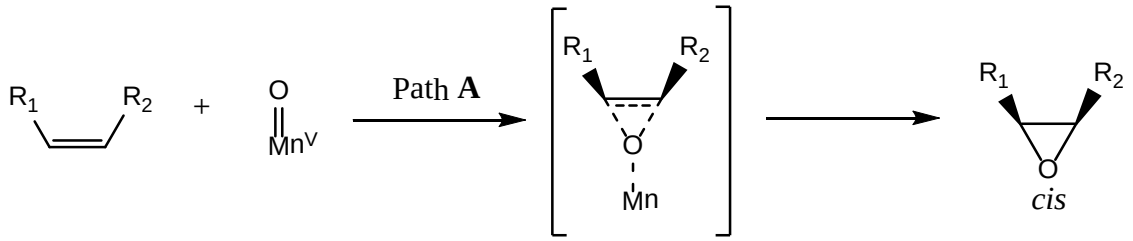

Scheme 1.7 [29]

The Mn(V)=O could potentially oxidize the alkene through two other pathways. The radical pathway **B** proceeds through a secondary carbon radical, allowing rotation of the C-C bond. In this case, a *trans* epoxide can form. Substrates with electron-withdrawing groups appear to prefer this pathway due to the stabilization of the radical. The manganoxetane pathway **C** proceeds through a four-membered metallocycle. In this case, a *cis* epoxide is formed. (Scheme 1.8)

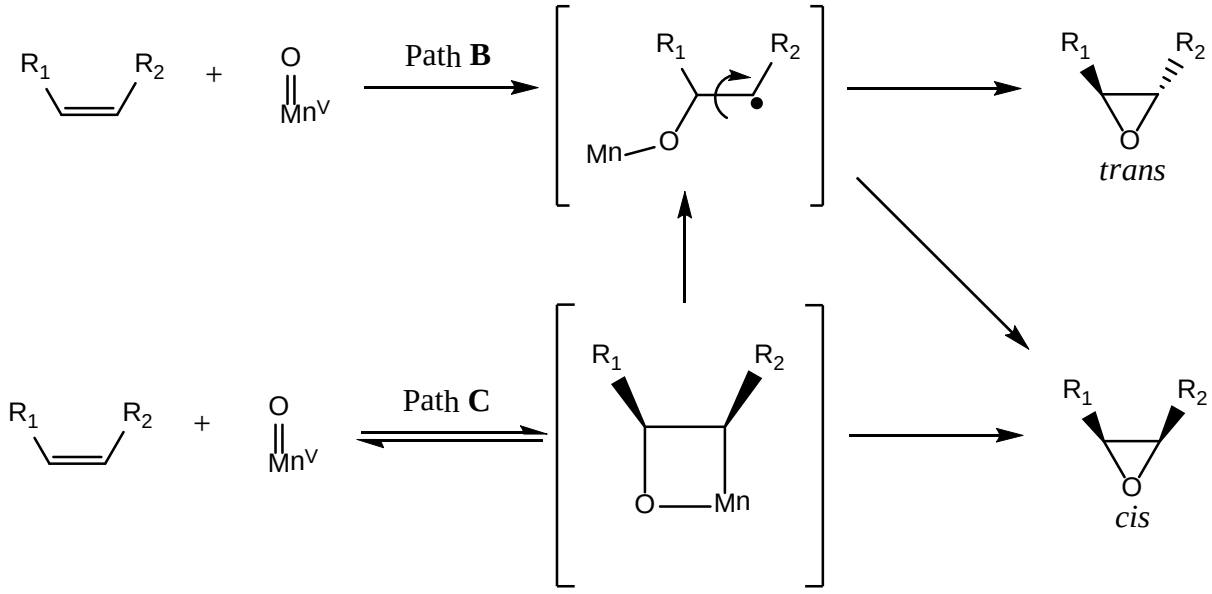

Scheme 1.8 [29]

[Mn(R,R-mcp)(OTf)$_2$]

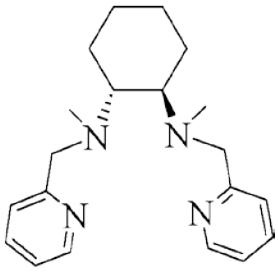

***R,R*-mcp**

Scheme 1.9. Ligand *R*,*R*-mcp.[30]

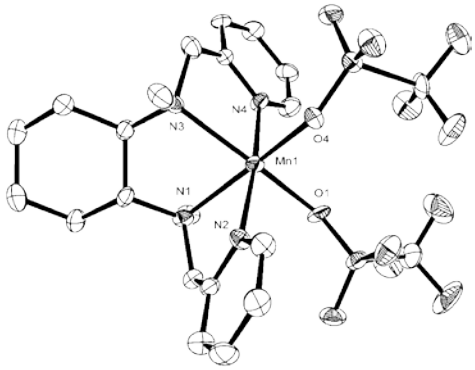

Figure 1.6. Crystal structure of [Mn(*R*,*R*-mcp)$(OTf)_2$].[30]

Stack and coworkers reported a polydentate N-donor ligand *R*,*R*-mcp and its Mn complex[30] (Scheme 1.9 and Figure 1.6). With a small loading (< 1.0 mol%), it catalyzed olefin epoxidation by peracetic acid with high yields within 5 min (Scheme 1.10 and Table 1.2).

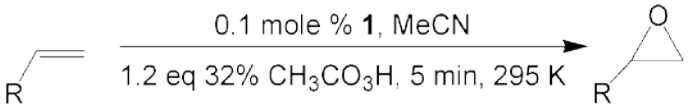

Scheme 1.10 [30]

Table 1.2. Epoxidations Catalyzed by [Mn(*R*,*R*-mcp)(OTf)$_2$] with CH_3CO_3H.[30] [a]

	aklene	%mol catalyst	oxidant (eq.)	GC yield[b]	isolated yield[c]
1	cyclooctene	0.1	1.2	99 (1)	90 (4)[d]
2	cyclohexene	0.1	1.2	98 (2)	85 (2)
3	1-methyl-cyclohexene	0.1	2	92 (3)	
4	*cis*-2-heptene	0.1	1.2	99 (1)[e]	
5	*trans*-2-heptene	0.1	1.2	99 (1)[f]	
6	2-methyl-1-pentene	0.1	1.2	97 (1)	
7	1-heptene	0.1	1.2	95 (3)	89 (3)
9	vinyl cyclohexane	0.1	1.2	99 (1)	90 (2)
9	allyl acetate	0.1	2	89 (3)	
10	methyl methacrylate	0.2	1.2	98 (1)	86 (6)
11	2-cyclohexen-1-one	0.5	1.2	97 (4)	88 (2)
12	ethyl sorbate[g]	0.1	1.2	94 (4)[h]	
13	*cis*-*β*-methylstyrene	1.0	1.2	90 (1)	
14	*trans*-*β*-methylstyrene	1.0	1.2	97 (1)	
15a	*R*-(-)-carvone	0.5	3	98 (1)[i]	88 (2)[i]
15b	*R*-(-)-carvone	0.5	1	97 (2)[j]	91 (2)[j]

[a] Olefin (0.5 M in CH_3CN), 32% CH_3CO_3H in acetic acid/water, 25 °C, 5 min. [b] Yields determined by GC versus internal standard, average of three runs. Conversion for all substrates is >95%. The numbers in parentheses represent a standard deviation of a minimum of three experiements. [c] Isolated yields, 1-g scale. [d] 0.25-mol scale, 88% yield. [e] 98% *cis*epoxide, 2% *trans*-epoxide. [f] 97% *trans*-epoxide, 3% *cis*-epoxide. [g] *trans*,*trans*-CH_3CH_2=CH_2CH_2=CH_2-$CO_2CH_2CH_3$. [h] 4:1 mixture of 4,5-monoepoxide and 2,3-monoepoxide. [i] 0 °C, diepoxide product, 20% de. [j] -20 °C, *R*carvone8,9-monoepoxide, 15% de.

The reactivities of the Mn(II) complexes with the neutral N-donors depend on the acidity of the reaction mixture.[31] Table 1.3 shows that moderate yields were obtained when using commercial peracetic acid (PAA_C, 32%). This contains traces of the H_2SO_4 used to prepare the oxidant. However, substantially greater yields are obtained with a custom-made low concentration peracetic acid (PAA_R, 9 ~ 10%) using AcOH, H_2O_2, and Amberlite IR120 cation exchange resin. This lacks the H_2SO_4 impurity. It has been proposed that higher concentrations of acid promote dissociation of the ligand; the Mn(II) salts by themselves are not competent catalysts.

Table 1.3. Epoxidation Reactivity of [Mn(II)(L)(OTf)$_2$] Complexes.[31] [a]

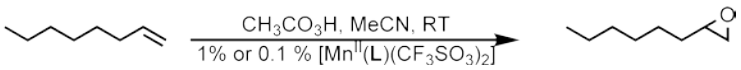

No.	Ligand	5 min		5 min				15 s[b]	
		PAA$_C$[c] oxidant		PAA$_R$[d] oxidant				PAA$_R$[d] oxidant	
		1% Catalyst loading		1% Catalyst loading		0.1% Catalyst loading		1% Catalyst loading	0.1% Catalyst loading
		Conv.	Epoxide	Conv.	Epoxide	Conv.	Epoxide	Epoxide	Epoxide
1	*R,R*-mcp	98	94	96	92	96	92	75	27
2	*R,R*-pcp	0	0	28	22	2	2	8	
3	*R,R*-6-Me-6′-H-mcp	18	15	91	88	36	31	19	
4	*R,R*-6-Me-mcp	6	2	60	55	6	4	10	
5	*R,R*-hcp	18	11	98	96	33	28	88	
6	*meso*-hcp	4	2	95	92	15	12	61	
7	mep	25	24	87	87	53	49	83	2
8	*uns*-mep	5	3	94	94	49	43	89	
9	bisp	97	91	92	84	23	18	19	
10	tmpa	3	2	96	92	6	4	23	
11	Me$_4$cyclam	5	2	11	11	1	1	1	
12	*R,R*-H$_1$pcdb[e]	6	6	51	49	6	5	50	
13	*R,R*-H$_2$cdb[e]	4	2	20	15	1	1	3	
14	Me$_3$tacn	80	71	95	91	85	82	44	8
15	terpy	2	1	94	91	50	46	84	43
16	bpma	0	0	88	83	82	77	83	2
17	*R,R*-tmcp	12	9	95	92	15	11	74	
18	tmep	1	1	88	86	10	9	57	
19	bpy[f]	2	2	99	95	99	94	94	93
20	phen[f]	2	2	99	93	99	93	93	93
21	2-Cl-phen[f]	1	1	46	40	7	3	7	
22	5-Cl-phen[f]	1	1	98	95	95	89	90	88
23	none	0	0	4	2	4	2	0	0

[a]Performed with 1-octene (0.5 M), [Mn(II)**L**(OTf)$_2$] (5 mM), *n*-nonane (50 mM), 2 equiv. of CH_3CO_3H, 25 °C, 5 min. Conversion and epoxide yields determined relative to an internal standard. Results are average of at least three runs. [b]32% CH_3CO_3H, 1% H_2SO_4 in CH_3CO_2H/H_2O (**PAA$_C$**). [c]9-10% CH_3CO_3H in CH_3CO_2H (**PAA$_R$**). [d]1-Octene (0.5 M), [Mn(II)**L**(OTf)$_2$] (5 mM), *n*-nonane (50 mM), 2 equiv of CH_3CO_3H (**PAA$_R$**), 25 °C. Reactions were quenched with Et_3N after 15 s. [e][Mn(III)**L**OAc] complexes, generated from $MnOAc_2 \cdot 4H_2O$ and O_2. [f] Performed with 2 equiv of **bipy**/Mn(II). [g]phenanthroline shows reactivity nearly identical to that of bipy under these conditions.

[Fe(mep)(MeCN)$_2$]$^{2+}$

In 2001, Jacobsen and coworkers developed a novel Fe complex [Fe(mep)(MeCN)$_2$]$^{2+}$ for fast epoxidation (Figure 1.7).[32] With a small catalyst loading (< 5 mol%), high yields of epoxides were obtained within 5 min (Scheme 1.11 and Table 1.4). Interestingly, in the presence of acetic acid, a μ-oxo, carboxylate bridged di-iron(III) complex reminiscent of the active site of iron-containing methane monooxygenase was formed (Figure 1.8).

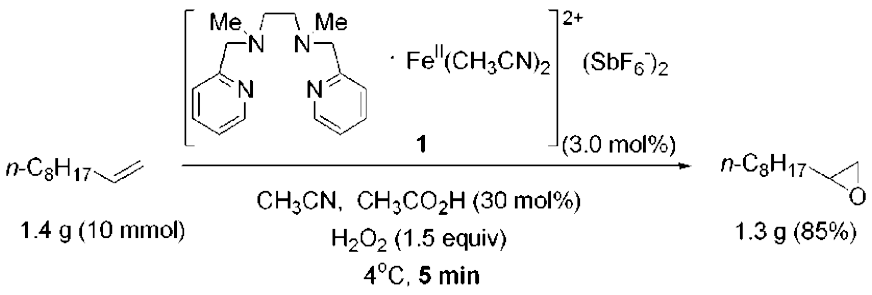

Scheme 1.11 [32]

Table 1.4. Epoxidations catalyzed by $[Fe(mep)(MeCN)_2]^{2+}$. [32 a]

Entry	Substrate	Isolated Yields[b] (GC yield)[c]
1	*n*-C_8H_{17}	85%
2	*n*-$C_{10}H_{21}$	90%[d]
3	*cyclo*-C_6H_{11}	76%[e]
4	EtO_2C	63%[f]
5	TBSO	61%[g]
6		77%
7	cyclooctene	86%
8		87%
9		80% (90%)
10		85% (90%)

[a] Reaction conditions[33]: olefin (2.0 mmol, 0.16 M in CH_3CN), **1** (3.0 mol %), CH_3CO_2H (10 equiv relative to **1**), H_2O_2 (aqueous 50 wt %, 3.0 mmol, 1.5 M in CH_3CN, added dropwise over 2 min), 4 °C, 5 min. [b] Isolated yields based on an average of 3 runs. [c] GC yields were determined using nitrobenzene as an internal standard for especially volatile substrates. [d] Reaction carried out at $[olefin]_0$) 0.13 M due to poor solubility in CH_3CN.[e] 5 mol % by $[Fe(mep)(MeCN)_2]^{2+}$. [f] 1.5 mol % **1**/1.5 mol % CH_3CO_2H. [g] 6 mol % CH_3CO_2H.

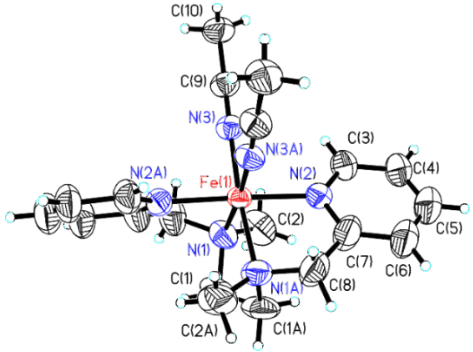

Figure 1.7. Crystal structure of $[Fe(mep)(MeCN)_2]^{2+}$.[32]

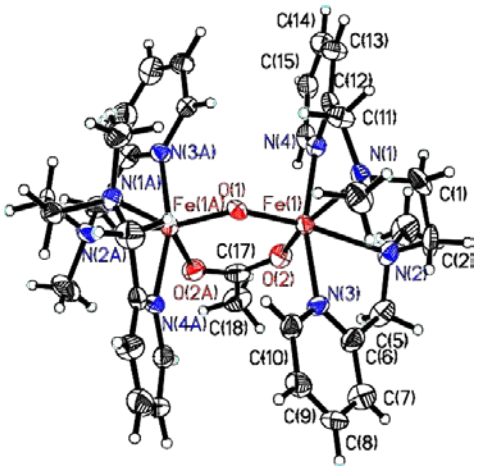

Figure 1.8. Crystal structure of the $[Fe_2(\mu\text{-}O)(\mu\text{-}CH_3CO_2)(mep)_2]^{2+}$.[32]

Que and coworkers proposed mechanisms for olefin epoxidation by H_2O_2 in the presence and absence of AcOH (Scheme 1.12).[34] With AcOH, a $[Fe(III)(OOH)(AcOH)]^{2+}$ adduct is proposed to form an Fe(V)=O oxidant (f in Scheme 1.12), which transfers an oxygen atom to the olefin. In Chapter 3, we explore the use of a more highly chelating analog of the mep ligand in iron- and manganese-catalyzed olefin epoxidation.

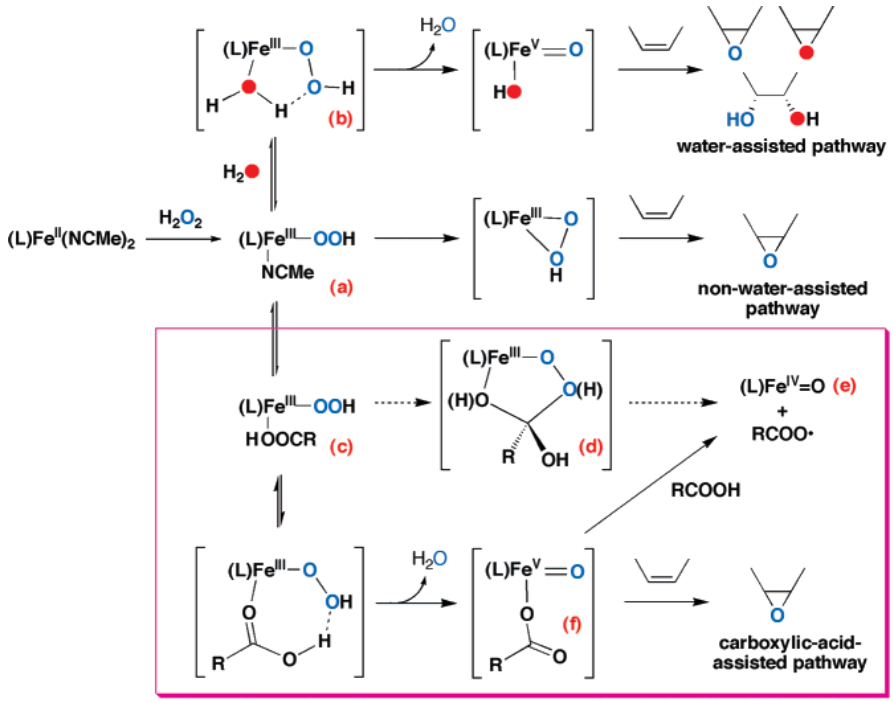

Scheme 1.12. Proposed mechanisms for non-heme iron catalyzed olefin epoxidation.[34]

1.3 Non-heme iron catalyzed C-H activation

Iron catalyzed C-H activation in nature

Nature uses iron hydroxylases to selectively oxidize C-H bonds under mild conditions. For both Cytochrome P450 (heme) and α-ketoglutaratedioxygenase (TauD, non-heme), Fe(IV)=O species have been proposed as the relevant oxidant (Scheme 1.13).[35-37]

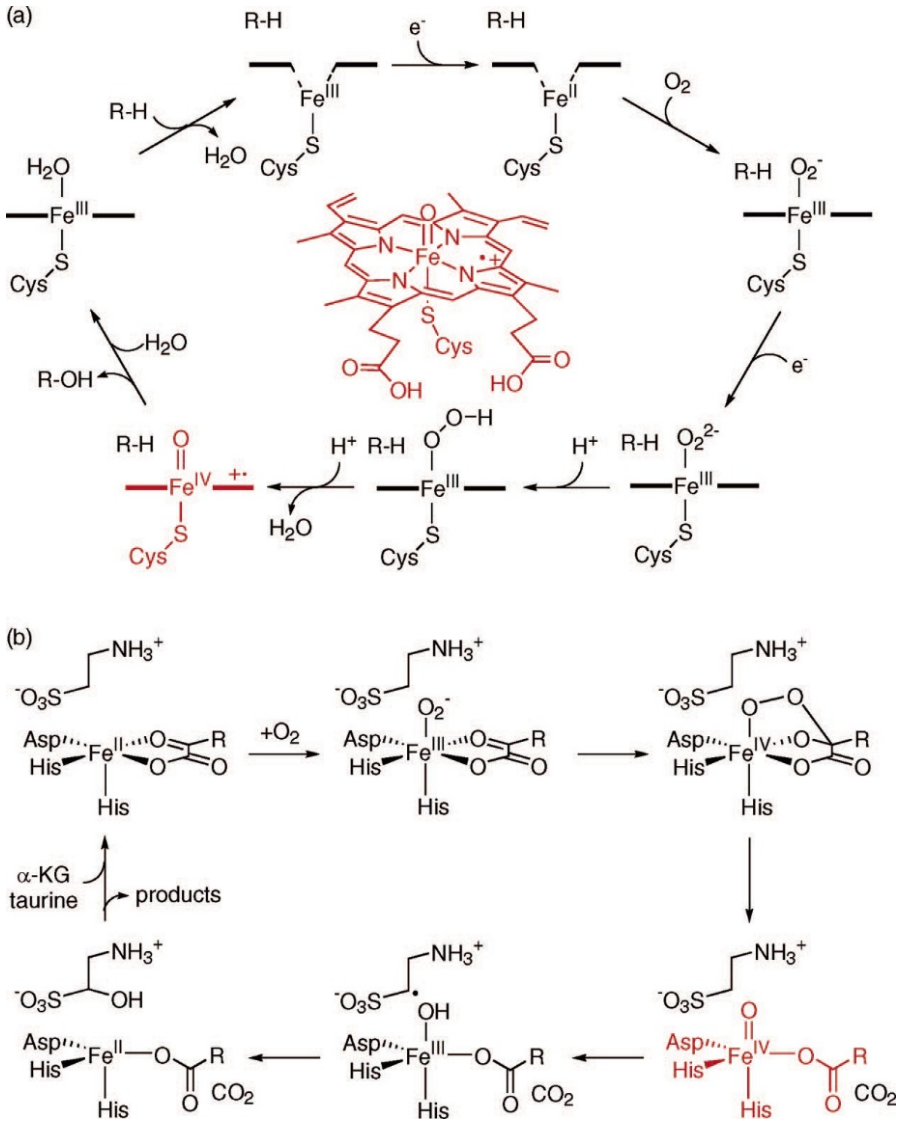

Scheme 1.13. Proposed mechanisms of catalytic cycle of Cytochrome P450 (a) and TauD (b).[35]

Non-heme iron complexes as catalysts for regioselective oxidation

Generally, secondary carbons are harder to oxidize than tertiary carbons. A method to oxidize secondary carbons selectively would complement existing methodology and allow synthetic chemists more ready access to new classes of oxidized products. In 2001, Que and coworkers reported the alkane hydroxylation by the non-heme iron catalyst [Fe(mep)$(OTf)_2$] (mep = bpmen).[38] Tertiary alcohols were the major products when *cis*-1,2-dimethylcyclohexane was the substrate, and the retention of configuration was 96%. However, there are few successful examples of regioselective oxidation towards positions that are considered to be less innately reactive.[39-42] In 2010, White and coworkers reported the substrate-guided selectivity of non-heme [Fe(*S*,*S*-pdp)$(MeCN)_2]^{2+}$ (*S*,*S*-pdp = (2-({(*S*)-2-[(*S*)-1-(pyridin-2-ylmethyl)pyrrolidin-2-yl]pyrrolidin-1-yl}methyl)pyridine)[41] catalyzed C-H oxidation (Figure 1.9).[43] It can predictably catalyze specific positions of substrates based on electronic, steric, and stereoelectronic effects. In this case, the ratio of secondary products to tertiary products is higher than [Fe(bpmen)$(OTf)_2$] (Table 1.5).

Potentially, one can use steric repulsions between the catalyst and substrate to tune the regioselectivity of the oxidation towards secondary carbons. Our laboratory recently prepared the ligand *N*,*N*'-di(phenylmethyl)-*N*,*N*'-bis(2-pyridinylmethyl)-1,2-cyclohexanediamine (bbpc).[44] (Figure 1.10) The complex [Fe(bbpc)$(MeCN)_2]^{2+}$ directed the oxidation towards secondary carbons to a greater extent than other reported non-heme iron complexes (Table 1.5).[43,44] In Chapter 4, we tune this reactivity more towards the secondary carbons by substituting neopentyl groups for the benzyl groups. The reactivity proceeds through [Fe(III)(bbpc)$(OOH)]^{2+}$ species.[44] The compound can also be generated from O_2 and a hydrocarbon with a weak C-H bond.[45] The formation and stability of the ferric hydroperoxide are discussed in Chapter 5.

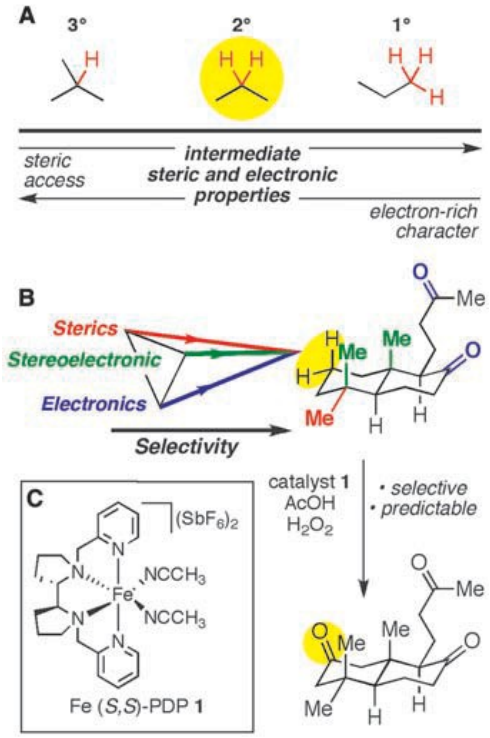

Figure 1.9. (A) Chemical properties of aliphatic C-H bonds. (B) Synergistic effects on site selectivity. Steric, stereoelectronic (influence of orientation of electron orbitals in space on reactivity), and electronic influences on reactivity with catalyst Fe(*S*,*S*)-pdp have an additive effect in complex molecule settings, which can lead to highly predictable and selective outcomes. (C) Electrophilic, bulky catalyst Fe(*S*,*S*)-pdp for predictably selective aliphatic C-H oxidation.[43]

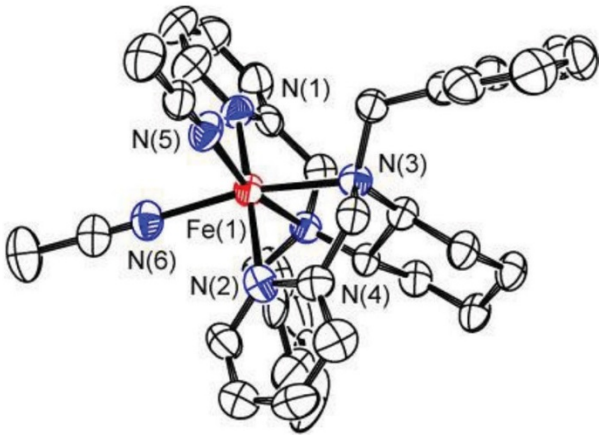

Figure 1.10. Crystal structure of $[Fe(bbpc)(MeCN_2)]^{2+}$.[44]

Table 1.5. Ratios of Tertiary (3°) to Secondary (2°) Carbon Oxidation Observed with Non-Heme Iron Catalysts.[44]

Compound	3°:2° with *cis*-1,2-dimethylcyclohexane	3°:2° with *trans*-1,2-dimethylcyclohexane	Reference
$[Fe(bpmen)(OTf)_2]$	2.8:1	1:1.5	44
$[Fe(bpmcn)(MeCN)_2]^{2+}$	1.8:1	1:1.9	44
$[Fe(S,S\text{-pdp})(MeCN)_2]^{2+}$	4.0:1	1:1.7	43
$[Fe(bbpc)(MeCN)_2]^{2+}$	1.4:1	1:4.8	44

Appendix

Copyright with permissions

(1) Figure 1.1 was reprinted with permission from Caravan, P. *Chem. Soc. Rev.* **2006**, *35*, 512-523. Copyright © 2006 Royal Society of Chemistry.

(2) Scheme 1.2 was reprinted with permission from Hermann, P.; Kotek, J.; Kubiček, V.; Lukeš, I. *Dalton Trans.* **2008**, 3027-3047. Copyright © 2008 Royal Society of Chemistry.

(3) Scheme 1.3 was reprinted with permission from Werner, E. J.; Datta, A.; Jocher, C. J.; Raymond, K. N. *Angew. Chem. Int. Ed.* **2008**, *47*, 8568-8580. Copyright © 2008 Wiley-VCH Verlag GmbH & Co. KGaA.

(4) Figure 1.2 was reprinted with permission from Caravan, P. *Chem. Soc. Rev.* **2006**, *35*, 512-523. Copyright © 2006 Royal Society of Chemistry.

(5) Figure 1.3 was reprinted with permission from Werner, E. J.; Datta, A.; Jocher, C. J.; Raymond, K. N. *Angew. Chem. Int. Ed.* **2008**, *47*, 8568-8580. Copyright 2008 © Wiley-VCH Verlag GmbH & Co. KGaA.

(6) Scheme 1.4 was reprinted with permission from Drahoš, B.; Lukeš, I.; Tóth, É. *Eur. J. Inorg. Chem.* **2012**, 1975-1986. Copyright © 2012 Wiley-VCH Verlag GmbH & Co. KGaA.

(7) Figure 1.4 was reprinted with permission from Drahoš, B.; Lukeš, I.; Tóth, É. *Eur. J. Inorg. Chem.* **2012**, 1975-1986. Copyright © 2012 Wiley-VCH Verlag GmbH & Co. KGaA.

(8) Figure 1.5 was reprinted with permission from Drahoš, B.; Lukeš, I.; Tóth, É. *Eur. J. Inorg. Chem.* **2012**, 1975-1986. Copyright © 2012 Wiley-VCH Verlag GmbH & Co. KGaA.

(9) Scheme 1.5 was reprinted with permission from Choi, W. J.; Choi, C. Y. *Biotechnol. Bioprocess Eng.* **2005**, *10*, 167-179. Copyright © 2005 Springer.

(10) Table 1.1 was reprinted with permission from Jacobsen, E. N.; Zhang, W.; Muci, A. R.;

Ecker, J. R.; Deng, L. *J. Am. Chem. Soc.* **1991**, *113*, 7063-7064. Copyright © 1991 American Chemical Society.

(11) Scheme 1.7 was reprinted with permission from Linker, T. *Angew. Chem. Int. Ed. Engl.* **1997**, *36*, 2060-2062. Copyright © 1997 Wiley-VCH Verlag GmbH & Co. KGaA.

(12) Scheme 1.8 was reprinted with permission from Linker, T. *Angew. Chem. Int. Ed. Engl.* **1997**, *36*, 2060-2062. Copyright © 1997 Wiley-VCH Verlag GmbH & Co. KGaA.

(13) Scheme 1.9 was reprinted with permission from Murphy, A.; Dubois, G.; Stack, T. D. P. *J. Am. Chem. Soc.* **2003**, *125*, 5250-5251. Copyright © 2003 American Chemical Society.

(14) Figure 1.6 was reprinted with permission from Murphy, A.; Dubois, G.; Stack, T. D. P. *J. Am. Chem. Soc.* **2003**, *125*, 5250-5251. Copyright © 2003 American Chemical Society.

(15) Scheme 1.10 was reprinted with permission from Murphy, A.; Dubois, G.; Stack, T. D. P. *J. Am. Chem. Soc.* **2003**, *125*, 5250-5251. Copyright © 2003 American Chemical Society.

(16) Table 1.2 was reprinted with permission from Murphy, A.; Dubois, G.; Stack, T. D. P. *J. Am. Chem. Soc.* **2003**, *125*, 5250-5251. Copyright © 2003 American Chemical Society.

(17) Table 1.3 was reprinted with permission from Murphy, A.; Pace, A.; Stack, T. D. P. *Org. Lett.* **2004**, *6*, 3119-3122. Copyright © 2004 American Chemical Society.

(18) Scheme 1.11 was reprinted with permission from White, M. C.; Doyle, A. G.; Jacobsen, E. N. *J. Am. Chem. Soc.* **2001**, *123*, 7194-7195. Copyright © 2001 American Chemical Society.

(19) Table 1.4 was reprinted with permission from White, M. C.; Doyle, A. G.; Jacobsen, E. N. *J. Am. Chem. Soc.* **2001**, *123*, 7194-7195. Copyright © 2001 American Chemical Society.

(20) Figure 1.7 was reprinted with permission from White, M. C.; Doyle, A. G.; Jacobsen, E. N. *J. Am. Chem. Soc.* **2001**, *123*, 7194-7195. Copyright © 2001 American Chemical Society.

(21) Figure 1.8 was reprinted with permission from White, M. C.; Doyle, A. G.; Jacobsen, E.

N. *J. Am. Chem. Soc.* **2001**, *123*, 7194-7195. Copyright © 2001 American Chemical Society.

(22) Scheme 1.12 was reprinted with permission from Mas-Ballesté, R.; Que, L., Jr. *J. Am. Chem. Soc.* **2007**, *129*, 15964-15972. Copyright © 2007 American Chemical Society.

(23) Scheme 1.13 was reprinted with permission from Nam, W. *Acc. Chem. Res.* **2007**, *40*, 522-531. Copyright © 2007 American Chemical Society.

(24) Figure 1.10 was reprinted with permission from Chen, M. S.; White, M. C. *Science* **2010**, *327*, 566-571. Copyright © 2010 American Association for the Advancement of Science.

(25) Figure 1.11 was reprinted with permission from He, Y.; Gorden, J. D.; Goldsmith, C. R. *Inorg. Chem.* **2011**, *50*, 12651-12660. Copyright © 2011 American Chemical Society.

(26) Table 1.5 was reprinted with permission from He, Y.; Gorden, J. D.; Goldsmith, C. R. *Inorg. Chem.* **2011**, *50*, 12651-12660. Copyright © 2011 American Chemical Society.

References

(1) Caravan, P.; Ellison, J. J.; McMurry, T. J.; Lauffer, R. B. *Chem. Rev.* **1999**, *99*, 2293-2352.

(2) Werner, E. J.; Datta, A.; Jocher, C. J.; Raymond, K. N. *Angew. Chem., Int. Ed.* **2008**, *47*, 8568-8580.

(3) Caravan, P. *Chem. Soc. Rev.* **2006**, *35*, 512-523.

(4) Beattie, P. F.; Meyers, S. P. *Phys. Ther.* **1998**, *78*, 738-753.

(5) Lauffer, R. B. *Chem. Rev.* **1987**, *87*, 901-927.

(6) Bottrill, M.; Kwok, L.; Long, N. J. *Chem. Soc. Rev.* **2006**, *35*, 557-571.

(7) Zhang, S.; Merritt, M.; Woessner, D. E.; Lenkinski, R. E.; Sherry, A. D. *Acc. Chem. Res.* **2003**, *36*, 783-790.

(8) Aime, S.; Botta, M.; Fasano, M.; Terreno, E. *Acc. Chem. Res.* **1999**, *32*, 941-949.

(9) Raymond, K. N.; Pierre, V. C. *Bioconjugate Chem.* **2005**, *16*, 3-8.

(10) Hermann, P.; Kotek, J.; Kubiček, V.; Lukeš, I. *Dalton Trans.* **2008**, 3027-3047.

(11) Caravan, P.; Cloutier, N. J.; Greenfield, M. T.; McDermid, S. A.; Dunham, S. U.; Bulte, J. W. M.; Amedio, J. C., Jr.; Looby, R. J.; Supkowski, R. M.; Horrocks, W. D., Jr.; McMurry, T. J.; Lauffer, R. B. *J. Am. Chem. Soc.* **2002**, *124*, 3152-3162.

(12) Lauffer, R. B.; Parmelee, D. J.; Dunham, S. U.; Ouellet, H. S.; Dolan, R. P.; Witte, S.; McMurry, T. J.; Walovitch, R. C. *Radiology* **1998**, *207*, 529-538.

(13) Parmelee, D. J.; Walovitch, R. C.; Ouellet, H. S.; Lauffer, R. B. *Invest. Radiol.* **1997**, *32*, 741-747.

(14) Kirchin, M. A.; Pirovano, G. P.; Spinazzi, A.; *Invest. Radiol.* **1998**, *33*, 798-809.

(15) van Beers, B. E.; Pastor, C. M.; Hussain, H. K. *J. Hepatol.* **2012**, *57*, 421-429.

(16) Drahoš, B.; Lukeš, I.; Tóth, É. *Eur. J. Inorg. Chem.* **2012**, 1975-1986.

(17) Kueny-Stotz, M.; Garofalo, A.; Felder-Flesch, D. *Eur. J. Inorg. Chem.* **2012**, 1987-2005.

(18) Paulter, R. G. *NMR Biomed.* **2004**, *17*, 595-601.

(19) Aschner, M.; Guilarte, T. R.; Schneider, J. S.; Zheng, W. *Toxicol. Appl. Pharmacol.* **2007**, *221*, 131-147.

(20) Rocklage, S. M.; Cacheris, W. P.; Quay, S. C.; Hahn, F. E.; Raymond, K. N. *Inorg. Chem.* **1989**, *28*, 477-485.

(21) Elizondo, G.; Fretz, C. J.; Stark, D. D.; Rocklage, S. M.; Quay, S. C.; Worah, D.; Tsang, Y. M.; Chen, M. C.; Ferrucci, J. T. *Radiology* **1991**, *178*, 73-78.

(22) Parker, R. E.; Isaacs, N. S. *Chem. Rev.* **1959**, *59*, 737-799.

(23) Bertolini, T. *J. Chem. Educ.* **2002**, *79*, 828.

(24) Choi, W. J.; Choi, C. Y. *Biotechnol. Bioprocess Eng.* **2005**, *10*, 167-179.

(25) Zhang, W.; Loebach, J. L.; Wilson, S. R.; Jacobsen, E. N. *J. Am. Chem. Soc.* **1990**, *112*, 2801-2803.

(26) Jacobsen, E. N.; Zhang, W.; Guler, M. L. *J. Am. Chem. Soc.* **1991**, *113*, 6703-6704.

(27) Jacobsen, E. N.; Zhang, W.; Muci, A. R.; Ecker, J. R.; Deng, L. *J. Am. Chem. Soc.* **1991**, *113*, 7063-7064.

(28) Jacobsen, E. N.; Deng, L.; Furukawa, Y.; Martínez, L. E. *Tetrahedron* **1994**, *50*, 4323-4334.

(29) Linker, T. *Angew. Chem., Int. Ed. Engl.* **1997**, *36*, 2060-2062.

(30) Murphy, A.; Dubois, G.; Stack, T. D. P. *J. Am. Chem. Soc.* **2003**, *125*, 5250-5251.

(31) Murphy, A.; Pace, A.; Stack, T. D. P. *Org. Lett.* **2004**, *6*, 3119-3122.

(32) White, M. C.; Doyle, A. G.; Jacobsen, E. N. *J. Am. Chem. Soc.* **2001**, *123*, 7194-7195.

(33) Fringuelli, F.; Piermatti, O.; Pizzo, F.; Vaccaro, L. *J. Org. Chem.* **1999**, *64*, 6094-6096.

(34) Mas-Ballesté, R.; Que, L., Jr. *J. Am. Chem. Soc.* **2007**, *129*, 15964-15972.

(35) Nam, W. *Acc. Chem. Res.* **2007**, *40*, 522-531.

(36) Makris, T. M.; von Koenig, K.; Schlichting, I.; Sligar, S. G. *J. Inorg. Biochem.* **2006**, *100*, 507–518.

(37) Bollinger, J. M., Jr.; Krebs, C. *J. Inorg. Biochem.* **2006**, *100*, 586–605.

(38) Chen, K.; Que, L., Jr. *J. Am. Chem. Soc.* **2001**, *123*, 6327-6337.

(39) Goldsmith, C. R.; Coates, C. M.; Hagan, K.; Mitchell, C. A. *J. Mol. Catal. A* **2011**, *335*, 24−30.

(40) Chen, J.; Che, C.-M. *Angew. Chem., Int. Ed.* **2004**, *43*, 4950−4954.

(41) Zhang, J.-L.; Che, C.-M. *Chem.−Eur. J.* **2005**, *11*, 3899−3914.

(42) Chen, M. S.; White, M. C. *Science* **2007**, *318*, 783-787.

(43) Chen, M. S.; White, M. C. *Science* **2010**, *327*, 566-571.

(44) He, Y.; Gorden, J. D.; Goldsmith, C. R. *Inorg. Chem.* **2011**, *50*, 12651-12660. Correction: *Inorg. Chem.* **2012**, *51*, 7431.

(45) He, Y.; Goldsmith, C. R. *Chem. Commun.* **2012**, *48*, 10532-10534.

Chapter 2

Manganese(II)-Containing MRI Contrast Agent Employing a Neutral and Non-Macrocyclic Ligand*

* This Chapter's content was previously published in the following manuscript:

Zhang, Q.; Gorden, J. D.; Beyers, R. J.; Goldsmith, C. R. *Inorg. Chem.* **2011**, *50*, 9365-9373.

2.1 Introduction

First-row transition metal ions are commonly found with coordination numbers of four through six. Seven-coordinate transition metal complexes, conversely, are relatively rare. A 2003 survey of the Cambridge Structural Database found that heptacoordinate metal ions were found in less than 2% of the total number of structures that contained elements from Groups 3 to 12.[1] Heptacoordinate metal centers have been sought and investigated for a number of reasons. They can serve as models of intermediates in associative ligand exchange mechanisms. Their electronic structures can differ markedly from those of lowercoordinate analogs, potentially enabling novel modes of reactivity.[2]

Heptacoordinate manganous complexes, in particular, have been investigated for their potential to serve both as superoxide dismutase mimics[3-5] and as contrast agents for magnetic resonance imaging (MRI).[6-10] The latter research has the goal of developing alternatives to gadolinium-containing contrast agents. Although many Gd(III) complexes have been approved for clinical use,[11,12] there exist concerns about both their adverse effects on the human body[13,14] and the potential entrance of toxic Gd(III) species into groundwater.[15] Manganese(II) ions are attractive alternatives as the paramagnetic reporter on the bases of their high paramagnetism (S = 5/2) and the prevalence of manganese in biology and the environment.[16,17] In the development of clinically useful Mn(II) compounds, the use of a highly coordinating ligand is essential to maintaining the stability of the complex in aqueous solutions and regulating the metal ion's reactivity. Previously found Mn(II)-containing contrast agents, including the clinically approved Teslascan, have made use of either a macrocycle or a highly anionic ligand to further ensure aqueous stability[6,7,9] and prevent manganism in biological subjects.[18]

The shortage of stable seven-coordinate transition metal complexes hinders attempts to understand their reactivity, make comparisons to related lower-coordinate species, and develop clinically useful Mn(II) compounds. One complication is the lack of ligands that can reliably coordinate metals to this extent. Heptacoordination around first-row transition metal ions often requires a constrained ligand, such as a pentadentate macrocycle.[1,2,6,19,20] In rarer cases, hexadentate ligands may allow an additional monodentate ligand to coordinate.[21-24]

Presented are a novel ligand, *N*,*N*'-bis(2-pyridylmethyl)-bis-(ethylacetate)-1,2-ethanediamine (debpn, Scheme 2.1), and its complexes with divalent first-row transition metal ions. The ligand binds to Mn(II), Fe(II), and Zn(II) in a hexadentate fashion, binding through the two pyridine rings, the two amine nitrogens, and the two carbonyl groups of the esters (Scheme 2.1). A water molecule completes the heptacoordination around Mn(II) and Fe(II); whereas, the Zn(II) is hexacoordinate. With smaller metal ions, such as Co(II) and Ni(II), debpn behaves as a pentadentate ligand, with one of the O-donors remaining unbound. The $[Mn(debpn)(H_2O)]^{2+}$ complex appears to be stable in water. The Mn(II) compound's ability to bind water molecules and remain intact in water over several hours, despite the absence of a macrocycle and anionic donor atoms within the ligand, led us to investigate its capacity to act as a MRI contrast agent.

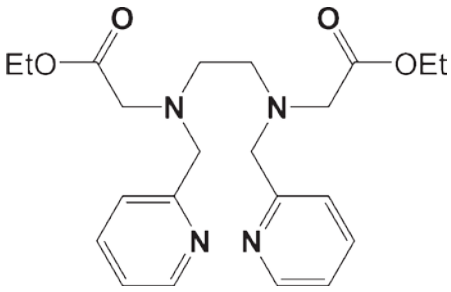

Scheme 2.1

2.2 Experimental Section

Materials

2-Pyridinecarboxaldehyde, ethyl bromoacetate, anhydrous acetonitrile (MeCN), manganese(II) perchlorate hydrate, iron(II) perchlorate hydrate, cobalt(II) perchlorate hydrate, nickel(II) perchlorate hydrate, copper(II) perchlorate hydrate, zinc(II) perchlorate hydrate, basic alumina (Brockmann I activity), silica (60 Å), potassiumcarbonate (K_2CO_3), sodiumborohydride (NaBH4), and 4-(2-hydroxyethyl)-1-piperazineethanesulfonic acid (HEPES) were purchased from Sigma-Aldrich and used as received, unless noted otherwise. Iron(II) triflate was prepared as previously described.[25] Diethyl ether (ether), ethyl acetate (EtOAc), methanol (MeOH), and potassium iodide (KI) were bought from Fisher. 1,2-Ethylenediamine, diethyl ether (ether), dichloromethane (CH_2Cl_2), and ethanol (EtOH) were purchased from Fluka, Mallinckrodt Baker, and Pharmco-AAPER, respectively. Chloroform-*d* ($CDCl_3$) and acetonitrile-*d3* (CD_3CN) were bought from Cambridge Isotopes and used as received. *N*,*N*'-bis(2-pyridylmethyl)-1,2-ethanediamine (bispicen) was prepared through a precedented procedure.[26]

CAUTION: Although no problems were encountered with the described chemistry, perchlorate salts of metal complexes are potentially explosive. The danger can be minimized by working with small quantities of these reagents and using appropriate safety measures, such as protective shields, for their preparation and handling.

Instrumentation

^{1}H and ^{13}C NMR spectra were recorded on a 250 or 400 MHz AV Bruker NMR spectrometer at 293 K unless stated otherwise and referenced to internal standards. Elemental analyses (C, H, N) were performed by Atlantic Microlabs (Norcross, GA). All samples subjected to elemental analysis were crystallized and dried under vacuum prior to their shipment. IR spectra

were collected by a Shimadzu IR Prestige-21 FT-IR spectrophotometer. Electron paramagnetic resonance (EPR) spectra were collected on a Bruker EMX-6/1 X-band EPR spectrometer operated in the perpendicular mode and analyzed with the program EasySpin. Each sample was run as a frozen solution in a quartz tube. A Johnson Matthey magnetic susceptibility balance (model MK I#7967) was used to measure the magnetic moments of solid samples. High resolution mass spectrometry (HR-MS) data were acquired at the Mass Spectrometer Center at Auburn University on a Bruker microflex LT MALDI-TOF mass spectrometer via direct probe analysis operated in the positive ion mode.

X-ray Crystallography

Crystals were mounted in paratone oil on glass fibers and aligned on a Bruker SMART APEX CCD X-ray diffractometer. Intensity measurements were performed using graphite monochromated Mo Kα radiation (λ = 0.71073 Å) from a sealed tube and monocapillary collimator. SMART (v 5.624) was used to determine the preliminary cell constants and regulate the data acquisition. The intensities of reflections of a sphere were collected through the compilation of three sets of exposures (frames). Each set had a different ϕ angle for the crystal, with each exposure spanning a range of 0.3° in ω. A total of 1800 frames were collected with exposure times of 40 s per frame. The data were corrected for Lorentz and polarization effects. Structures were solved using direct methods and expanded using Fourier techniques. All non-hydrogen atomswere refined anisotropically. Hydrogen atoms were included at idealized positions 0.95 Å from their parent atoms prior to the final refinement. Further details regarding the data acquisition and analysis are included in Table 2.1. Structural overlays were performed using the Mercury software (v. 2.4.5) available from the Cambridge Crystallographic Database Center.

Magnetic Resonance Imaging (MRI)

All MRI data were collected at the Auburn University MRI Research Center. All measurements were run on a Siemens Verio open-bore 3-T MRI clinical scanner using a 15-channel knee coil to simultaneously image 12 ~ 15 samples. An inversion recovery (IR) sequence was used that featured a nonselective adiabatic inversion pulse followed by a slice-selective gradient recalled echo (GRE) readout after a delay period corresponding to the inversion time (TI).[27, 28] The GRE was a saturation readout, such that only one line of k-space was acquired per repetition time (TR), in order to maximize both signal strength and the accuracy of the T1 estimates. The specific imaging parameters were as follows: TR was set to 4 s, TI was varied from 4.8 to 2500 ms over 37 steps, the echo time (TE) was set to 3.6 ms, the flip angle equaled 90°, averages = 1, slice thickness = 5 mm, field of view = 140 × 140 mm, matrix = 128 × 128, resulting in a pixel size of 1.1 × 1.1 × 5.0 mm. All samples were run in 50 mM solutions of HEPES in water that were buffered to pH 7.00 and kept at 22 °C. $[Mn(H_2O)_6](ClO_4)_2$, $Na_2[Mn(EDTA)(H_2O)]$, and $[Mn(debpn)(H_2O)](ClO_4)_2$ were investigated. The manganese content was systematically varied from 0.10 to 1.00 mM. The inverses of the T_1 values were plotted versus the concentration of Mn(II) to obtain r_1 values.

MRI Data Analysis

Image analysis was performed using custom Matlab programs (Mathworks, Natick, MA). The initial TI = 4.8 ms image was used as a baseline to determine circular region of interest (ROI) boundaries for each sample; from these, the mean pixel magnitudes for each ROI were calculated. For each of the 36 subsequent TI images, the same ROI boundaries were applied and the mean pixel magnitude calculations were repeated. This gave consistent ROI spatial definitions and a corresponding time course of magnitudes for each of the samples over all the TI time points. Each

sample's complex phase was used to correct the magnitude polarity to produce a complete exponential T_1 inversion recovery curve. The Nelder-Mead simplex algorithm[29] was applied to each sample's exponential curve to estimate its corresponding T_1 value.

Synthesis

***N,N'*-Bis(2-pyridylmethyl)-bis(ethylacetate)-1,2-ethanediamine (debpn).** Ethyl bromoacetate (3.34 g, 20.0 mmol), K_2CO_3 (2.76 g, 20.0 mmol), and KI (3.32 g, 20.0 mmol) were added to a solution of bispicen (2.42 g, 10.0 mmol) in 20 mL of anhydrous MeCN. The resultant mixture was stirred under N_2 for 48 h at room temperature. After this period, the solution was filtered to remove inorganic salts, and the filtrate was concentrated to a brown oil under reduced pressure. The product was purified through column chromatography. The crude material was run first on a basic alumina support, using CH_2Cl_2 as an elutant, then a silica support with a 10:1 EtOAc/EtOH solution as the elutant (R_f = 0.47). The product is isolated as a yellow oil (1.10 g, 31%). ^{1}H NMR (250 MHz, $CDCl_3$): δ 1.23 (t, 3H, OCH_2CH_3), 2.84 (s, 2H, NCH_2CH_2N), 3.42 (s, 2H, NCH_2-Py), 3.92 (s, 2H, NCH_2CO_2Et), 4.13 (q, 2H, OCH_2CH_3), 7.12 (t, 1H, 5-Py*H*), 7.46 (d, 1H, 3-Py*H*), 7.61 (t, 1H, 4-Py*H*), 8.51 (d, 1H, 6-Py*H*). ^{13}C NMR (62.5 MHz, $CDCl_3$): δ 14.1, 52.1, 54.5, 60.3, 60.5, 121.9, 123.0, 136.4, 149.0, 159.5, 171.4. IR (KBr, cm^{-1}): 3052 (w), 2982 (m), 2937 (m), 2908 (m), 2847 (m), 2374 (w), 2318 (w), 2276 (w), 1738 (s, C=O), 1729 (s, C=O), 1590 (s), 1570 (m), 1475 (s), 1434 (s), 1370 (s), 1299 (m), 1260 (s), 1191 (s), 1029 (s), 995 (m), 761 (s). MS (ESI): Calcd for MH^+, 415.2345; Found, 415.2343.

Aqua(*N,N'*-bis(2-pyridylmethyl)-bis(ethylacetate)-1,2-ethanediamine)manganese(II) Perchlorate ([Mn(debpn)(H_2O)](ClO_4)$_2$). An anaerobic solution of debpn (0.830 g, 2.00 mmol) in 5.0 mL of anhydrous MeCN was added to 0.506 g of $Mn(ClO_4)_2$ (1.86 mmol). The mixture stirred under N_2 for 60 min, yielding a yellow solution. At the end of the 60 min, 15 mL of ether

was added to precipitate the product as pale yellow crystals suitable for single crystal X-ray diffraction (0.69 g, 52%). Solid-state magnetic susceptibility (295 K): μ_{eff} = 6.1 μ_B. EPR (H_2O, 77 K, X-band): g_{eff} = 6.07, 3.28, 2.00. IR (KBr, cm^{-1}): 2953 (w), 2915 (w), 2903 (w), 2360 (w), 2344 (w), 1729 (w), 1678 (s, C=O), 1645 (w, C=O), 1605 (m, C=O), 1571 (w), 1434 (m), 1410 (m), 1387 (m), 1321 (m), 1302 (m), 1277 (w), 1239 (m), 1161 (m), 1115 (s), 1101 (s), 1059 (s), 1015 (m), 1000 (m), 990 (w), 947 (m), 932 (w), 867 (w), 834(m), 770 (m), 732 (m), 622 (s). Elemental Analysis: Calcd for $C_{22}H_{32}N_4O_{13}MnCl_2$: C, 38.50; H, 4.70; N, 8.16; Found: C, 38.46; H, 4.63; N, 7.67.

Aqua(*N,N'*-bis(2-pyridylmethyl)-bis(ethylacetate)-1,2-ethanediamine) iron(II) Perchlorate ([Fe(debpn)(H_2O)](ClO_4)$_2$). An anaerobic solution of debpn (0.830 g, 2.00 mmol) in 5.0 mL of anhydrous MeCN was added to 0.508 g iron(II) perchlorate hydrate (1.86 mmol). The mixture was stirred under an anaerobic atmosphere for 60 min. At the end of this time, 15 mL of ether was added to the brown solution to precipitate the product as a brownish yellow microcrystalline powder (1.13 g, 85%). Crystals suitable for single-crystal X-ray diffraction were grown from saturated solutions of the triflate analog in MeCN. The following measurements pertain to the perchlorate complex. Solid-state magnetic susceptibility (295 K): μ_{eff} = 4.7 μ_B. Optical spectroscopy (MeCN): 260 nm (8000 M^{-1} cm^{-1}), 343 nm (1000 M^{-1} cm^{-1}). IR (KBr, cm^{-1}): 2986 (w), 2958 (w), 2911 (w), 2873 (w), 2362 (w), 2331 (w), 1673 (s, C=O), 1644 (m, C=O), 1608 (m, C=O), 1572 (w), 1479 (w), 1443 (m), 1422 (m), 1488 (m), 1360 (w), 1322 (m), 1285 (s), 1249 (s), 1225 (s), 1171 (s), 1160 (s), 1138 (s), 1029 (s), 1004 (w), 990 (w), 948 (m), 871 (w), 840 (m), 772 (m), 758 (m), 729 (m), 640 (s). Elemental Analysis: Calcd for $C_{22}H_{32}N_4O_{13}FeCl_2$: C, 38.45; H, 4.69; N, 8.15; Found: C, 37.87; H, 4.53; N, 8.03.

Acetonitrilo(*N,N'*-bis(2-pyridylmethyl)-bis(ethylacetate)-1,2-ethanediamine) cobalt(II) Perchlorate ([Co(debpn)(MeCN)](ClO_4)$_2$). An anaerobic solution of debpn (0.414 g, 1.00 mmol) in 5.0 mL of anhydrous MeCN was added to 0.366 g of $Co(ClO_4)_2 \cdot 6H_2O$ (1.00 mmol). The mixture stirred under N_2 for 60 min, yielding a red solution. At the end of the 60 min, 15 mL of ether was added to precipitate the product as red crystals suitable for single crystal X-ray diffraction (0.300 g, 42%). Solid-state magnetic susceptibility (295 K): μ_{eff} = 4.0 μ_B. Optical spectroscopy (MeCN): 475 nm (45 $M^{-1}\,cm^{-1}$). IR (KBr, cm^{-1}): 2987 (w), 2959 (w), 2938 (w), 2359 (w), 2343 (w), 2331 (w), 2284 (w), 2016 (w), 1733 (s, C=O), 1666 (s, C=O), 1609 (m, C=O), 1414 (w), 1382 (w), 1355 (w), 1344 (w), 1306 (m), 1292 (m), 1262 (m), 1211 (s), 1162 (w), 1092 (s), 1019 (m), 996 (w), 953 (w), 878 (w), 843 (w), 822 (w), 797 (w), 768 (m), 734 (w), 718 (w), 648 (w), 623 (s). Elemental Analysis: Calcd for $C_{24}H_{33}N_5O_{12}CoCl_2$: C, 40.41; H, 4.66; N, 9.82; Found: C, 39.95; H, 4.58; N, 9.64.

Acetonitrilo(*N,N'*-bis(2-pyridylmethyl)-bis(ethylacetate)-1,2-ethanediamine) nickel(II) Perchlorate ([Ni(debpn)(MeCN)](ClO_4)$_2$). The ligand debpn (0.144 g, 0.348 mmol) was put under nitrogen and dissolved in 5.0 mL of anhydrous MeCN. This solution was added to 0.110 g of $Ni(ClO_4)_2 \cdot 6H_2O$ (0.300 mmol). The resultant purple solution stirred under N_2 for 60 min. The product crystallized as a purple solid (0.119 g, 56%) upon the addition of 15 mL of ether. These crystals were suitable for X-ray diffraction. Solid-state magnetic susceptibility (295 K): μ_{eff} = 2.8 μB. Optical spectroscopy (MeCN): 550 nm (16 $M^{-1}\,cm^{-1}$), 890 nm (17 $M^{-1}\,cm^{-1}$). IR (KBr, cm^{-1}): 2988 (w), 2964 (w), 2938 (w), 2314 (w), 2286 (w), 2016 (w), 1737 (s, C=O), 1668 (s, C=O), 1610 (m, C=O), 1429 (m), 1414 (w), 1381 (w), 1355 (w), 1343 (w), 1290 (w), 1262 (w), 1210 (m), 1093 (s), 1059 (m), 1022 (m), 998 (w), 939 (w), 881 (w), 840 (w), 824 (w), 799 (w), 776 (m), 767

(m), 734 (w), 718 (w), 666 (w), 623 (s). Elemental Analysis: Calcd for $C_{24}H_{33}N_5O_{12}NiCl_2$: C, 40.42; H, 4.66; N, 9.82; Found: C, 39.93; H, 4.64; N, 9.64.

(*N,N'*-bis(2-pyridylmethyl)-bis(ethylacetate)-1,2-ethanediamine) zinc(II) Perchlorate ([Zn(debpn)](ClO$_4$)$_2$). An anaerobic solution of debpn (0.124 g, 0.300 mmol) in 5.0 mL of anhydrous MeCN was added to 0.112 g of $Zn(ClO_4)_2 \cdot 6H_2O$ (0.300 mmol). The pale yellow mixture stirred under N_2 for 60 min. The product crystallized as pale yellow crystals (0.145 g, 69%) upon the addition of 15 mL of ether. These crystals were suitable for X-ray diffraction. IR (KBr, cm^{-1}): 2987 (w), 2979 (w), 2939 (w), 2876 (w), 2361 (w), 2340 (w), 2253 (w), 2021 (w), 1738 (w), 1733 (w), 1673 (s, C=O), 1613 (s, C=O), 1488 (m), 1464 (m), 1447 (s), 1435 (s), 1398 (m), 1374 (s), 1347 (m), 1310 (m), 1284 (m), 1264 (s), 1162 (m), 1093 (s), 1028 (s), 1012 (s), 995 (s), 970 (m), 953 (m), 936 (m), 898 (w), 871 (m), 841 (m), 830 (w), 817 (m), 764 (s), 745 (w), 730 (w), 668 (w), 651 (m), 601 (s). Elemental Analysis: Calcd for $C_{22}H_{30}N_4O_{12}ZnCl_2 \cdot H_2O$: C, 37.92; H, 4.63; N, 8.04; Found: C, 37.45; H, 4.54; N, 8.10.

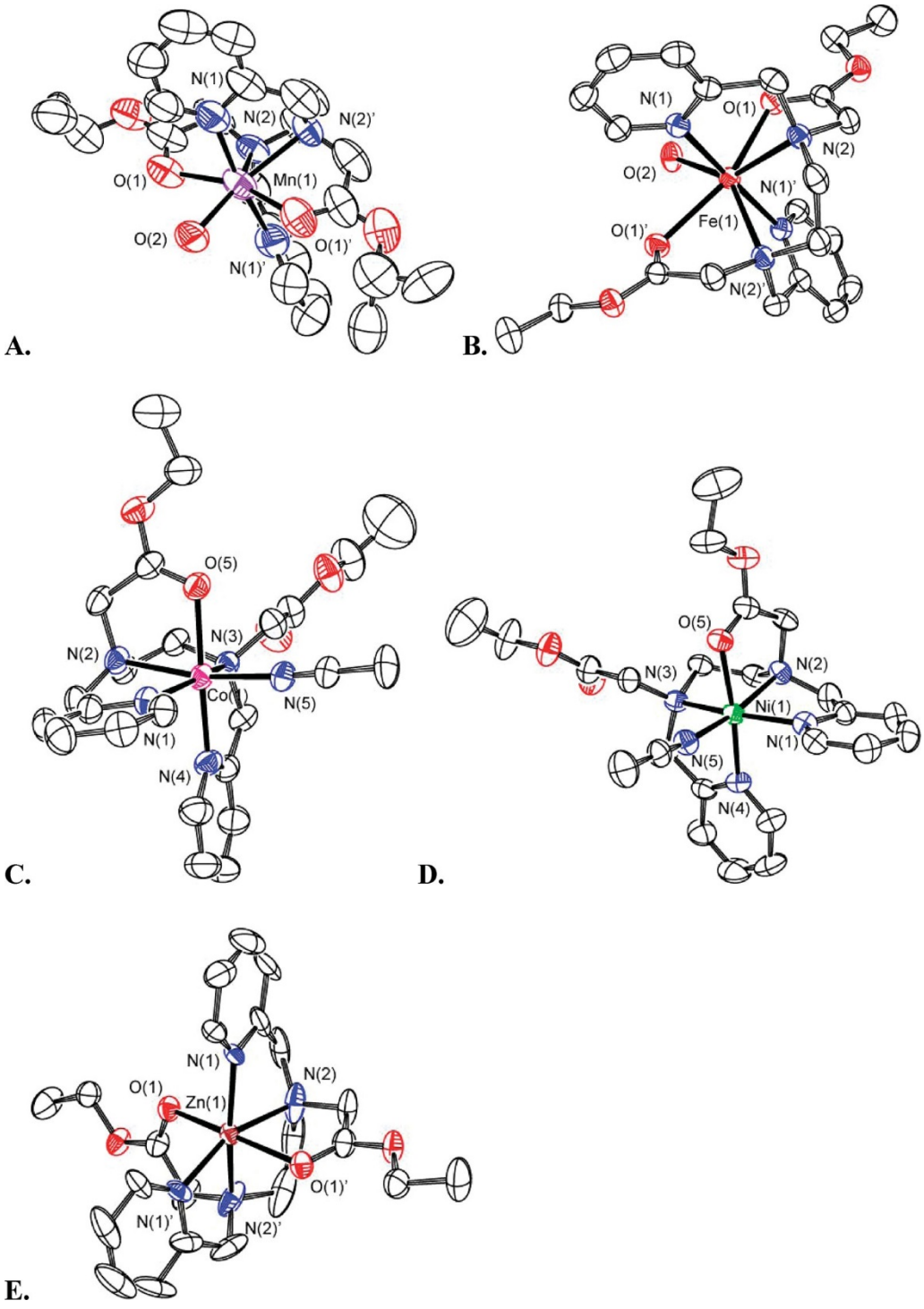

Figure 2.1. ORTEP representations of the dications (A) $[Mn(debpn)(H_2O)]^{2+}$ (Cambridge Crystallographic Database Center (CCDC) No. 838911), (B) $[Fe(debpn)(H_2O)]^{2+}$ (CCDC No. 838912), (C) $[Co(debpn)(MeCN)]^{2+}$ (CCDC No. 838913), (D) $[Ni(debpn)(MeCN)]^{2+}$ (CCDC No. 838914), and (E) $[Zn(debpn)]^{2+}$ (CCDC No. 838915). All hydrogen atoms, counterions, and noncoordinated solvent molecules have been removed for clarity. All thermal ellipsoids are drawn at 50% probability.

Table 2.1. Selected Crystallographic Data for Coordination Complexes

parameter	[Mn(debpn)(H_2O)] (ClO_4)$_2$	[Fe(debpn)(H_2O)] (CF_3SO_3)$_2$
formula	$C_{22}H_{32}Cl_2MnN_4O_{13}$	$C_{24}H_{32}F_6FeN_4O_6S_6$
MW	686.36	754.45
cryst. syst.	monoclinic	orthorhombic
space group	*C2/c* (#15)	*Fdd2* (#43)
a (Å)	13.5732(10)	13.983(2)
b (Å)	9.5786(10)	47.723(8)
c (Å)	22.716(2)	9.4858(15)
α (deg)	90	90
β (deg)	99.247(3)	90
γ (deg)	90	90
V (Å^3)	2915.0(5)	6330.1(18)
Z	4	8
crystal color	colorless	yellow
T (K)	193(2)	198(2)
reflns collected	11666	15823
unique reflns	3597	3390
*R*1 (F, I > 2σ(I))[a]	0.0518	0.0409
w*R*2 (F^2, all data)[a]	0.1589	0.0998

[a] $R1 = \Sigma||F_o| - |F_c||/\Sigma|F_o|$; $wR2 = [\Sigma w(F_o^2 - F_c^2)^2/\Sigma w(F_o^2)^2]^{1/2}$.

Table 2.1. (Cont'd) Selected Crystallographic Data for Coordination Complexes

parameter	[Co(debpn)(MeCN)] $(ClO_4)_2$	[Ni(debpn)(MeCN)] $(ClO_4)_2$	[Zn(debpn)] $(ClO_4)_2$
formula	$C_{24}H_{33}Cl_2CoN_5O_{12}$	$C_{24}H_{33}Cl_2N_5NiO_{12}$	$C_{22}H_{30}Cl_2N_4O_{12}Zn$
MW	713.38	713.16	678.77
cryst. syst.	triclinic	triclinic	monoclinic
space group	$P\bar{1}$ (#2)	$P\bar{1}$ (#2)	*C2/c* (#15)
a (Å)	10.2626(6)	10.3714(7)	15.7195(14)
b (Å)	12.7750(8)	12.6946(9)	13.5426(12)
c (Å)	13.5173(8)	13.5156(10)	13.0717(12)
α (deg)	72.270(1)	71.807(2)	90
β (deg)	70.608(1)	70.823(2)	100.910(2)
γ (deg)	73.394(1)	73.280(2)	90
V ($Å^3$)	1558.25(16)	1562.35(19)	2732.4(4)
Z	2	2	4
crystal color	orange	purple	white
T (K)	193(2)	193(2)	198(2)
reflns collected	15863	16017	13634
unique reflns	7617	4364	2336
*R*1 (F, I > 2σ(I))[a]	0.0577	0.0705	0.080
wR2 (F^2, all data)[a]	0.1847	0.1976	0.1901

[a] $R1 = \Sigma||F_o| - |F_c||/\Sigma|F_o|$; $wR2 = [\Sigma w(F_o^2 - F_c^2)^2/\Sigma w(F_o^2)^2]^{1/2}$.

2.3 Results

Synthesis

The ligand is prepared in moderate yield in two steps from commercially available reagents. The preparation of the metal complexes is straightforward, with yields ranging from 52% to 85%. Attempts to prepare a Cu(II) complex yielded a blue crystalline material which did not diffract X-ray radiation.

The elemental analysis of the copper compound was not consistent with $[Cu(debpn)(X)](ClO_4)_2$ with X = MeCN, H_2O, or null. Due to the ambiguity of its composition, the copper compound will not be discussed further in this work.

Structural Characterization

The M(II) complexes with debpn crystallize from saturated MeCN solutions upon cooling or the addition of ether. In each case, the cations contain mononuclear metal centers with a 1:1 ratio of ligand to metal. The w*R*2 values (Table 2.1) are relatively high due to disorder in both the ester groups of the debpn ligand and the perchlorate anions.

The Mn(II) and Fe(II) compounds contain heptacoordinate metal ions (Figure 2.1, A and B). The debpn ligand coordinates through six atoms: the four nitrogen atoms from the pyridine rings and the tertiary amines and the two carbonyl oxygen atoms from the pendant esters. Although the crystals are grown in MeCN, a molecule of H_2O completes the coordination around each of these two metal ions. The source of the water is likely the perchlorate salt. The coordination around each is best described as a distorted pentagonal bipyramid, as assessed by the L-M-L bond angles, with the pyridine rings occupying the axial positions (Table 2.2). On the basis of a least-squares analysis of the L-M-L bond angles, the Fe(II) complex appears to have the less distorted geometry. The N-donors coordinate the metal ions in a distorted *cis*-α conformation, with the amine nitrogens

closer together than in their hexacoordinate analogs.[30] As anticipated, the M-L bond distances are shorter for the Fe(II) complex.[31]

In the structures of the Co(II) and Ni(II) compounds (Figure 2.1, C and D), the metal ions are hexacoordinate, with the debpn ligand providing five donor atoms and an MeCN molecule completing the octahedral geometry. On the basis of the L-M-L bonds, the Ni(II) complex more closely approximates an ideal octahedron. The debpn ligates the metals through the four N-donors and one of the ester's carbonyl oxygen atoms. The pyridine rings are *cis* to each other (Table 2.3), and the coordination of the N-donors resembles the *cis*-β conformation occasionally found for tetradentate ligands with reduced imine linkages.[32,33] As anticipated, the M-L bond distances are shorter for the Ni(II) complex.[31] These average 2.09 Å, whereas, those for the Co(II) complex average 2.13 Å.

In the structure of the Zn(II) complex (Figure 2.1, E), the metal ion is hexacoordinate, with the debpn ligand providing all six donor atoms. The esters of the ligand coordinate *trans* to each other; the four N-donors are roughly coplanar. Of the three hexacoordinate metal centers, the Zn(II) complex displays the greatest distortions from an ideal octahedral geometry, as assessed by a least-squares analysis of the L-M-L bond angles (Tables 2.3 and 2.4). The average of the M-L bond distances, 2.15 Å, is greater than those measured for the Co(II) and Ni(II) complexes.

Table 2.2. Comparison of the Bond Lengths (Å) and Bond Angles (deg) for the Heptacoordinate Complexes $[Mn(debpn)(H_2O)]^{2+}$ and $[Fe(debpn)(H_2O)]^{2+}$ [a]

bond length	Mn	Fe
M-O(1)	2.374(3)	2.2946(19)
M-O(2)	2.159(3)	2.184(3)
M-N(1)	2.260(3)	2.204(2)
M-N(2)	2.371(3)	2.322(2)
bond angle	**Mn**	**Fe**
O(1)-M-O(1)'	159.23(13)	154.27(11)
O(1)-M-O(2)	79.61(6)	77.14(5)
O(1)-M-N(1)	82.67(11)	85.05(7)
N(1)-M-N(1)'	172.33(15)	176.68(13)
O(1)-M-N(1)'	98.73(10)	95.70(7)
O(1)-M-N(2)	68.58(10)	69.70(8)
O(1)-M-N(2)'	130.57(11)	134.27(8)
O(2)-M-N(1)	93.84(7)	91.66(7)
O(2)-M-N(2)	142.28(8)	142.05(6)
N(1)-M-N(2)	101.42(11)	103.07(8)
N(1)-M-N(2)'	72.31(12)	74.22(8)
N(2)-M-N(2)'	75.43(15)	75.91(11)

[a] Note that the ligands' donor atoms have been relabeled in accordance with Figure 2.1 in order to facilitate comparison of the structures.

Table 2.3. Comparison of the Bond Lengths (Å) and Bond Angles (deg) for the Heptacoordinate Complexes $[Co(debpn)(MeCN)]^{2+}$ and $[Ni(debpn)(MeCN)]^{2+}$ [a]

bond length	Co	Ni
M-N(1)	2.208(2)	2.088(4)
M-N(2)	2.161(2)	2.097(4)
M-N(3)	2.112(2)	2.169(4)
M-N(4)	2.116(2)	2.062(4)
M-N(5)	2.073(2)	2.044(4)
M-O(5)	2.098(2)	2.086(4)
bond angle	**Co**	**Ni**
N(1)-M-N(2)	83.40(9)	80.07(15)
N(1)-M-N(3)	158.73(9)	162.80(14)
N(1)-M-N(4)	79.18(10)	93.12(15)
N(1)-M-N(5)	100.29(9)	98.51(15)
N(1)-M-O(5)	90.41(9)	94.70(14)
N(2)-M-N(3)	78.58(10)	84.53(14)
N(2)-M-N(4)	97.38(10)	97.26(15)
N(2)-M-N(5)	168.29(10)	168.64(15)
N(2)-M-O(5)	80.00(9)	81.64(14)
N(3)-M-N(4)	91.96(10)	81.22(15)
N(3)-M-N(5)	99.61(10)	98.08(14)
N(3)-M-O(5)	97.42(9)	90.56(13)
N(4)-M-N(5)	94.23(10)	94.07(16)
N(4)-M-O(5)	83.40(9)	80.07(15)
N(5)-M-O(5)	158.73(9)	162.80(14)

[a] Note that the ligands' donor atoms from the have been relabeled in accordance with Figure 2.1 in order to facilitate comparison of the structures.

Table 2.4. Bond Lengths (Å) and Bond Angles (deg) for the Heptacoordinate Complex $[Zn(debpn)]^{2+}$

	bond length
Zn-N(1)	2.063(4)
Zn-N(2)	2.173(5)
Zn-O(1)	2.201
	bond angle
N(1)-Zn-N(2)	79.2(2)
N(1)-Zn-O(1)	95.13(14)
N(1)-Zn-N(1)'	119.8(2)
N(1)-Zn-N(2)'	159.0(2)
N(1)-Zn-O(1)'	90.12(14)
N(2)-Zn-O(1)	78.63(15)
N(2)-Zn-N(2)'	83.8(3)
N(2)-Zn-O(1)'	93.52(15)
O(1)-Zn-O(1)	169.54(17)

Solution Characterization

The metal complexes with debpn were analyzed by EPR, NMR, and optical spectroscopy. The EPR spectrum of the Mn(II) complex in water (Figure 2.2) resembles those of other Mn(II) complexes with N-donor ligands.[32,34-36] Zero-field splitting gives rise to three features with g_{eff} = 6.07, 3.28, and 2.00. Under the conditions used to acquire the spectrum, we cannot resolve the hyperfine interactions anticipated for a nucleus with I = 5/2. The UV/vis spectrum of the Fe(II) compound resembles other heptacoordinate Fe(II) species, with a relatively low intensity LMCT band in the 300 ~ 400 nm region.[37] The spectrophotometric features of both the Co(II) and Ni(II) complexes are consistent with octahedrally coordinated metal ions,[38,39] suggesting that the hexacoordination observed in the solid-state is largely preserved in solution. The ^{1}H NMR

spectrum of the Zn(II) crystals in CD_3CN defies simple explanation and appears to contain at least four diamagnetic species at room temperature, as assessed by the number of ester CH_3 peaks. Upon warming the sample from 25 to 65 °C (Figure 2.A1), the peaks broaden and begin to coalesce. The ^1H NMR spectrum of the Ni(II) undergoes similar changes over this range in temperature, albeit with fewer visible resonances due to the paramagnetism of the sample (Figure 2.A2). The only conclusions that we can definitively draw from these data are that the solid-state structures are not exclusively maintained in solution and that the coordination of the debpn ligand to the metal ions is not static.

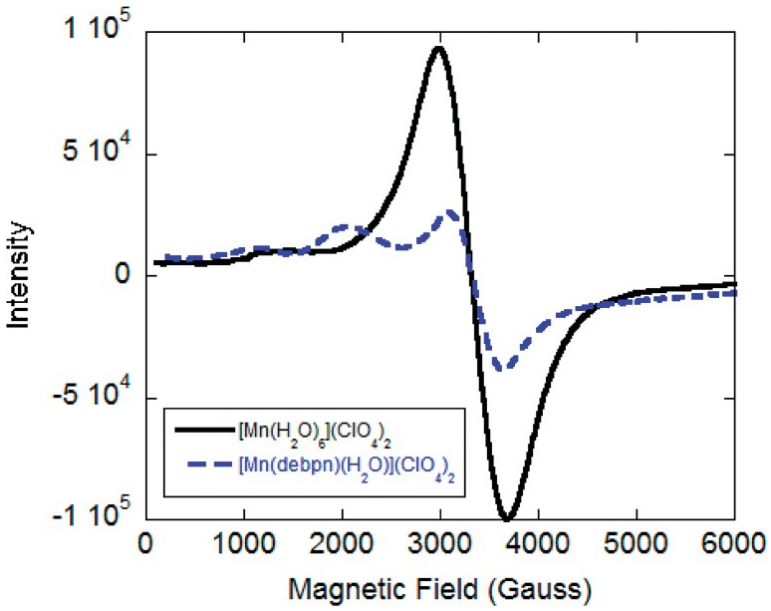

Figure 2.2. X-Band electron paramagnetic resonance spectra of $[Mn(H_2O)_6](ClO_4)_2$ (black) and $[Mn(debpn)(H_2O)](ClO_4)_2$ (blue) in H_2O at 77 K. The concentration of each sample is 1.0 mM. For the debpn complex, g_{eff} = 6.07, 3.28, and 2.00. For $[Mn(H_2O)_6]^{2+}$, g = 2.03.

Solid-State Characterization

The magnetic susceptibility of each debpn complex was measured in the solid state at 295 K. The Mn(II), Fe(II), and Co(II) have μ_{eff} values consistent with high-spin d^5, d^6, and d^7 metal

ions, respectively. These assignments are consistent with the aforementioned structural and spectroscopic data. The 2.8 μB value for $[Ni(debpn)(MeCN)]^{2+}$ is consistent with an octahedrally coordinated d^8 metal ion. The $[Zn(debpn)]^{2+}$ complex is diamagnetic, as anticipated.

The debpn ligand and its five metal complexes were also analyzed by infrared spectroscopy (IR), with a focus on the carbonyl stretching frequencies. The assigned ester C=O stretches are listed in Table 2.5. The frequencies of the C=O stretches for the debpn ligand (1738 cm^{-1}, 1729 cm^{-1}) are typical for organic esters. When the esters bind to the metal ion, their stretching frequencies decrease to values ranging from 1600 to 1675 cm^{-1}. The two complexes which contain nonbound esters, $[Co(debpn)(MeCN)]^{2+}$ and $[Ni(debpn)(MeCN)]^{2+}$, retain IR stretches in the 1725 ~ 1740 cm^{-1} region. The Mn(II) and the Zn(II) complexes also have weak bands in this region, which may indicate partial dissociation of the esters within the KBr pellets.

Table 2.5. Carbonyl Stretching Frequencies for Debpn Species[a]

species	carbonyl stretches (cm^{-1})
debpn	1738, 1729
$[Mn(debpn)(H_2O)]^{2+}$	1678, 1645, 1605[b]
$[Fe(debpn)(H_2O)]^{2+}$	1673, 1644, 1608
$[Co(debpn)(MeCN)]^{2+}$	1733, 1666, 1609
$[Ni(debpn)(MeCN)]^{2+}$	1737, 1668, 1610
$[Zn(debpn)]^{2+}$	1673, 1613[c]

[a] All samples were prepared as KBr pellets. [b] Additional weak band at 1729 cm^{-1}. [c] Additional weak bands at 1738 and 1733 cm^{-1}.

MRI Measurements

The magnetic properties of the $[Mn(debpn)(H_2O)]^{2+}$ complex were further analyzed, with a particular focus on the relaxation time of the ^1H nuclei of the bulk water molecules. T_1 values for

different concentrations of the Mn(II) species in a 50 mM solution of HEPES buffered to pH 7.0 were obtained with the aid of a 3 T MRI instrument (Figure 2.3) at 22 °C. The inverses of these T_1 values were plotted as a function of $[Mn(debpn)(H_2O)]^{2+}$ concentration to obtain an r_1 value, which was subsequently compared to those measured for $[Mn(H_2O)_6](ClO_4)_2$ and $Na_2[Mn(EDTA)(H_2O)]$ (Figure 2.4) under the same conditions. The numbers of water molecules in the coordination spheres of these latter two manganous species are well established as q = 6 and q = 1, respectively.[6,8,10] Comparison of the r_1 values of the three Mn(II) compounds serves two goals. First, it can confirm that the debpn ligand remains bound to the metal in aqueous solution. Second, it can potentially assess whether additional equivalents of water are displacing portions of the debpn ligand, which is more weakly bound to the metal ion than the EDTA ligand on account of its charge neutrality.

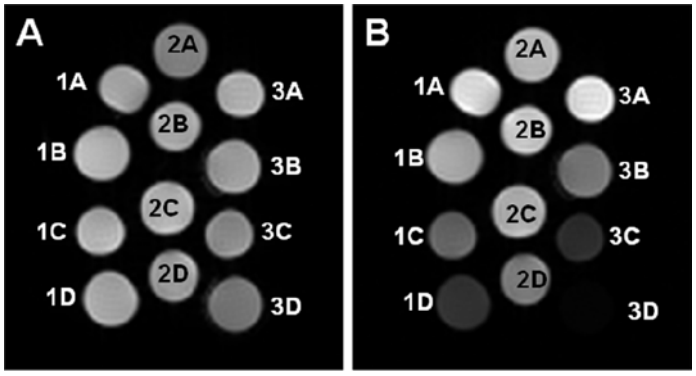

Figure 2.3. Inversion recovery magnetic resonance images of samples at initial time of inversion (TI) = 4.8 ms (Panel A) and TI = 160 ms (Panel B), exemplifying the different T_1 relaxation rates by the contrast change. The images with TI = 4.8 ms occur almost immediately after inversion. In the TI = 160 ms images, the more quickly relaxing samples are approaching their T_1 minima and appear darker as a consequence. Samples contained Mn(II) complexes in 50 mM HEPES solutions buffered to pH 7.00. Samples 1A-D contained $[Mn(debpn)(H_2O)](ClO_4)_2$, samples 2A-D contained $Na_2[Mn(EDTA)(H_2O)]$, and samples 3A-D contained $[Mn(H_2O)_6](ClO_4)_2$. The concentrations of the Mn(II) in the samples included: 0.10 mM (A), 0.40 mM (B), 0.70 mM (C), and 1.00 mM (D).

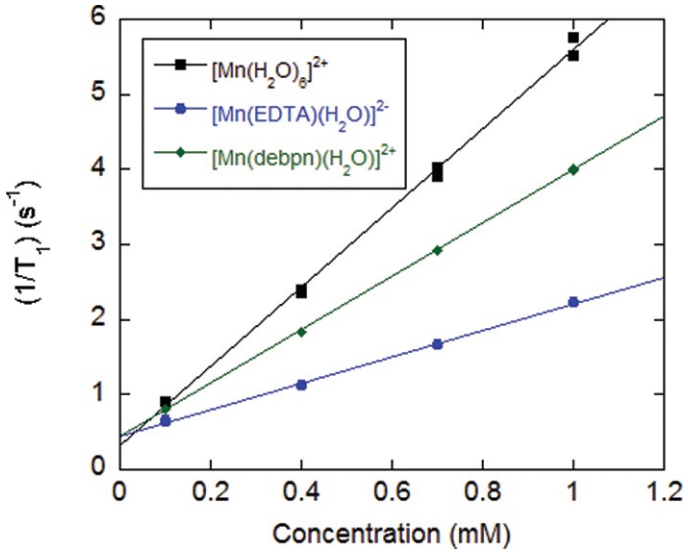

Figure 2.4. Plots of $(1/T_1)$ as functions of Mn(II) concentration for $[Mn(H_2O)_6](ClO_4)_2$, $Na_2[Mn(EDTA)(H_2O)]$, and $[Mn(debpn)(H_2O)](ClO_4)_2$. The shown data were collected from two sets of independently prepared samples and fit to the following equations: $[Mn(H_2O)_6]^{2+}$, $y = 0.32834 + 5.258x$ ($R = 0.99893$); $[Mn(EDTA)(H_2O)]^{2-}$, $y = 0.45333 + 1.7607x$ ($R = 0.99914$); $[Mn(debpn)(H_2O)]^{2+}$, $y = 0.43613 + 3.5573x$ ($R = 0.9999$).

The r_1 value for the $[Mn(debpn)(H_2O)]^{2+}$ complex was found to be 3.56 (± 0.14) $mM^{-1}\,s^{-1}$. As anticipated, this is less than the 5.26 (± 0.21) $mM^{-1}\,s^{-1}$ value for $[Mn(H_2O)_6]^{2+}$. This r_1 value, however, is greater than the 1.76 (± 0.07) $mM^{-1}\,s^{-1}$ value we measured for the other monoaqua species, $[Mn(EDTA)(H_2O)]^{2-}$. The measured r_1 values for $[Mn(H_2O)_6]^{2+}$ and $[Mn(EDTA)(H_2O)]^{2-}$ are similar but not identical to those that had been previously measured at 90 MHz and 37 °C.[8,40] Discrepancies between our values and the previously reported ones are anticipated, given the different solution media, temperature, and magnetic field strength used in the prior work.[8] The linearity of the $1/T_1$ plot over concentrations ranging from 0.1 to 1.0 mM suggests that the debpn ligand remains associated with the Mn(II) ion over these concentrations. If a significant percentage of the complexes were to fully dissociate in solution, then the r_1 value should more closely approximate that of the $[Mn(H_2O)_6]^{2+}$ species at lower concentrations, resulting in a curved plot. The T_1 values associated with each concentration of $[Mn(debpn)(H_2O)]^{2+}$ remained constant over

a 15 h period, providing a lower limit of the complex's stability. Mass spectrometry of the debpn ligand after this 15 h period confirmed that the ligand remained intact, with no hydrolysis of its ester groups.

2.4 Discussion

Structural analyses of ligands that encourage heptacoordination are rare; in most instances, only certain complexes within a series are structurally characterized, which limits systematic analysis of the ligand's binding tendencies.[2,21]

The ligand *N*,*N*'-bis(2-pyridylmethyl)-bis(ethylacetate)-1,2-ethanediamine (debpn) can be made in two steps from commercially available chemicals. The only complication is that two sequential chromatography columns are needed to purify the product at the end of the second step. Although the yield is modest (30%), multigram quantities of debpn can be made relatively quickly. One attractive feature of the synthesis is that it should be readily modifiable. A wide array of diamine backbones and esters could be substituted without necessitating drastic changes in the general procedure. The debpn ligand readily forms complexes with divalent first-row transition metal ions, with yields of crystalline material ranging from moderate (42%, cobalt) to excellent (85%, iron). In each case, the isolated product is a mononuclear species with a 1:1 ligand/metal ratio. The composition and structure of an isolated Cu(II) complex with debpn were never assigned with certainty.

The largest metal ions, Mn(II) and Fe(II), are heptacoordinate when bound to debpn; whereas, the others are hexacoordinate. The donor atoms in the heptacoordinate complexes are arrayed in distorted pentagonal bipyramidal geometries that are nearly isostructural. A structural overlay of the seven donor atoms and the metal center from the two complexes yields a rms value of 0.0775 $Å^{-1}$. According to a least-squares analysis of the L-M-L bond angles, the Fe(II) complex

is slightly less distorted from the ideal pentagonal bipyramid. The analysis suggests that the distortions arise largely from the positions of the ester oxygen atoms and the amine nitrogen atoms. The N(1)-M-N(2)', O(1)-M-N(2)', and O(1)-M-O(1)' bond angles are farthest from their idealized values (90°, 144°, and 144°), with greater digressions observed for $[Mn(debpn)(H_2O)]^{2+}$ (Table 2.2).

Among the hexacoordinate complexes, $[Ni(debpn)(MeCN)]^{2+}$ has its donor atoms arrayed in the closest approximation of an ideal octahedral geometry, as assessed by a least-squares analysis of the L-M-L bond angles. Under the same criteria, the Zn(II) complex is the most distorted, in large part due to the 119.8° N(1)-Zn-N(1)' bond angles. Given that Zn(II), as a d^{10} metal ion, has no strong electronic structural preferences, it may be anticipated to better tolerate deviations from octahedral coordination. The Co(II) complex more closely resembles the Ni(II) than the Zn(II) with respect to the composition of its coordination sphere, the relative orientation of the ligand's donor atoms, and its approximation of an ideal octahedral geometry. The M-N bonds for these three compounds have lengths similar to those found in other M(II) complexes with sterically encumbered bispicen ligands.[41,42]

The mode of debpn coordination is strongly linked to the size of the metal ion, with a predisposition to bind smaller metal ions in an octahedral fashion. When the metal ion is too large, overall pentagonal bipyramidal geometries ensue. Although Co(II) is electronically compatible with heptacoordination, unlike Ni(II),[2] its ionic radius appears to be too small to accommodate all seven of the donor atoms from this particular ligand. The structures of the debpn complexes are reminiscent of the coordinative behavior of ethylenediaminetetraacetate (EDTA), which forms heptacoordinate complexes with Fe(II) and Mn(II) but hexacoordinate complexes with Ni(II) and Co(II).[4,23,43]

The coordination of ester carbonyl groups to metal ions is unusual, but precedented, in nonorganometallic coordination chemistry. The M-O_{ester} bond distances in the debpn complexes are similar to those previously reported for metal-ester complexes with comparable coordination numbers, oxidation numbers, and spin-states.[37,44-49] The M-O bond distances for $[Co(debpn)(MeCN)]^{2+}$ and $[Ni(debpn)(MeCN)]^{2+}$ are among the shortest measured for nonorganometallic Co(II) and Ni(II) complexes with ester O-donors.[46-49] Upon coordination of the ester to the metal ion, the C=O stretches decrease (Table 2.5), analogous to what has been observed for CO chemistry.[50] The seven-coordinate complexes each contain an additional C=O band around 1645 cm^{-1}, but otherwise, the frequencies of the metal-bound ester C=O stretches remain relatively constant throughout the series.

The ^1H NMR spectrum of the Zn(II) complex is inconsistent with the solid-state structure, since it displays many more resonance peaks than anticipated from the complex's C_2 symmetry (Figure 2.A1). Upon heating the solution sample, these resonances broaden and begin to coalesce. The variable temperature data suggest that the coordination of the debpn ligand is both flexible and dynamic, with the flexibility being anticipated from the structural data. The exact Zn(II) species in solution cannot be assigned with certainty. These may include stereoisomers of the solid-state structure with the N-donors of the debpn ligand in a *cis*-α or *cis*-β conformation around the Zn(II) center. These conformers may exchange with each other through either partial, temporary ligand dissociation or Bailar or Ray-Dutt twists. Other reasonable possibilities for the additional species in solution include higher-coordinate complexes such as $[Zn(\kappa\text{-6-debpn})(MeCN)]^{2+}$, which would be analogous to the Fe(II) and Mn(II) complexes. Alternatively, the esters could be displaced by solvent molecules to yield species such as $[Zn(\kappa\text{-5- debpn})(MeCN)]^{2+}$, analogous to the Co(II) and Ni(II) complexes. The ^1H NMR spectrum of the Ni(II) complex undergoes similar

changes upon heating (Figure 2.A2), and we speculate that similar speciation likely occurs for the other metal complexes.

The EPR spectrum of the Mn(II) complex in H_2O is distinct than that for $[Mn(H_2O)_6]^{2+}$ (Figure 2.2). This suggests that the debpn ligand remains at least mostly coordinated to the metal ion in aqueous solution. On the basis of the NMR data for the other metal complexes, we believe that it is unlikely that the solid-state structure is exclusively maintained in water. Spectroscopic analysis found no signs of metal dissociation or ligand decomposition over 15 h. The aqueous stability and the presence of the bound water molecule in the crystal structure prompted us to investigate $[Mn(debpn)(H_2O)]^{2+}$ as a potential contrast agent for magnetic resonance imaging. The measurements were performed on aqueous solutions of the Mn(II) compounds buffered to pH 7.00 and used a 3 T MRI scanner that is also used for clinical purposes. Comparison of the r_1 value to that of $[Mn(H_2O)_6](ClO_4)_2$ corroborates the aqueous stability of the Mn-debpn adduct, which should and does have a lower r_1 on the basis of its fewer coordinated molecules of water (q). The r_1 value is greater than our measured value for $[Mn(EDTA)(H_2O)]^{2-}$, despite the ostensibly equal q values.

Three explanations may rationalize this difference. First, additional water molecules may be coordinating to the Mn(II) in $[Mn(debpn)(H_2O)]^{2+}$. The ester groups, as seen in the crystal structures of the Co(II) and Ni(II) complexes with debpn, are relatively easy to detach from the divalent metal ions. The anionic carboxylate groups of the EDTA ligand are more difficult to displace, and the deprotonated EDTA ligand binds much more strongly to Mn(II) than debpn as assessed by ^1H NMR analysis of the titration of $[Mn(debpn)(H_2O)]^{2+}$ by EDTA. In this titration, 1 equiv. of EDTA quantitatively displaces the debpn ligand from the metal. In aqueous solution, water molecules may displace one or both of the debpn esters bound to the Mn(II), resulting in a

mixture of species with $q = 1$, $q = 2$, or possibly even $q = 3$. Alternatively, transiently stable higher-coordinate species with $q = 2$ may form.[6] The solution data for the other metal complexes suggest that the debpn coordination is flexible enough to allow either of these mechanisms. Second, the rate of water exchange may be significantly different for $[Mn(debpn)(H_2O)]^{2+}$ and $[Mn(EDTA)(H_2O)]^{2-}$, which should result in different r_1 values for compounds with equal q values.[8] Third, the complexes may have substantially different interactions with outer-sphere water molecules. Given that EDTA should be able to more effectively hydrogen bond with water molecules than debpn, on the basis of its greater number of uncoordinated carbonyl groups, we find this third explanation unlikely.

The r_1 of 3.56 (± 0.14) $mM^{-1}\ s^{-1}$ for $[Mn(debpn)(H_2O)]^{2+}$ compares favorably with values measured for Teslascan® (2.8 $mM^{-1}\ s^{-1}$) and other mononuclear Mn(II)-containing contrast agents.[6,9,18,51] Direct comparisons are difficult, given the different conditions under which these complexes were analyzed and the paucity of theoretical work correlating the relaxitivities of manganese compounds with to such parameters. Five complexes recently reported by Wang and Westmoreland, for instances, were studied in water at 20 MHz.[6] The relaxitivity of the debpn complex also compares well to those of clinically relevant, mononuclear, Gd(III)-containing contrast agents, which generally have r_1 values of about 4 $mM^{-1}\ s^{-1}$.[11] The ability of $[Mn(debpn)(H_2O)]^{2+}$ to serve as a contrast agent is notable since the debpn ligand lacks both a macrocycle and an anionic charge, two features thought to be key to the stabilization of the aforementioned Mn(II) complexes in water.[7,8] The results may suggest that the design limitations for Mn(II) contrast agents may be more relaxed than previously thought and that other Mn(II) complexes with neutral, nonmacrocyclic ligands may also facilitate biological imaging.

The Mn(II) complex seems relatively robust. No hydrolysis of the ligand's ester groups is observed over 15 h in the HEPES buffer, as assessed by mass spectrometry. However, if the complex were to enter cells, esterases could potentially degrade the ligand. Other metal ions are capable of exchanging for the Mn(II) ion, but this exchange occurs slowly (Figure 2.A6). When 1.0 mM $Fe(ClO_4)_2$ and 1.0 mM $[Mn(debpn)(H_2O)]^{2+}$ are allowed to react in MeCN, only 30% of the Mn(II) is displaced by the Fe(II) after 3 h. It should also be noted that physiological concentrations of chelatable metal ions are much lower than the 1.0 mM concentration of free iron used to achieve this modest rate of substitution.[52-55] Metal scavenging proteins and biomolecules may pose a more significant problem. EDTA, which may be thought of as a mimic of such species, quantitatively removes Mn(II) from the debpn complex.

The ability to use different sorts of Mn(II) complexes as imaging agents has potential clinical benefits. The positive charge of the $[Mn(debpn)(H_2O)]^{2+}$ complex may significantly alter its pharmacological properties relative to Teslascan, which is anionic. These properties include the sensor's abilities to permeate biological membranes and associate with particular tissues or cell types. Studies of the biological behavior of $[Mn(debpn)(H_2O)]^{2+}$ will explore these issues.

2.5 Conclusions

The novel ligand *N*,*N*'-bis(2-pyridylmethyl)-bis(ethylacetate)-1,2-ethanediamine (debpn) was found to chelate divalent first-row transition metal ions in both penta- and hexadentate fashions. With larger first-row transition metal ions, the ligand is hexadentate, with an exogenous water molecule completing an overall pentagonal bipyramidal geometry. Despite the lack of a negative charge or a macrocycle within the debpn ligand's framework, the heptacoordinate Mn(II)

complex with debpn can serve as a stable and effective MRI contrast agent under physiologically and clinically relevant conditions.

Appendix

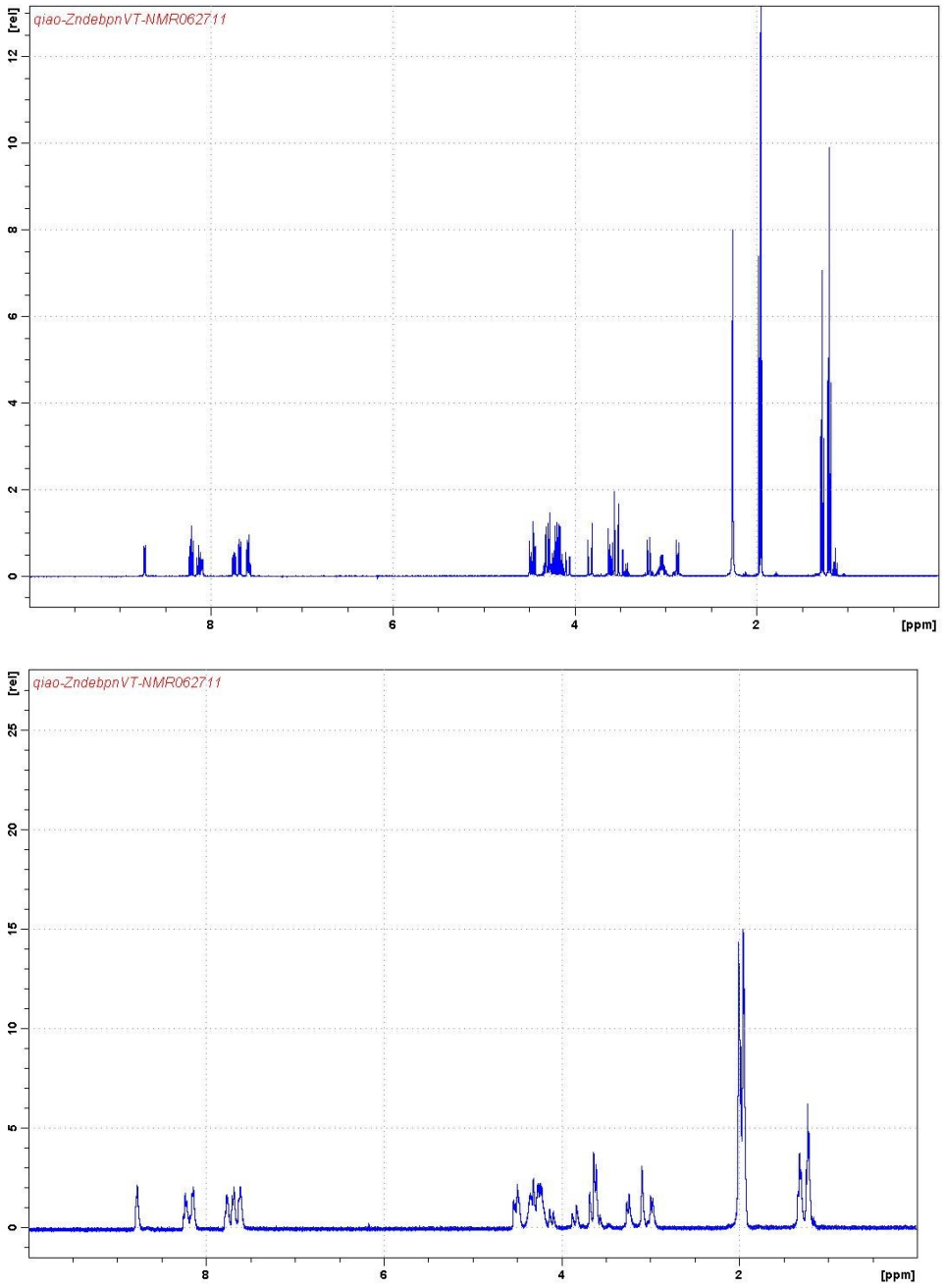

Figure 2.A1. ^{1}H NMR spectrum of [Zn(debpn)]$(ClO_4)_2$ in CD_3CN at 298 K (top) and 338 K (bottom). The field strength was 400 MHz. Note that the NMR sample was prepared from crystalline [Zn(debpn)]$(ClO_4)_2$. At 298 K, the major resonance peaks are observed at δ 8.73, 8.21, 8.12, 7.74, 7.67, 7.58, 4.46, 4.27, 4.20, 4.06, 3.85, 3.58, 3.47, 3.17, 3.04, 2.86, 1.28, 1.20, and 1.13 ppm.

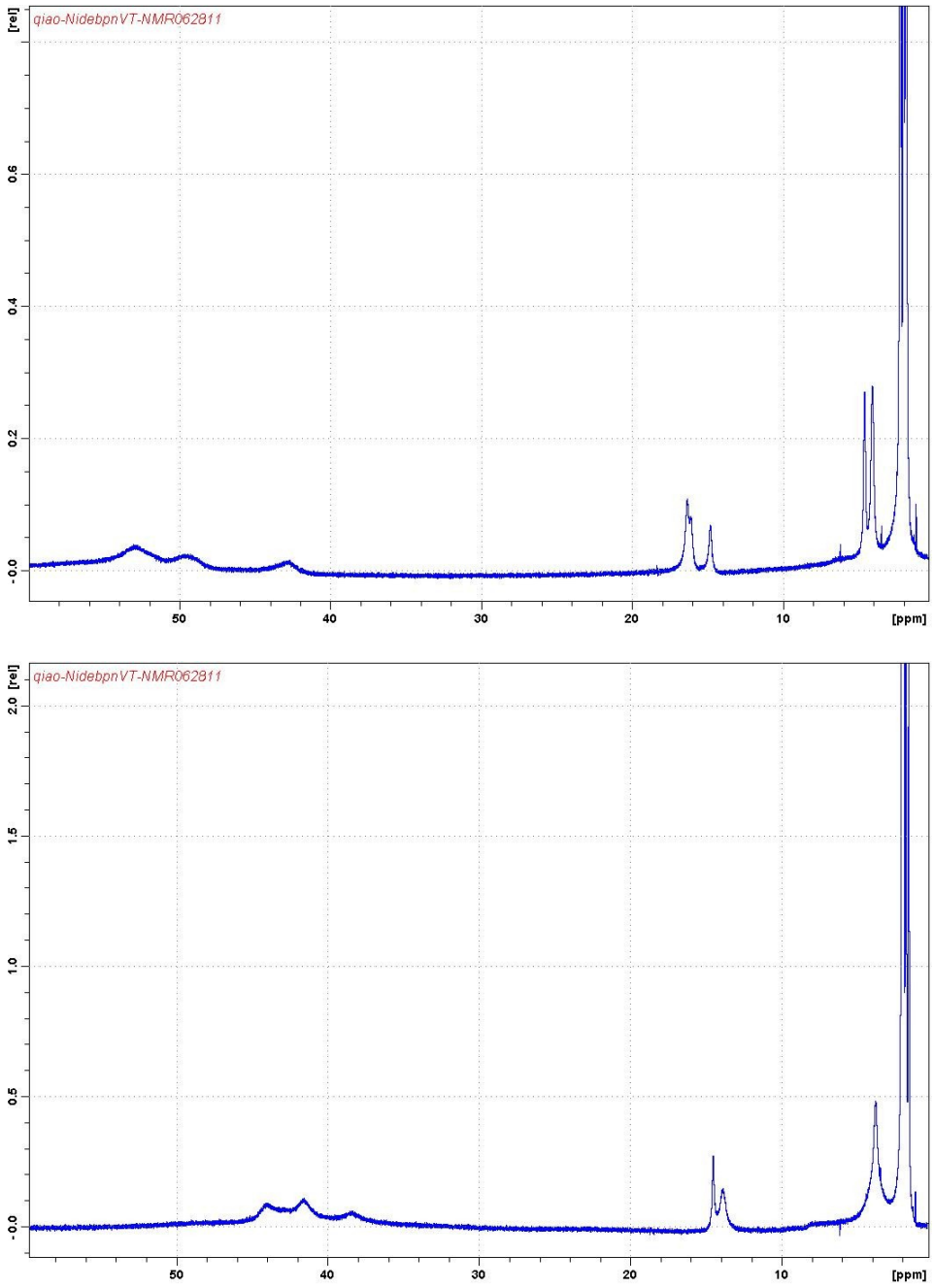

Figure 2.A2. ^{1}H NMR spectrum of [Ni(debpn)(MeCN)]$(ClO_4)_2$ in CD_3CN at 298 K (top) and 338 K (bottom). The field strength was 400 MHz. Note that the NMR sample was prepared from crystalline [Ni(debpn)(MeCN)]$(ClO_4)_2$. At 298 K, peaks are observed at δ 52, 49, 42, 16, 15, 6, 4.6, 4.0, and 2.2 ppm.

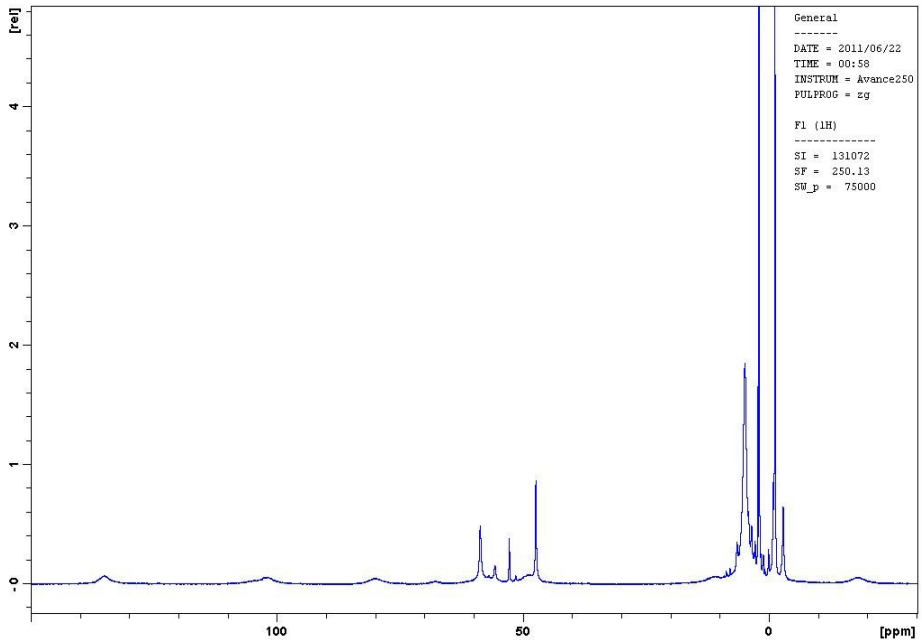

Figure 2.A3. ^{1}H NMR spectrum of $[Fe(debpn)(H_2O)](ClO_4)_2$ in CD_3CN at 294 K. The field strength was 400 MHz. Peaks are observed at δ 135, 102, 80, 68, 59, 57, 56, 53, 52, 49, 47, 11, 4.9, 3.5, 2.9, 2.3, 1.2, 0.1, -1.2, -2.9, and -18 ppm. The NMR sample was prepared from a crystalline sample of the Fe(II) complex.

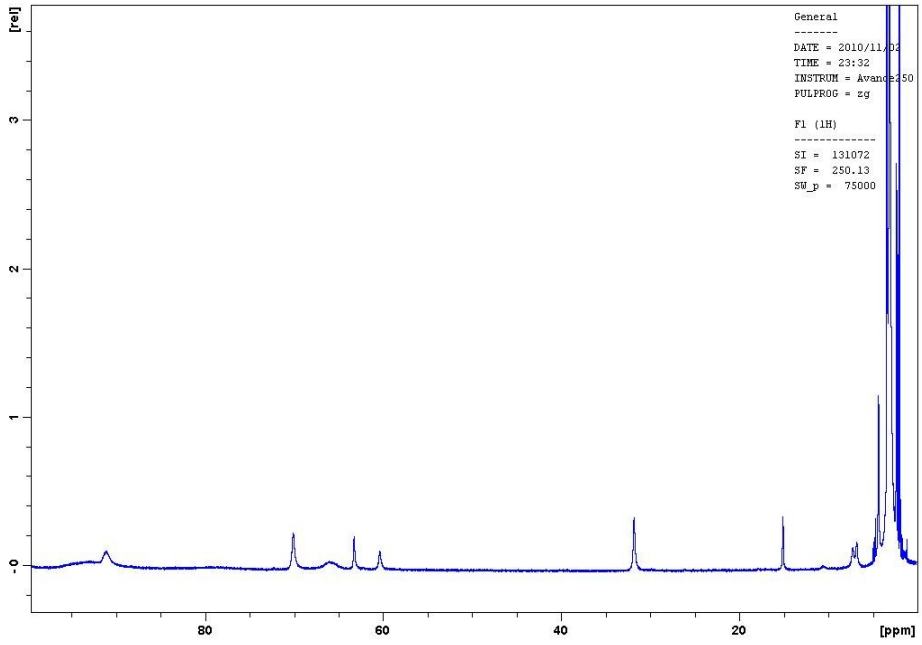

Figure 2.A4. ^{1}H NMR spectrum of $[Co(debpn)(MeCN)](ClO_4)_2$ in CD_3CN at 294 K. The field strength was 400 MHz. Peaks are observed at δ 99, 93, 91, 70, 66, 63, 60, 32, 15, 7.3, 6.8, 4.9, 4.7, 4.4, 3.4, 3.1, 2.3, 2.1, -4.9, and -5.1 ppm. The NMR sample was prepared from a crystalline sample of the Co(II) complex.

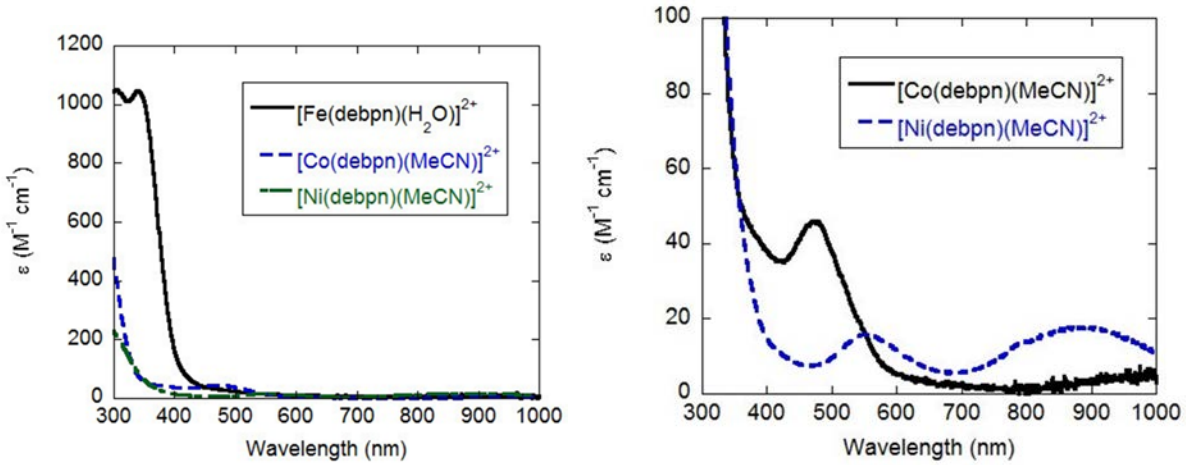

Figure 2.A5. Comparative UV/vis spectra of $[Fe(debpn)(H_2O)]^{2+}$, $[Co(debpn)(MeCN)]^{2+}$, and $[Ni(debpn)(MeCN)]^{2+}$ in MeCN at 294 K. The concentrations of the samples used for the measurements were as follows: 0.40 mM (Fe), 0.50 mM (Co), and 1.60 mM (Ni).

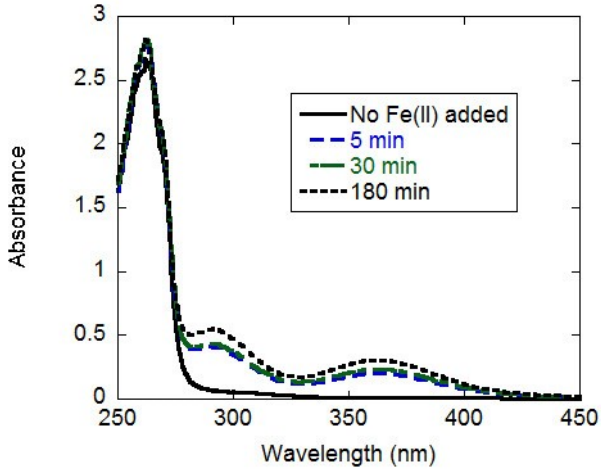

Figure 2.A6. Reaction between 1.0 mM $[Mn(debpn)(H_2O)](ClO_4)_2$ and 1.0 mM $Fe(ClO_4)_2$ in MeCN at 294 K. The reaction was monitored spectrophotometrically over a 3 h period. At 180 min, 30% of the Mn(II) has been displaced by Fe(II).

References

(1) Casanova, D.; Alemany, P.; Bofill, J. M.; Alvarez, S. *Chem. −Eur. J.* **2003**, *9*, 1281–1295.

(2) Platas-Iglesias, C.; Vaiana, L.; Esteban-Gómez,D.; Avecilla, F.; Real, J. A.; de Blas, A.; Rodríguez-Blas, T. *Inorg. Chem.* **2005**, *44*, 9704–9713.

(3) Aston, K.; Rath, N.; Naik, A.; Slomczynska, U.; Schall, O. F.; Riley, D. P. *Inorg. Chem.* **2001**, *40*, 1779–1789.

(4) Summers, J. S.; Baker, J. B.; Meyerstein, D.; Mizrahi, A.; Zilbermann, I.; Cohen, H.; Wilson, C. M.; Jones, J. R. *J. Am. Chem. Soc.* **2008**, *130*, 1727–1734.

(5) Liu, G.-F.; Dürr, K.; Puchta, R.; Heinemann, F. W.; van Eldik, R.; Ivanović-Burmazović, I. *Dalton Trans.* **2009**, 6292–6295.

(6) Wang, S.; Westmoreland, T. D. *Inorg. Chem.* **2009**, *48*, 719–727.

(7) Troughton, J. S.; Greenfield, M. T.; Greenwood, J. M.; Dumas, S.; Wiethoff, A. J.; Wang, J.; Spiller, M.; McMurry, T. J.; Caravan, P. *Inorg. Chem.* **2004**, *43*, 6313–6323.

(8) Lauffer, R. B. *Chem. Rev.* **1987**, *87*, 901–927.

(9) Rocklage, S. M.; Cacheris, W. P.; Quay, S. C.; Hahn, F. E.; Raymond, K. N. *Inorg. Chem.* **1989**, *28*, 477–485.

(10) Oakes, J.; Smith, E. G. *J. Chem. Soc., Faraday Trans. 2* **1981**, *77*, 299–308.

(11) Caravan, P.; Ellison, J. J.; McMurry, T. J.; Lauffer, R. B. *Chem. Rev.* **1999**, *99*, 2293–2352.

(12) Caravan, P. *Acc. Chem. Res.* **2009**, *42*, 851–862.

(13) Thomsen, H. S. *Eur. Radiol.* **2004**, *14*, 1654–1656.

(14) Buhaescu, I.; Izzedine, H. *Int. J. Clin. Pract.* **2008**, *62*, 1113–1118.

(15) Kümmerer, K.; Helmers, E. *Environ. Sci. Technol.* **2000**, *34*, 573–577.

(16) Mukhopadhyay, S.; Mandal, S. K.; Bhaduri, S.; Armstrong, W. H. *Chem. Rev.* **2004**, *104*, 3981–4026.

(17) Wieghardt, K. *Angew. Chem., Int. Ed. Engl.* **1989**, *28*, 1153–1172.

(18) Schwert, D. D.; Davies, J. A.; Richardson, N. *Top. Curr. Chem.* **2002**, *221*, 165–199.

(19) Drew, M. G. B.; bin Othman, A. H.; McFall, S. G.; McIlroy, P. D. A.; Nelson, S. M. *J. Chem. Soc., Dalton Trans.* **1977**, 1173–1180.

(20) Seitz, M.; Kaiser, A.; Stempfhuber, S.; Zabel, M.; Reiser, O. *Inorg. Chem.* **2005**, *44*, 4630–4636.

(21) Hulsbergen, F. B.; Driessen, W. L.; Reedijk, J.; Verschoor, G. C. *Inorg. Chem.* **1984**, *23*, 3588–3592.

(22) Hoard, J. L.; Pedersen, B.; Richards, S.; Silverton, J. V. *J. Am. Chem. Soc.* **1961**, *83*, 3533–3534.

(23) Zetter, M. S.; Grant, M. W.; Wood, E. J.; Dodgen, H. W.; Hunt, J. P. *Inorg. Chem.* **1972**, *11*, 2701–2706.

(24) El Ghachtouli, S.; Mohamadou, A.; Barbier, J.-P. *Inorg. Chim. Acta* **2005**, *358*, 3873–3880.

(25) Haynes, J. S.; Sams, J. R.; Thompson, R. C. *Can. J. Chem.* **1981**, *59*, 669–678.

(26) Toftlund, H.; Pedersen, E.; Yde-Andersen, S. *Acta. Chem. Scand. A* **1984**, *38*, 693–697.

(27) Bernstein, M. A.; King, K. F.; Zhou, X. J. *Handbook of MRI Pulse Sequences*; Elsevier Academic Press: Amsterdam, **2004**.

(28) Haacke, E. M.; Brown, R. W.; Thompson, M. R.; Venkatesan, R. *Magnetic Resonance Imaging: Physical Principles and Sequence Design*; John Wiley & Sons: New York, NY, **1999**.

(29) Nelder, J. A.; Mead, R. *Comput. J.* **1965**, *7*, 308–313.

(30) Britovsek, G. J. P.; England, J.; White, A. J. P. *Dalton Trans.* **2006**, 1399–1408.

(31) Shannon, R. D. *Acta Crystallogr.* **1976**, *A32*, 751–767.

(32) Coates, C. M.; Hagan, K.; Mitchell, C. A.; Gorden, J. D.; Goldsmith, C. R. *Dalton Trans.* **2011**, *40*, 4048–4058.

(33) Costas, M.; Que, L., Jr. *Angew. Chem., Int. Ed.* **2002**, *41*, 2179–2181.

(34) Coates, C. M.; Nelson, A.-G. D.; Goldsmith, C. R. *Inorg. Chim. Acta* **2009**, *362*, 4797–4803.

(35) Goldsmith, C. R.; Cole, A. P.; Stack, T. D. P. *J. Am. Chem. Soc.* **2005**, *127*, 9904–9912.

(36) Dowsing, R. D.; Gibson, J. F.; Goodgame, M.; Hayward, P. J. *J. Chem. Soc. A* **1969**, 187–193.

(37) Gosiewska, S.; Cornelissen, J. J. L. M.; Lutz, M.; Spek, A. L.; van Koten, G.; Klein Gebbink, R. J. M. *Inorg. Chem.* **2006**, *45*, 4214–4227.

(38) Klein Gebbink, R. J. M.; Jonas, R. T.; Goldsmith, C. R.; Stack, T. D. P. *Inorg. Chem.* **2002**, *41*, 4633–4641.

(39) Drago, R. S. *Physical Methods for Chemists, 2 ed.*; Surfside Scientific Publishers: Gainesville, FL, **1992**.

(40) Brown, M. A.; Johnson, G. A. *Med. Phys.* **1984**, *11*, 67–72.

(41) Bandara, H. M. D.; Kennedy, D. P.; Akin, E.; Incarvito, C. D.; Burdette, S. C. *Inorg. Chem.* **2009**, *48*, 8445–8455.

(42) Glerup, J.; Goodson, P. A.; Hodgson, D. J.; Michelsen, K. *Inorg. Chem.* **1995**, *34*, 6255–6264.

(43) Maigut, J.; Meier, R.; Zahl, A.; van Eldik, R. *J. Am. Chem. Soc.* **2008**, *130*, 14556–14569.

(44) Buschhaus, B.; Hampel, F.; Grimme, S.; Hirsch, A. *Chem. −Eur. J.* **2005**, *11*, 3530–3540.

(45) López-Deber, M.; Bastida de la Calle, R.; Macías, A.; Pérez-Lourido, P.; Rodríguez, A.; Valencia Matarranz, L. Z. *Anorg. Allg. Chem.* **2007**, *633*, 1842–1846.

(46) Waynant, K. V.; White, J. D.; Zakharov, L. *Chem. Commun.* **2010**, *46*, 5304–5306.

(47) March, R.; Clegg, W.; Coxall, R. A.; González-Duarte, P. *Inorg. Chim. Acta* **2003**, *346*, 87–94.

(48) Singh, G.; Sowerby, D. B. *J. Chem. Soc., Dalton Trans.* **1977**, 490–492.

(49) Kang, S.-G.; Kweon, J. K.; Jeong, J. H. *Inorg. Chim. Acta* **2007**, *360*, 1875–1882.

(50) Zhou, M.; Andrews, L.; Bauschlicher, C. W., Jr. *Chem. Rev.* **2001**, *101*, 1931–1962.

(51) Elizondo, G.; Fretz, C. J.; Stark, D. D.; Rocklage, S. M.; Quay, S. C.; Worah, D.; Tsang, Y.-M.; Chen, M. C.; Ferrucci, J. T. *Radiology* **1991**, *178*, 73–78.

(52) Outten, C. E.; O'Halloran, T. V. *Science* **2001**, *292*, 2488–2492.

(53) Theil, E. C.; Goss, D. J. *Chem. Rev.* **2009**, *109*, 4568–4579.

(54) Zhang, Y.; Gladyshev, V. N. *Chem. Rev.* **2009**, *109*, 4828–4861.

(55) Ba, L. A.; Doering, M.; Burkholz, T.; Jacob, C. *Metallomics* **2009**, *1*, 292–311.

Chapter 3

Hydrocarbon Oxidation Catalyzed by Manganese and Iron Complexes with the Hexadentate Ligand *N,N'*-Di(ethylacetate)-*N,N'*-bis(2-pyridylmethyl)-1,2-ethanediamine*

* This Chapter's content was previously published in the following manuscript:

Zhang, Q.; Goldsmith, C. R. *Inorg. Chim. Acta* **2013**, *406*, 301-306.

3.1 Introduction

Manganese(II) and iron(II) complexes with tetradentate, neutral N-donor ligands have found application as homogeneous catalysts for the oxidation of hydrocarbons. The Mn(II) compounds have been used to catalyze the epoxidation of alkenes by peracids and other two-electron oxidants;[1-6] whereas, the Fe(II) complexes have been found to facilitate the oxidation of both alkenes[7,8] and alkanes.[9-18] The chemistry is widely believed to proceed through higher-valent metal oxidants that are produced from initial reactions between the M(II) complexes and the terminal oxidants.[4,6,7,16-27] The structurally characterized M(II) complexes with the aforementioned tetradentate ligands contain hexacoordinate centers with two readily exchangeable coordination sites capable of allowing inner-sphere oxidation of the metal ions to proceed.

One disadvantage that is commonly encountered with such catalysts is their limited stability. Removal of the metal from the tetradentate ligand often halts or greatly diminishes the catalysis.[1-3] In manganese-catalyzed alkene epoxidation, the use of ligands that are less highly coordinating, through either the removal of donor atoms or the installation of steric bulk, generally decreases the activity.[3] Most of the metal complexes are unstable in water, which limits the potential "greenness" of their reactions. The use of a more highly coordinating ligand may sufficiently stabilize such compounds to allow oxidative catalysis in water. The additional chelate arms necessary for this stability, however, could hinder or preclude the coordination of the terminal oxidant required for the catalysis.

Earlier work from our laboratory involved the synthesis and characterization of two heptacoordinate metal complexes with the ligand *N*,*N*'-di(ethylacetate)-*N*,*N*'-bis(2-pyridylmethyl)-1,2-ethanediamine (debpn, Scheme 3.1).[28] The Mn(II) complex with debpn was sufficiently stable in water to serve as a contrast agent for magnetic resonance imaging. Although

the optical spectrum of the Fe(II) complex resembles those of other known heptacoordinate ferrous compounds,[28,29] it is difficult to tell for certain whether the heptacoordination of the Mn(II) and Fe(II) complexes is maintained in solution. The debpn ligand resembles the tetradentate *N*,*N*'-dimethyl-*N*,*N*'-bis(2-pyridylmethyl)-1,2-ethanediamine (bpmen, Scheme 3.1) which has been used to prepare hexacoordinate first-row transition metal catalysts for both alkene epoxidation and alkane hydroxylation.[1-3,8,13-16] Electronically, the two organic ligands are similar. The ester groups of the debpn ligand interact weakly with the metal center and do not impact the overall charge of either the ligand or its metal complexes.[28] More importantly, the debpn complexes with Mn(II) and Fe(II) each contain a readily exchangeable coordination site that can accommodate an inner-sphere oxidant, such as hydrogen peroxide or peracetic acid. The O-donors from the esters are not fully bound to the Co(II) and Ni(II) ions in other structures,[28] suggesting that these groups are weakly coordinating and can detach from the Mn(II) and Fe(II) to provide additional coordination sites for inner-sphere oxidants.

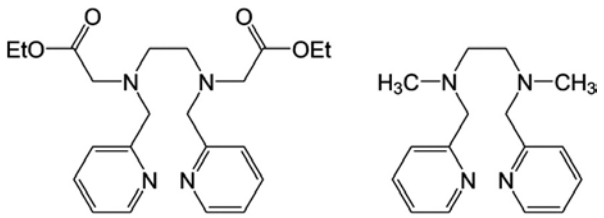

Scheme 3.1

In the present work, we have assessed the catalytic capabilities of the Mn(II) and Fe(II) complexes with debpn (Scheme 3.2). Specifically, we have studied their abilities to accelerate the activation of aliphatic C-H bonds and the conversion of olefins to epoxides and compared these to the catalytic activities of analogous complexes with the less highly coordinating bpmen.

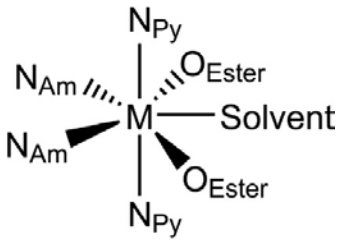

Scheme 3.2. Inner-sphere coordination of $[Mn(debpn)(H_2O)]^{2+}$ and $[Fe(debpn)(H_2O)]^{2+}$.

3.2 Experimental Section

Materials

Unless otherwise stated, all chemicals were bought from Sigma–Aldrich and used without further purification. *cis*-Cyclooctene, 1-octene, ethyl sorbate, and anhydrous acetonitrile (MeCN) were purchased from Acros. Hydrogen peroxide (H_2O_2, 30% or 50% in water) was purchased from Fisher and stored in a refrigerator when not in use. Glacial acetic acid (CH_3CO_2H) was bought from Pharmco-Aaper. The peracetic acid (PAA_R, 7.5%) was custom-made through a previously described process.[3] In this procedure, 50% H_2O_2 and CH_3CO_2H react in the presence of the acidic resin Amberlite IR-120. This synthesis produces a less acidic grade of peracetic acid that lacks the H_2SO_4 impurity found in commercial sources (PAA_C). The concentration of the peracid was determined and periodically checked by ^{13}C NMR. The compounds $[Mn(debpn)(H_2O)](ClO_4)_2$ and $[Fe(debpn)(H_2O)](OTf)_2$ were prepared as previously described.[28] Crystalline samples of these two compounds were used for all catalytic reactions.

CAUTION: Although no accidents occurred in the described studies, peracids, peroxides, and metal perchlorate salts, such as $[Mn(debpn)(H_2O)](ClO_4)_2$, are potentially explosive. As precautionary measures, most reactivity assays involving peracids were performed at 0 °C behind a blast shield, using minimal amounts of these reagents. The peracetic acid was stored in a freezer when not in use.

Instrumentation

All ^{1}H magnetic resonance (NMR) spectra were acquired on a 400 MHz AV Bruker NMR spectrometer at 294 K; all observed resonance peaks were assigned relative to known internal standards. Gas chromatography (GC) was obtained on a Thermo Scientific Trace GC Ultra spectrometer with a flame ionization detector (FID). All cyclic voltammetry was performed under N_2 at 294 K using a Pine Instrument Co. AFCBP1 bipotentiostat, a glassy carbon working electrode, a platinum wire auxiliary electrode, a silver wire reference electrode, and tetrabutylammonium perchlorate as a supporting electrolyte. Since all electrochemistry was done in MeCN, ferrocene was added as an internal reference.[30] The scan rate was 100 mV/s.

Reactivity

All reactions were run under N_2. The protocols for the alkene epoxidation reactions were adapted from previously reported procedures.[1-3,8] In the reactions with the Mn(II) catalyst, $[Mn(debpn)(H_2O)]^{2+}$, the substrate and oxidant were combined in a glass vial and dissolved in MeCN. The internal standard, 1,2-dichlorobenzene, was added and the solution was cooled to 0 °C with an ice bath. The terminal oxidant, PAA_R, was added over the course of 2 min. Aliquots of the reaction mixture were taken for GC analysis at set time points after the reaction began (the start of the addition of the oxidant). Each aliquot was run through a plug of silica gel prior to analysis; this removed the metal salts and the excess oxidant without removing the organic products.[31-33] After the samples were diluted with ether, the identities and quantities of the products were assessed by GC. All products were identified through comparison of their GC retention times to those of known standards. ^{1}H NMR spectroscopy was used to confirm the identities of isolated products. All reactions were repeated at least three times; the provided yields are the averages of those independent runs.

The alkene epoxidation protocol with the Fe(II) catalyst, $[Fe(debpn)(H_2O)]^{2+}$, was similar to that corresponding to the Mn(II) catalysis with two modifications. First, CH_3CO_2H was added to the initial MeCN solution of the catalyst and substrate. Second, H_2O_2 was used as the terminal oxidant instead of PAA_R. The isolated yields on Table 3.3 were obtained from reactions between 232 mg *cis*-cyclooctene (2.0 mmol), 23.5 mg $[Fe(debpn)(H_2O)](OTf)_2$ (0.060 mmol), 34 μL CH_3CO_2H (0.60 mmol), and 173 μL H_2O_2 (50 wt %, 3.0 mmol) in 14 mL of MeCN. After 5, 30, or 60 min, 40 mL of a saturated solution of Na_2CO_3 in water was added to quench the reaction. The product was extracted with CH_2Cl_2 (3 × 30 mL). The extracts were dried over $MgSO_4$ and filtered. The solvent and starting material were removed from the mixture through rotavaporation, yielding the cyclooctene oxide as a colorless oil.

The protocol for the alkane oxidation reactions was based on previously reported procedures in order to facilitate comparison to prior research.[13-15,17] The Fe(II) catalyst and alkane substrate were dissolved in MeCN, with initial concentrations of 1.0 mM and 1.0 M, respectively, unless noted otherwise. The terminal oxidant, H_2O_2, was diluted in MeCN and added dropwise over the course of 1 min in order to minimize changes to the reaction temperature. The final volume of each reaction solution was 2.50 mL. At various time points, aliquots of the solution were taken via syringe, filtered through silica gel, and analyzed via GC. Prior to GC analysis, 1,2-dichlorobenzene was added as an internal standard.

3.3 Results

Alkene Epoxidation-Manganese

The heptacoordinate $[Mn(debpn)(H_2O)]^{2+}$ complex (**1**) was tested as a catalyst for the epoxidation of various olefins by peracetic acid (PAA_R). The reaction protocol was chosen to

facilitate comparison to the previously reported catalytic capabilities of [Mn(bpmen)(OTf)$_2$] (**3**), although in most instances the reactions using **1** were run at 0 °C, rather than 25 °C.[1,2] Although **1** catalyzes the reaction between alkenes and peracetic acid, the activity is inferior to that of the bpmen compound, as assessed by the lower conversions of 1-octene (Table 3.1). With both ligands, the epoxide is the only observed organic product; the yields of epoxides and conversions of alkene starting material are equal within error.

Table 3.1. Epoxidation of 1-Octene Catalyzed by [Mn(debpn)(H_2O)]$^{2+}$ (**1**) and [Mn(bpmen)(OTf)$_2$] (**3**).

Catalyst	Loading (mol %)	Time (s)	GC Yield (%)
1	0.1	15	1
	0.1	300	38
	1.0	15	9
	1.0	300	77
3	0.1	15	2
	0.1	300	49
	1.0	15	83
	1.0	300	87

All reactions were run at 298 K in MeCN under N_2, with initial concentrations of 100 mM 1-octene and 150 mM PAA_R. The reported yields are the averages of at least three independent reactions. The only observed product is 1-octene oxide; no other oxidized organic products were observed above the limit of detection. The data for **3** are from Ref. 3 these were reproduced by our laboratory.

The observed reactivity is unusual in that 1-octene and *cis*-cyclooctene are oxidized to similar extents, with essentially identical yields of the corresponding epoxides at 5 min (Table 3.2). This is noteworthy since the more electron deficient C=C bond in 1-octene is generally less reactive.[1,2,7,26,33,34] Styrene is also more reactive than one might otherwise anticipate, for the measured yields at 5 and 30 min are not much lower than their counterparts for dimethylstyrene.

The catalyst is not stable under the reaction conditions; over 30 min, the debpn ligand is oxidized, as evidenced by mass spectrometry (Figure 3.A5). Further, the reaction mixture changes color from light yellow to brown, indicating that the manganese is oxidized as well.

Table 3.2. Epoxidation of Alkenes by 7.5% Peracetic Acid Catalyzed by $[Mn(debpn)(H_2O)]^{2+}$ (**1**).

Substrate	Product	Catalyst Loading (mol %)	Time (min)	GC Yield (%)
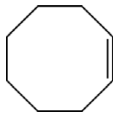	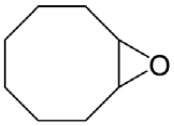	1.0	5	78
		1.0	30	79
		0.10	5	52
		0.10	30	78
		0.0	5	3
		0.0	30	8
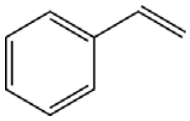	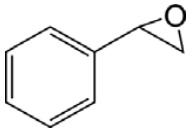	1.0	5	44
		1.0	30	62
		0.0	5	0
		0.0	30	0
	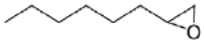	1.0	5	75
		1.0	30	77
		0.0	5	0
		0.0	30	0
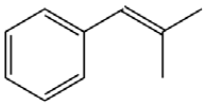	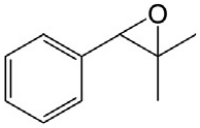	1.0	5	62
		1.0	30	78
		0.0	5	0
		0.0	30	0

All reactions were run at 273 K in MeCN under N_2, with initial concentrations of substrate and PAA_R equal to 100 and 150 mM, respectively. The initial concentrations of **1** in the 1.0 and 0.10 mol% catalyst loadings were 1.0 and 0.10 mM respectively. The shown epoxides are the only observed organic products; the remaining material is non-oxidized starting material. All reported yields are the averages of at least three independent reactions.

Alkene Epoxidation-Iron

The epoxidation of alkenes by H_2O_2 proceeds more slowly and to a lesser extent with $[Fe(debpn)(H2O)]^{2+}$ (**2**) as the catalyst relative to similar reactions reported by White, Doyle, and Jacobsen using $[Fe(bpmen)(MeCN)_2](SbF_6)_2$ (**4**).[8] *cis*-Cyclooctene is oxidized to half the extent (40% isolated yield) and requires 60 min, rather than 5 min, for this maximum yield to be reached (Table 3.3). The ferrous debpn complex also appears to catalyze the oxidation of terminal alkenes less avidly relative to both 1 and its bpmen analog **4**. 1-Octene is converted to 1-octene oxide in 47% yield over 30 min with a 5 mol% loading of **2**; with **4**, conversely, non-functionalized terminal alkenes are oxidized to epoxides in yields of 76 ~ 90% within 5 min.[8] As with the aforementioned **1**, **2** is itself oxidized under the reaction conditions. Mass spectrometry reveals that the debpn ligand is oxidized over the 30 min allowed for the reactions (Figure 3.A6). The solutions also discolor, suggesting that the iron oxidizes as well.

Table 3.3. Epoxidation of Alkenes by Hydrogen Peroxide Catalyzed by $[Fe(debpn)(H_2O)]^{2+}$ (**2**) and $[Fe(bpmen)(MeCN)_2](SbF_6)_2$ (**4**).

Catalyst	Substrate	Product	Catalyst Loading (mol %)	Time (min)	Yield (%)	TON
2	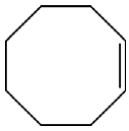	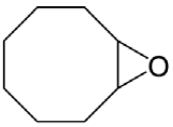	3.0	5	33, 29[a]	11.0
			3.0	30	38, 33[a]	12.7
			3.0	60	44,40[a]	14.7
			5.0	5	68	13.6
			5.0	30	82	16.4
			5.0	60	87	17.4
2	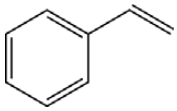	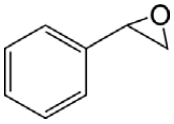	5.0	5	5	1.0
			5.0	30	5	1.0
			5.0	60	6	1.2
2	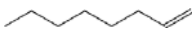	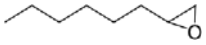	5.0	5	35	7.0
			5.0	30	47	9.4
			5.0	60	47	9.4
2	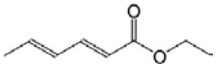	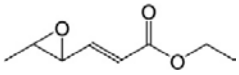	5.0	5	27	5.4
			5.0	30	27	5.4
			5.0	60	27	5.4
4	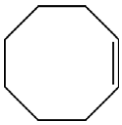	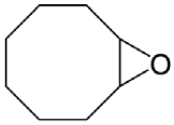	3.0	5	86[a,b]	28.3[b]

All reactions were run in MeCN at 273 K under N_2. The initial concentrations of substrate, H_2O_2, and acetic acid were 100 mM, 150 and 50 mM. The reported yields are the averages of at least three independent reactions. The epoxides are the sole observed organic products. All yields are GC yields unless stated otherwise.
[a] Isolated yield. [b] Data from Ref. 8; these results were independently reproduced by our laboratory.

Alkane Oxidation-Iron

Compound **2** also catalyzes the oxidation of alkanes by H_2O_2 to alcohols and ketones (Table 3.4). As with the alkene epoxidation, this activity is not as extensive as that previously

observed with the bpmen ligand. Cyclohexane is oxidized to a mixture of cyclohexanol and cyclohexanone. When 10 equiv. of H_2O_2 are provided as the terminal oxidant, the catalyst only turns over 2.1 times; this activity is exceptionally mild relative to the catalysis reported for other non-heme iron compounds.[13–17] [Fe(bpmen)(MeCN)$_2$] (OTf)$_2$, for instance, can catalyze 7.0 turnovers under identical reaction conditions (5.6 TON for cyclohexanol, 0.7 TON for cyclohexanone which requires two equiv. of H_2O_2).[15,16] Additionally, the selectivity for the alcohol product is lost; the products of cyclohexane oxidation promoted by **2** contain nearly equal amounts of cyclohexanol and cyclohexanone. A kinetic isotope effect of 2.4 was measured from a competition experiment with protonated and deuterated cyclohexane (C_6D_{12}), suggesting that C-H bond cleavage is involved in the product-determining step of the reaction. Compound **2** catalyzes 1.3 turnovers over 30 min when C_6D_{12} is the sole substrate with a 3:1 ratio of alcohol to ketone products. This reactivity is more extensive than one would expect from the KIE and the TON reported for the protonated cyclohexane. In order to assess the potential impact of steric repulsions between the catalyst and the substrate on the C-H activation, the more sterically complex alkanes *cis*- and *trans*-1,2-dimethylcyclohexane were investigated as substrates using a protocol first employed by White[35] and subsequently by ourselves.[17] In these experiments, the ratio of secondary to tertiary carbon oxidation is used as a measure of the accessibility of the metal-based oxidant to substrates. More sterically congested catalysts will direct the oxidation to the thermodynamically stronger but more accessible C-H bonds on secondary carbons.[13,17,35] The ratios of secondary/tertiary oxidation observed for **2** are similar to those observed for reactions catalyzed by other non-heme iron compounds but are lower than those of [Fe(bbpc)(MeCN)$_2$]$^{2+}$ (bbpc = *N*,*N*'-bis(phenylmethyl)-*N*,*N*'-bis(2-pyridinylmethyl)-1,2-cyclohexanediamine), which is a

markedly superior catalyst for cyclohexane oxidation (4.5 TON, 7.3:1 alcohol:ketone (A:K) ratio with 10 equiv. H_2O_2).[17]

Table 3.4. Oxidation of Alkanes by Hydrogen Peroxide Catalyzed by $[Fe(debpn)(H_2O)]^{2+}$ (**2**).

Substrate	Products[a]	TON[b]	Notes
cyclohexane	cyclohexanol	0.76	1.1:1 A:K ratio
	cyclohexanone	0.67	
1-hexane	2-hexanol	0.049	1.1:1 A:K ratio
	3-hexanol	0.19	no 1° carbon oxidation
	2-hexanone	0.074	
	3-hexanone	0.15	
cis-1,2-dimethylcyclohexane	*trans*-1,2-dimethylcyclohexanol	3.3	modified procedure[c]
	cis-1,2-dimethylcyclohexanol	0.3	
	cis-2,3-dimethylcyclohexanone	2.2	
	cis-3,4-dimethylcyclohexanone	0.1	
trans-1,2-dimethylcyclohexane	*trans*-1,2-dimethylcyclohexanol	0.9	modified procedure[c]
	cis-1,2-dimethylcyclohexanol	1.5	
	trans-2,3-dimethylcyclohexanol	1.8	
	trans-2,3-dimethylcyclohexanone	2.8	
	cis-3,4-dimethylcyclohexanone	1.7	

Standard reaction conditions: All reactions were run at 298 K in MeCN under N_2. For cyclohexane and hexane, the starting concentrations of **2** and the substrate were 1.0 and 1.0 M, respectively. A solution of H_2O_2 diluted in MeCN was added dropwise over the course of 1 min. The final volume of each reaction solution was 2.50 mL. The duration of each reaction was 30 min. After this time, the solution was filtered through silica gel and analyzed via GC.

[a] The products were identified by GC/MS and comparison of the retention times with those of authentic samples. The concentrations of each organic product were calibrated relative to that of an internal standard (dichlorobenzene) with a known concentration.

[b] Turnover number, defined as the number of moles of cyclohexanol and cyclohexanone generated per mole of **2**.

[c] Modified procedure reaction conditions: the general protocol was adapted from Ref. 35 in order to facilitate direct comparison of the data to previously reported results. The substrate (0.056 g, 0.50 mmol, 1 equiv) was dissolved in 1.0 mL of MeCN. The iron catalyst and the terminal oxidant, H_2O_2, were added to this solution in three portions. For each addition, the H_2O_2 was added dropwise over the course of 90 s. After the first additions, the concentrations were as follows: [Fe] = 4.26 μM, [substrate] = 85.2 μM, [H_2O_2] = 0.102 mM. 10 min after the first portion of H_2O_2 was added, further equivalents of catalyst and oxidant were added, yielding the following concentrations: [Fe] = 4.65 μM, [substrate] = 46.5 μM, [H_2O_2] = 0.112 mM. 20 min after the first portion of H_2O_2 was added, the third portions of catalyst and oxidant were added, yielding the following concentrations: [Fe] = 4.80 μM, [substrate] = 32.0 μM, [H_2O_2] = 0.115 mM.

Electrochemistry

Cyclic voltammetry (CV) was performed for compounds **1** ~ **4** in anaerobic MeCN. Each debpn and bpmen compound except for **4** has a single irreversible redox feature, which we assign to the M(III/II) couple. The manganese complexes have oxidation peaks at 1020 mV (debpn) and 960 mV (bpmen) (vs. ferrocene); whereas, the iron complexes have similar features at 1010 mV (debpn) and 835 mV (bpmen). The feature for $[Fe(bpmen)(MeCN)_2]^{2+}$ is quasi-reversible. Although the ΔE of 60 mV is consistent with a reversible process, the current of the cathodic peak is much less than that of the anodic. The +2 oxidation state is stabilized by the additional ester arms of the debpn ligand, with Fe(II) being stabilized to a much greater extent than $[Fe(bpmen)(MeCN)_2]^{2+}$.

3.4 Discussion

The use of a more highly coordinating ligand can potentially impact the catalytic properties of a bound metal ion in several ways. First, the additional donor atoms can alter the fundamental electronic structure through a change in the coordination geometry, which could better stabilize certain oxidation states over others. Second, a more highly chelating ligand can stabilize metal–ligand adducts crucial to the desired reactivity. Third, the ligand could hinder the ability of inner-sphere terminal oxidants to ligate the metal, due to the more crowded coordination sphere. Fourth, the extra binding groups can block substrates from interacting with the generated metal-based oxidants, which remain nebulous in many instances.[3,4,27,36-39]

In their investigation of alkene epoxidation catalyzed by manganese complexes with bidentate, tridentate, and tetradentate ligands, Murphy and Stack found that ligands with higher denticities tend to promote superior reactivity, with respect to both the ultimate yield and speed of

the reaction.[3] The better activity of the complexes with the tetradentate ligands was attributed to the greater stability of the manganese complexes; the use of a less highly chelating ligand or the introduction of steric modifications that lengthened and weakened the Mn-L bonds generally led to a pronounced loss of catalytic activity.[3] The Mn(II) complex with the debpn ligand promotes slightly less active epoxidation than the Mn(II) complexes with most tetradentate ligands, using the epoxidation of 1-octene as the basis for comparison (Table 3.1). The yield of the 1-octene epoxide is ~90% of that of the reaction catalyzed by its most closely related six-coordinate analog [Mn(bpmen)$(OTf)_2$]. The reactivity promoted by **1** also proceeds more slowly, evidenced most clearly by the yields measured at 15 s. The results demonstrate that factors other than the stability of the manganese-ligand adduct influence the catalysis of alkene epoxidation by peracetic acid. That 1-octene and cis-cyclooctene are oxidized to essentially the same extent (Table 3.1) suggests that steric interactions between the catalyst's ligand and the organic substrate may hinder the oxidation of more sterically congested olefins; normally, *cis*-cyclooctene is far more reactive than 1-octene.[1,7,26,33,34] The similar reactivities of styrene and dimethylstyrene also support this conclusion. With the latter two substrates, the reactions are substantially slower, requiring 30 min for completion instead of 5 min.

Slower alkene epoxidation activity is also observed when the Fe(II) complex **2** is used as a catalyst using a protocol developed by White, Doyle, and Jacobsen in their analysis of [Fe(bpmen)$(MeCN)_2]^{2+}$ (**4**).[8] Epoxidations catalyzed by **4** finish within 5 min; whereas, analogous reactions catalyzed by **2** need 30 min to reach their optimal yields. The final yield of the *cis*-cyclooctene epoxidation catalyzed by **2** is lower, being approximately 50% of that reported for the reaction promoted by [Fe(bpmen)$(MeCN)_2]^{2+}$. Compared to its Mn(II) analog **1**, **2** is not as effective at catalyzing the oxidation of terminal olefins, and the reactivity with styrene, in

particular, is negligible. The loss of epoxidation activity associated with the use of a hexadentate ligand in place of a tetradentate one is greater for iron than it is for manganese. Steric effects are not as evident for the iron-catalyzed epoxidation. The yields of 1-octene oxide from 1-octene are about half those of cyclooctene oxide from *cis*-cyclooctene.

The Fe(II) complex **2** was also tested as a catalyst for the oxidation of alkanes by H_2O_2 (Table 3.4). Iron complexes with bpmen have been explored extensively as catalysts for these reactions.[13-16] The addition of the ethyl esters to the ligand framework reduces the activity to a greater extent than the previously described epoxidation reactions. Using the oxidation of cyclohexane by 10 equiv. of H_2O_2 as a comparative standard, about 70% of the catalytic activity is lost upon switching the catalyst from [Fe(bpmen)$(OTf)_2$] to **2**. The debpn ligand does appear to be relatively bulky, as assessed by the retention of configuration (RC) for the oxidation of *cis*-1,2-dimethylcyclohexane. RC has been previously defined as [(1*R*,2*R* + 1*S*,2*S*) – (1R,2S + 1*S*,2*R*)] / (total amount of tertiary alcohol), where (1*R*,2*R*), (1*S*,2*S*), (1*R*,2*S*), and (1*S*,2*R*) are the various isomers of 1,2-dimethylcyclohexanol.[13] The RC for *cis*-1,2-dimethylcyclohexane oxidation has been found to decrease upon switching to an iron catalyst with a bulkier ligand. The 83% RC for **2** is significantly lower than the 96% value for [Fe(bpmen)$(OTf)_2$] but is higher than those associated with more catalytically active iron complexes with doubly and triply methylated tris(picolylamine) ligands.[13]

The reduced C-H activation catalysis therefore cannot be solely attributed to increased steric interactions between **2** and potential substrates. The ratios of secondary to tertiary carbon oxidation for the two 1,2-dimethylcyclohexane substrates provide an alternative means of assessing the steric hindrance between the substrate and catalysts. The ratios observed for **2** are similar to those reported for other non-heme iron catalysts with bulky N-donor ligands.[17,35] Further,

another Fe(II) complex of ours, $[Fe(bbpc)(MeCN)_2]^{2+}$, shows much stronger preferences for secondary over tertiary carbon oxidation (a ratio of 4.8:1 with *trans*-1,2-dimethylcyclohexane) without as marked a decrease in the catalysis.[17] The installation of the weakly binding ethyl esters also eliminates the selectivity for the alcohol over the ketone product that was observed for both the bpmen and bbpc systems.[15-17]

Cyclic voltammetry (CV) measurements suggest that the +2 oxidation state is better stabilized by the debpn ligand than by the bpmen, with the iron being particularly stabilized by the additional chelate arms. In each of the CV of compounds **1** ~ **4**, a single irreversible or quasi-reversible feature is observed, which we assign to the divalent metal ion's oxidation to the +3 state. The CV of **1** has a redox feature 60 mV higher than that observed for **3**. The redox event observed for **2** is 175 mV higher than that of **4**. The comparative increased difficulty in converting the Fe(II) to higher oxidation states may explain why the iron loses more of its activity than the Mn(II) upon the bpmen-for-debpn switch. For the alkane hydroxylation, the oxidation of the iron does not appear to be fully rate-limiting, however. The measured KIE for cyclohexane is consistent with C–H bond cleavage in the product-determining step. More turnovers are observed with C_6H_{12} than with C_6D_{12} suggesting that C-H bond cleavage is still relevant to the rate-determining step. The ratio of these turnover numbers (1.4:1), however, is much less than what one would expect based on the KIE of 2.4. An alternative explanation for the reduced activity may be that the higher reduction potentials destabilize the higher-valent iron oxidant responsible for alkane oxidation. This oxidant may consequently exhibit faster rates of intramolecular ligand oxidation[6], thereby eliminating opportunities for the oxidant to react with exogenous substrates. The observed debpn ligand degradation may be consistent with this alternative explanation.

Although the additional chelate arms of debpn were previously found to stabilize and solubilize ligand-metal adducts in water,[28] neither the Mn(II) nor the Fe(II) compound is a competent catalyst for hydrocarbon oxidation in aqueous solutions. Reactions were run in anaerobic distilled water; otherwise the reaction conditions were identical to those of the MeCN reactions. Due to the immiscibility of the substrate with water, the reactions were stirred quickly to ensure that the reaction proceeded.[40] The yields of cyclohexene oxide from cyclohexene for the uncatalyzed reactions with peracetic acid and H_2O_2 are equal to those with a debpn compound present. The $[Fe(debpn)(H_2O)]^{2+}$ complex fails to catalyze the oxidation of cyclohexane by H_2O_2 in water. Although the debpn ligand should remain more tightly bound to the metals due to their potential hexadenticity, the Mn(II) and Fe(II) complexes are still susceptible to degradation through side reactions with the terminal oxidants used for hydrocarbon oxidation.

3.5 Conclusions

Although the use of a neutral ligand that promotes heptacoordination appears to be a poor design feature for a first-row transition metal catalyst for hydrocarbon oxidation, such ligands may be beneficial for other applications. One concern in using transition metal ions for biological imaging, for instance, is that they often catalyze unwanted redox activity. Preparing a biological imaging agent with a more highly coordinating ligand may significantly limit these reactions by better stabilizing the metals in lower oxidation states.

Appendix

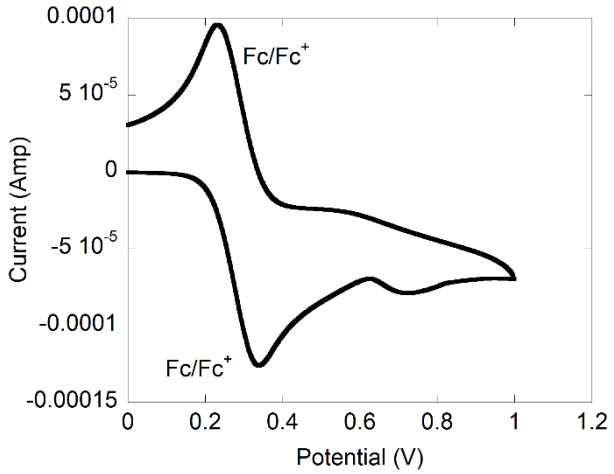

Figure 3.A1. Cyclic voltammogram for $[Mn(debpn)(H_2O)]^{2+}$ (**1**) in a 0.10 M solution of tetrabutylammonium perchlorate in MeCN. Ferrocene (Fc) has been added as an internal standard. For **1**: E_{pa} = +1020 mV vs. NHE. Scan rate = 100 mV/s.

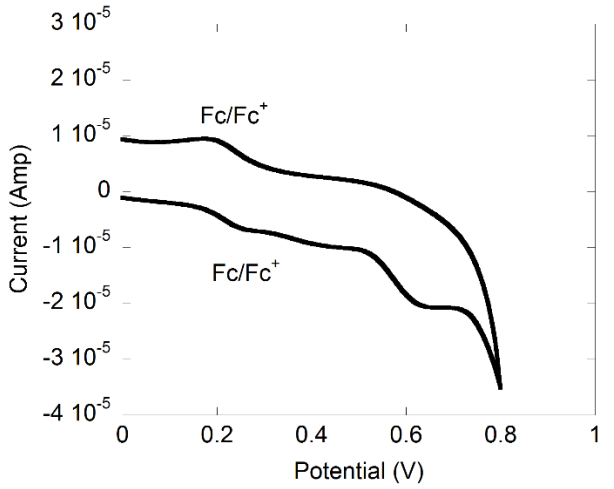

Figure 3.A2. Cyclic voltammogram for $[Fe(debpn)(H_2O)]^{2+}$ (**2**) in a 0.10 M solution of tetrabutylammonium perchlorate in MeCN. Ferrocene (Fc) has been added as an internal standard. For **2**: E_{pa} = +1010 mV vs. NHE. Scan rate = 100 mV/s.

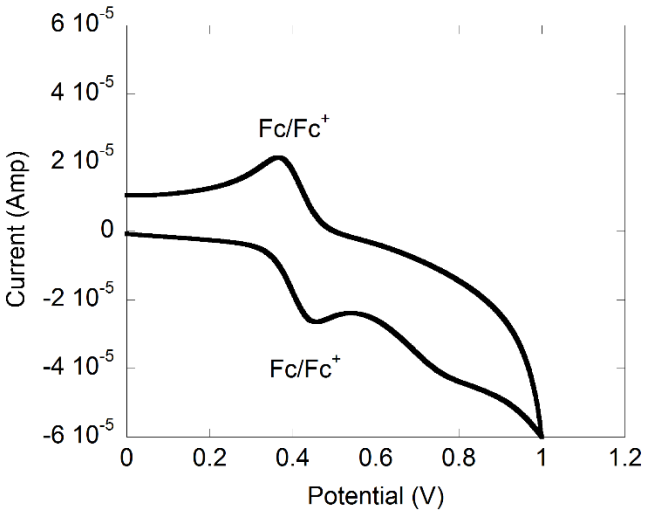

Figure 3.A3. Cyclic voltammogram for [Mn(bpmen)$(OTf)_2$] (**3**) in a 0.10 M solution of tetrabutylammonium perchlorate in MeCN. Ferrocene (Fc) has been added as an internal standard. For **3**: E_{pa} = +960 mV vs. NHE. Scan rate = 100 mV/s.

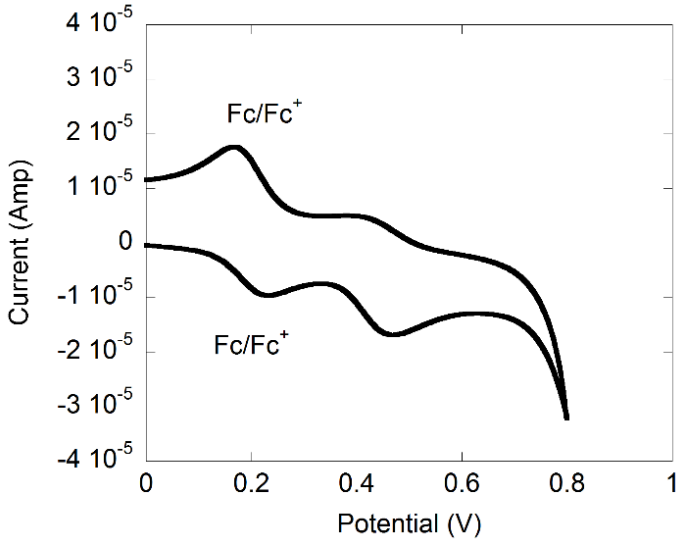

Figure 3.A4. Cyclic voltammogram for $[Fe(bpmen)(MeCN)_2]^{2+}$ (**4**) in a 0.10 M solution of tetrabutylammonium perchlorate in MeCN. Ferrocene (Fc) has been added as an internal standard. For **4**: $E_{1/2}$ = +835 mV vs. NHE. ΔE = 60 mV. Scan rate = 100 mV/s.

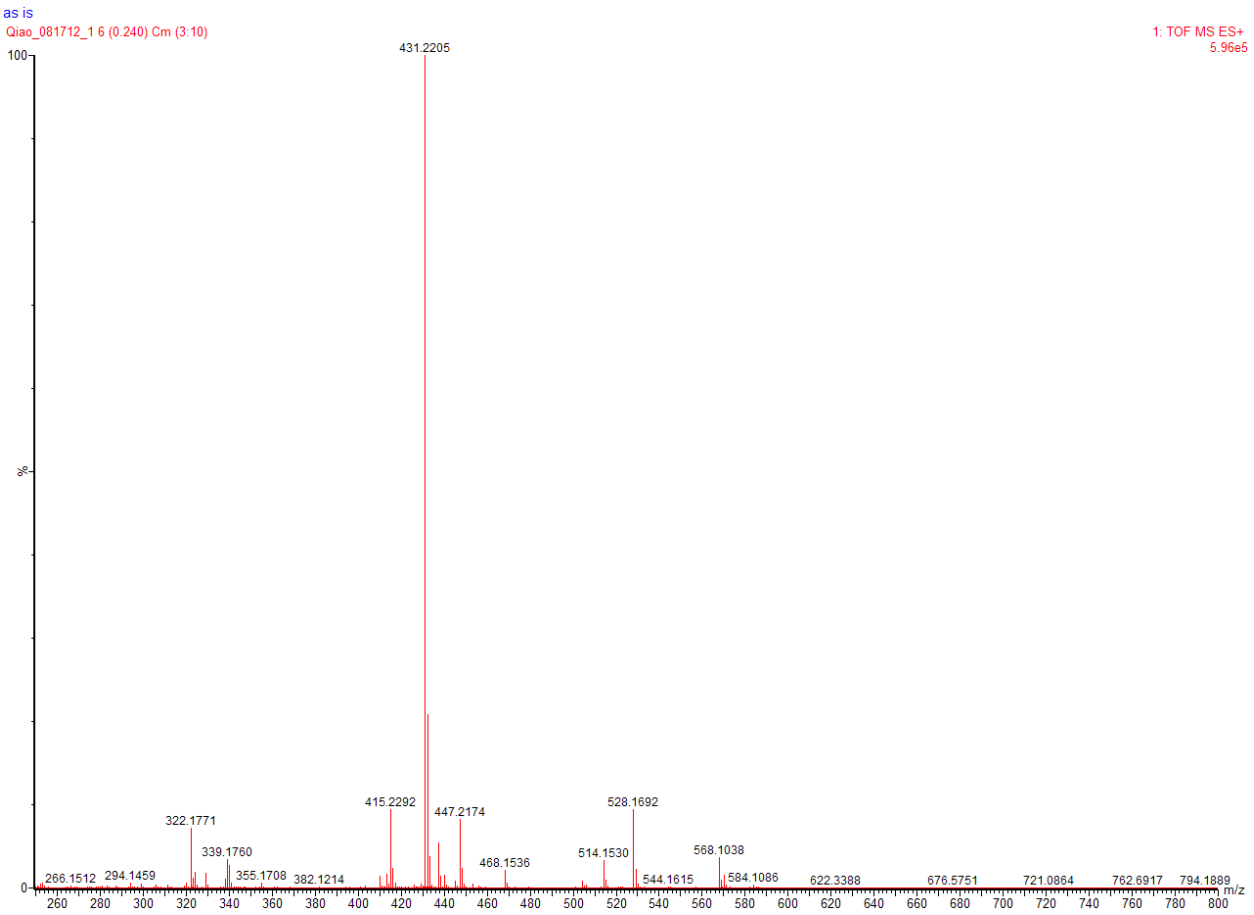

Figure 3.A5. Mass spectrum (ESI) of aliquot from reaction between 1.0 mM [Mn(debpn)(H_2O)](ClO_4)$_2$ and 5.0 mM PAA_R in 294 K MeCN. The reaction was allowed to proceed for 30 min. The *m*/*z* feature at 431.2205 is assigned to the oxidized debpn ligand ($[L+OH]^+$ calculated *m*/*z* = 431.2295). The *m*/*z* feature at 447.2174 is assigned to the doubly oxidized debpn ligand ($[L+O_2H]^+$ calculated *m*/*z* = 447.2289).

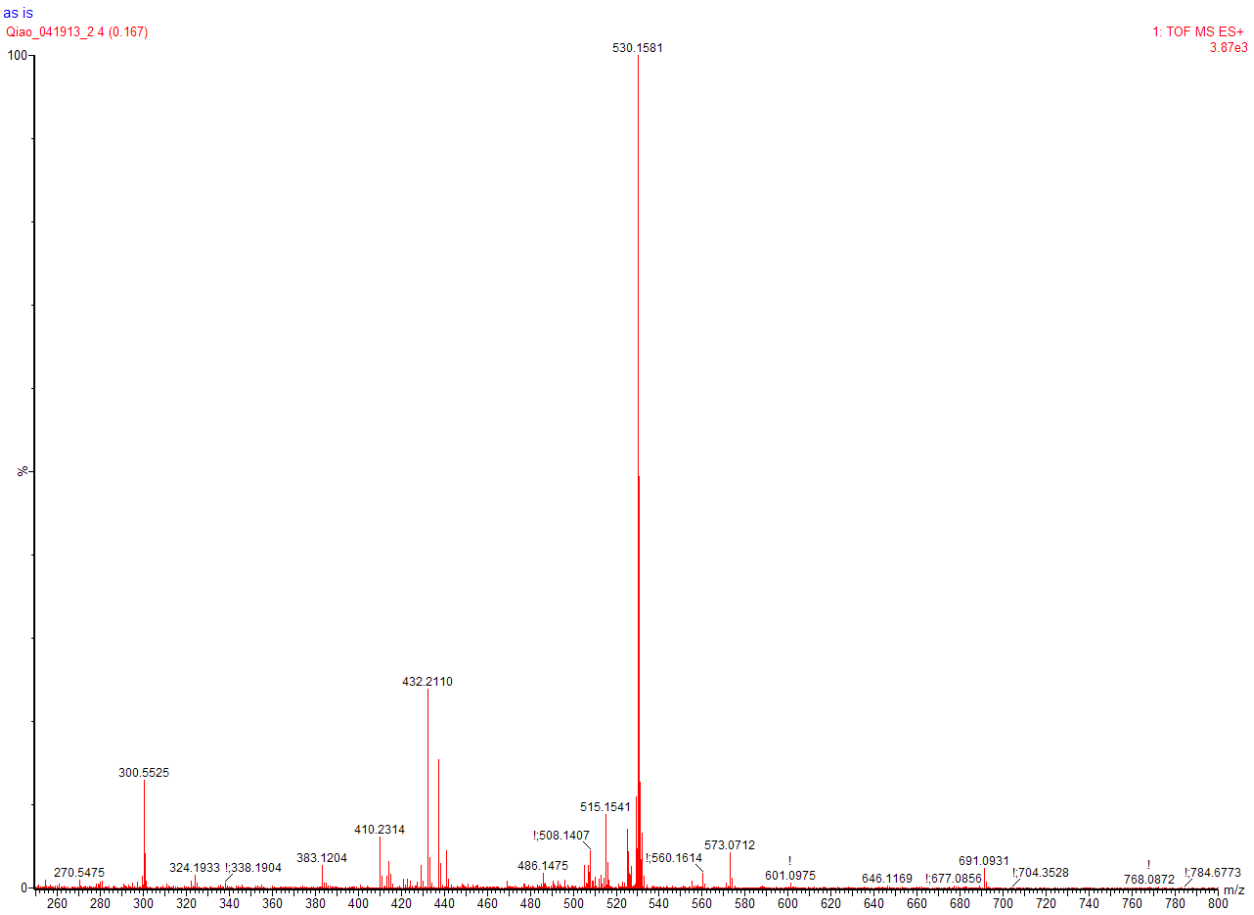

Figure 3.A6. Mass spectrum (ESI) of aliquot from reaction between 1.0 mM [Fe(debpn)(H_2O)](OTf)$_2$, 5.0 mM acetic acid, and 5.0 mM H_2O_2 in 294 K MeCN. The reaction was allowed to proceed for 30 min. The *m*/*z* feature at 432.2110 is assigned to the oxidized debpn ligand ($[L+OH_2]^+$ calculated *m*/*z* = 432.2373). The m/z feature at 530.1581 corresponds to the formula $[C_{23}H_{30}N_4O_7Fe]^+$.Given that formic acid was present in the ionization medium in addition to the acetic acid from the reaction mixture, a definitive assignment of this species cannot be made.

References

(1) Murphy, A.; Dubois, G.; Stack, T. D. P. *J. Am. Chem. Soc.* **2003**, *125*, 5250-5251.

(2) Murphy, A.; Pace, A.; Stack, T. D. P. *Org. Lett.* **2004**, *6*, 3119-3122.

(3) Murphy, A.; Stack, T. D. P. *J. Mol. Catal. A* **2006**, *251*, 78-88.

(4) Ottenbacher, R. V.; Bryliakov, K. P.; Talsi, E. P. *Inorg. Chem.* **2010**, *49*, 8620-8628.

(5) Wu, M.; Wang, B.; Wang, S.; Xia, C.; Sun, W. *Org. Lett.* **2009**, *11*, 3622-3625.

(6) Saisaha, P.; de Boer, J. W.; Browne, W. R. *Chem. Soc. Rev.* **2013**, *42*, 2059-2074.

(7) Mas-Ballesté, R.; Que, L., Jr. *J. Am. Chem. Soc.* **2007**, *129*, 15964-15972.

(8) White, M. C.; Doyle, A. G.; Jacobsen, E. N. *J. Am. Chem. Soc.* **2001**, *123*, 7194-7195.

(9) Costas, M.; Que, L., Jr. *Angew. Chem., Int. Ed.* **2002**, *41*, 2179-2181.

(10) Company, A.; Gómez, L.; Güell, M.; Ribas, X.; Luis, J. M.; Que, L., Jr., Costas, M. *J. Am. Chem. Soc.* **2007**, *129*, 15766-15767.

(11) Jaafar, H.; Vileno, B.; Thibon, A.; Mandon, D. *Dalton Trans.* **2011**, *40*, 92-106.

(12) Chen, M. S.; White, M. C. *Science* **2007**, *318*, 783-787.

(13) Chen, K.; Que, L., Jr. *J. Am. Chem. Soc.* **2011**, *123*, 6327-6337.

(14) England, J.; Britovsek, G. J. P.; Rabadia, N.; White, A. J. P. *Inorg. Chem.* **2007**, *46*, 3752-3767.

(15) Britovsek, G. J. P.; England, J.; White, A. J. P. *Inorg. Chem.* **2005**, *44*, 8125-8134.

(16) Chen, K.; Que, L., Jr. *Chem. Commun.* **1999**, 1375-1376.

(17) He, Y.; Gorden, J. D.; Goldsmith, C. R. *Inorg. Chem.* **2011**, *50*, 12651-12660. Correction: *Inorg. Chem.* **2012**, *51*, 7431.

(18) He, Y.; Goldsmith, C. R. *Chem. Commun.* **2012**, *48*, 10532-10534.

(19) Lim, M. H.; Rohde, J.-U.; Stubna, A.; Bukowski, M. R.; Costas, M.; Ho, R. Y. N.; Münck, E.; Nam, W.; Que, L., Jr. *Proc. Natl. Acad. Sci. USA* **2003**, *100*, 3665-3670.

(20) Kumar, D.; Hirao, H.; Que, L., Jr.; Shaik, S. *J. Am. Chem. Soc.* **2005**, *127*, 8026-8027.

(21) Roelfes, G.; Vrajmasu, V.; Chen, K.; Ho, R. Y. N.; Rohde, J.-U.; Zondervan, C.; la Crois, R.M.; Schudde, E.P.; Lutz, M.; Spek, A. L.; Hage, R.; Feringa, B. L.; Münck, E.; Que, L., Jr. *Inorg. Chem.* **2003**, *42*, 2639-2653.

(22) Sastri, C. V.; Lee, J.; Oh, K.; Lee, Y. J.; Lee, J.; Jackson, T. A.; Ray, K.; Hirao, H.; Shin, W.; Halfen, J. A.; Kim, J.; Que, L., Jr.; Shaik, S.; Nam, W. *Proc. Natl. Acad. Sci. USA* **2007**, *104*, 19181-19186.

(23) Que, L., Jr. *Acc. Chem. Res.* **2007**, *40*, 493-500.

(24) Kaizer, J.; Klinker, E. J.; Oh, N. Y.; Rohde, J.-U.; Song, W. J.; Stubna, A.; Kim, J.; Münck, E.; Nam, W.; Que, L., Jr. *J. Am. Chem. Soc.* **2004**, *126*, 472-473.

(25) Lyakin, O. Y.; Bryliakov, K. P.; Talsi, E. P. *Inorg. Chem.* **2011**, *50*, 5526-5538.

(26) Chen, K.; Costas, M.; Kim, J.; Tipton, A. K.; Que, L., Jr. *J. Am. Chem. Soc.* **2002**, *124*, 3026-3035.

(27) Lee, Y.-M.; Hong, S.; Morimoto, Y.; Shin, W.; Fukuzumi, S.; Nam, W. *J. Am. Chem. Soc.* **2010**, *132*, 10668-10670.

(28) Zhang, Q.; Gorden, J. D.; Beyers, R. J.; Goldsmith, C. R. *Inorg. Chem.* **2011**, *50*, 9365-9373.

(29) Gosiewska, S.; Cornelissen, J. J. L. M.; Lutz, M.; Spek, A. L.; van Koten, G.; Klein Gebbink, R. J. M. *Inorg. Chem.* **2006**, *45*, 4214-4227.

(30) Connelly, N. G.; Geiger, W. E.; *Chem. Rev.* **1996**, *96*, 877-910.

(31) Goldsmith, C. R.; Coates, C. M.; Hagan, K.; Mitchell, C. A. *J. Mol. Catal. A* **2011**, *335*, 24-30.

(32) Jiang, W.; Gorden, J. D.; Goldsmith, C. R. *Inorg. Chem.* **2013**, *52*, 5814-5823.

(33) Jiang, W.; Gorden, J. D.; Goldsmith, C. R. *Inorg. Chem.* **2012**, *51*, 2725-2727.

(34) Dubois, G.; Murphy, A.; Stack, T. D. P. *Org. Lett.* **2003**, *5*, 2469-2472.

(35) Chen, M. S.; White, M. C. *Science* **2010**, *327*, 566-571.

(36) Das, P.; Que, L., Jr. *Inorg. Chem.* **2010**, *49*, 9479-9485.

(37) Linde, C.; Koliaï, N.; Norrby, P.-O.; Åkermark, B. *Chem. −Eur. J.* **2002**, *8*, 2568-2573.

(38) Yin, G.; Buchalova, M.; Danby, A. M.; Perkins, C. M.; Kitko, D.; Carter, J. D.; Scheper, W. M.; Busch, D. H. *J. Am. Chem. Soc.* **2005**, *127*, 17170-17171.

(39) Park, M. J.; Lee, J.; Suh, Y.; Kim, J.; Nam, W. *J. Am. Chem. Soc.* **2006**, *128*, 2630-2634.

(40) He, Y.; Goldsmith, C. R. *Synlett* **2010**, *21*, 1377-1380.

Chapter 4

C-H Oxidation by H_2O_2 and O_2 Catalyzed by a Non-Heme Iron Complex with a Sterically Encumbered Tetradentate N-Donor Ligand*

* This Chapter's content was previously published in the following manuscript:

Zhang, Q.; Gorden, J. D.; Goldsmith, C. R. *Inorg. Chem.* **2013**, *52*, 13546-13554.

4.1 Introduction

The ability of mononuclear non-heme iron hydroxylases to catalyze the regio- and stereoselective activation of C-H bonds by O_2 has inspired many synthetic chemists to explore functional small molecule mimics of these enzymes.[1,2] Most reported mononuclear non-heme iron catalysts use H_2O_2 as a terminal oxidant for alkane oxidation instead of O_2. The few examples of non-heme iron-catalyzed hydrocarbon oxidation by O_2 have thus far required either a sacrificial reductant[3,4] or a weak C-H bond on the substrate.[5-9] The selectivity of the hydroxylase-catalyzed oxidation has also been difficult to replicate, and most small molecule catalysts simply direct the oxidation towards the weakest C-H bonds of their hydrocarbon substrates. Systems with alternate preferences are rare; as a consequence, the application of non-heme iron catalyzed C-H bond activation within organic synthesis has thus far been limited to a few instances.[10-12]

In an effort to tune the regioselectivity of the oxidation towards less sterically hindered but thermodynamically stronger C-H bonds, our research group previously prepared the bulky tetradentate ligand *N*,*N*'-di(phenylmethyl)-*N*,*N*'-bis(2-pyridinylmethyl)-1,2-cyclohexanediamine (bbpc) and its ferrous complex $[Fe(bbpc)(MeCN)_2](SbF_6)_2$.[13] The bbpc complex is capable of catalyzing the oxidation of hydrocarbons by either H_2O_2 or O_2, with the O_2 reactivity requiring a tertiary aliphatic or weaker C-H bond on the substrate.[9,13] The bulk of the benzyl groups and cyclohexane ring of bbpc were found to guide the H_2O_2-driven oxidation towards secondary carbons over tertiary carbons to a greater extent than had been previously observed with non-heme iron catalysis. We attributed this to steric repulsions between the generated iron-based oxidant and the relevant portions of the substrates. Despite these intermolecular repulsions, tertiary carbon oxidation is still favored over secondary carbon oxidation with certain substrates, such as *cis*-1,2-

dimethylcyclohexane and adamantane. Similarly, substrates with aliphatic C-H bonds on primary and secondary carbons are oxidized exclusively on the secondary carbons.

In an effort to shift the catalyzed oxidation even farther away from the C-H bonds on tertiary carbons, we prepared the ligand *N*,*N*'-bis(2-pyridylmethyl)-*N*,*N*'-bis(neopentyl)-1,2-ethanediamine (dnbpn, Scheme 4.1), which has even bulkier neopentyl groups[14,15] installed on the amine N-donors. We were unable to prepare an analogous compound with a 1,2-cyclohexanediamine backbone, thereby necessitating the 1,2-ethanediamine linkage. We subsequently prepared the complex [Fe(dnbpn)$(OTf)_2$] and investigated its ability to catalyze C-H activation by both H_2O_2 and O_2.

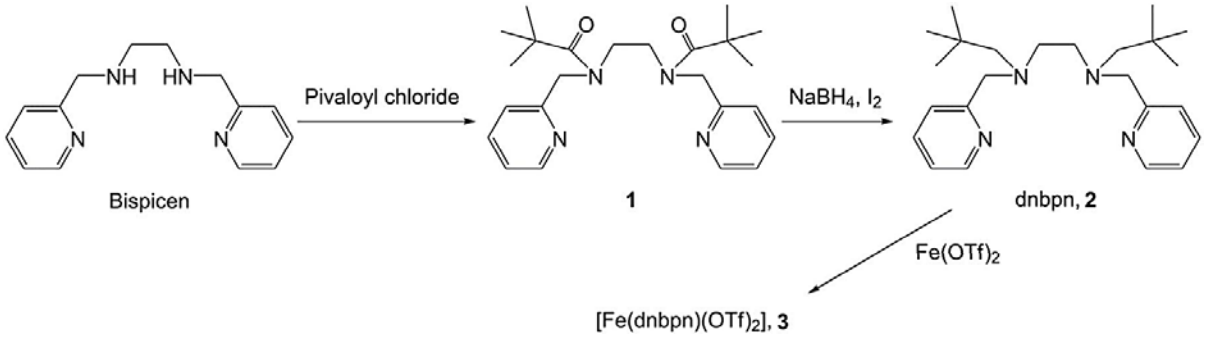

Scheme 4.1

4.2 Experimental Section

Materials

Except where noted otherwise, chemicals were purchased from Sigma-Aldrich and used as received. 9,10-Dihydroanthracene (DHA) was crystallized twice from ethanol (EtOH) prior to its use. Anhydrous acetonitrile (MeCN) was purchased from Acros Organics and stored in a glovebox free of moisture and oxygen. Hydrogen peroxide (H_2O_2, 50% wt) was bought from Fisher. Dry nitrogen (N_2) and oxygen (O_2) were purchased from Airgas. Tetrahydrofuran (THF) was dried

over 4 Å molecular sieves. Chloroform-*d* ($CDCl_3$), acetonitrile-*d3* (CD_3CN), and cyclohexane-*d12* (C_6D_{12}) were bought from Cambridge Isotopes. Tetradeuterated 9,10-dihydroanthracene (DHA-*d4*) was synthesized using a previously reported procedure.[16] *trans*-1,2- Dimethylcyclohexane was purchased from TCI America. *N*,*N*'-Bis(2-pyridinylmethyl)-1,2-ethanediamine (bispicen) and *N*,*N*'-bis(2-pyridylmethyl)-1,2-cyclohexanediamine were synthesized as described previously.[17,18]

Instrumentation

^1H and ^{13}C nuclear magnetic resonance (NMR) spectra were recorded on either a 400 MHz or a 250 MHz AV Bruker NMR spectrometer at 295 K. A Varian Cary 50 spectrophotometer was used to collect optical data, which were processed and analyzed using software from the WinUV Analysis Suite. A Thermo Scientific Trace GC Ultra Gas Chromatograph and Thermo Scientific TR-1 and TG-WAXMS columns were used for gas chromatography (GC). A Johnson Matthey magnetic susceptibility balance (model MK I#7967) was used to measure the magnetic moments of solid samples. Electron paramagnetic resonance (EPR) spectra were collected on a Bruker EMX-6/1 X-band EPR spectrometer operated in the perpendicular mode. High-resolution mass spectrometry (HR-MS) data were collected at the Mass Spectrometer Center at Auburn University on a Bruker microflex LT MALDI-TOF mass spectrometer via direct probe analysis operated in the positive ion mode. Crystalline samples were dried, stored under N_2, and sent to Atlantic Microlabs (Norcross, GA) for elemental analysis. A Renishaw inVia Raman microscope was used for the described Raman spectroscopy. A wavelength-stabilized high power laser diode system (model SDL-8530, SDL Inc.) provided the 785 nm excitation for resonance Raman spectroscopy. Control studies used an air-cooled argon ion laser (model 163-C42, Spectra-Physics Lasers, Inc.) to provide 514 nm excitation. All samples were run at 22 °C. Raman signals were accumulated for 10 s.

Crystallographic Studies

Single crystals of **3** were mounted on CryoLoops with Krytox oil and optically aligned on a Bruker APEXII Quazar X-ray diffractometer using a digital camera. Initial intensity measurements were performed using an IμSX-ray source, a 30 W microfocused sealed tube (MoKα, λ = 0.71073 Å) with high-brilliance and high-performance focusing Quazar multilayer optics. Standard APEXII software was used for determination of the unit cells and data collection control. The intensities of reflections of a sphere were collected by a combination of four sets of exposures (frames). Each set had a different φ angle for the crystal, and each exposure covered a range of 0.5° in ω. A total of 1464 frames were collected with an exposure time per frame of 20 to 60 s, depending on the crystal. The SAINT software was used for data integration including Lorentz and polarization corrections. Semi-empirical absorption corrections were applied using the program SADABS or TWINABS. Selected crystallographic information is listed on Tables 4.1 and 4.2.

Synthesis

***N,N'*-Bis-(2,2-dimethylpropanamide)-*N,N'*-bis(2-pyridylmethyl)-1,2-ethanediamine (1)**. The synthesis was inspired by that used to prepare the related compound (1*R*,2*R*)-*N*,*N*'-dineopentyl-1,2-cyclohexanediamine.[19] Bispicen (2.42 g, 10.0 mmol) and NaOH (0.80 g, 20 mmol) were dissolved in 50 mL of H_2O. Pivaloyl chloride (12.5 g, 100 mmol) was slowly added to the aqueous solution and heated at 50 °C for 12 h. The reaction was allowed to cool to room temperature (RT), after which a 2.0 M NaOH solution was added dropwise to increase the pH to 10. The product was extracted with three 50 mL portions of methylene chloride (CH_2Cl_2). The combined extracts were dried over Na_2SO_4. The solution was filtered, and the CH_2Cl_2 was removed through rotavaporation. The residue was washed with 30 mL of diethyl ether (Et_2O) and

dried to yield the product as a white solid (1.72 g, 42% yield). ^{1}H NMR ($CDCl_3$, 400 MHz): 8.53 (2H, d, *J* = 2.8 Hz), 7.65 (2H, t, *J* = 7.2 Hz), 7.17 (2H, t, *J* = 6.0 Hz), 7.13 (2H, d, *J* = 8.0 Hz), 4.83 (4H, s), 3.60 (4H, s), 1.27 (18H, s). ^{13}C NMR ($CDCl_3$, 100 MHz): 176.28, 157.75, 149.59, 136.77, 122.26, 120.88, 53.98, 46.40, 39.08, 28.53. HR-MS (ESI): Calcd MH^+ 411.2760; Found 411.2774.

***N,N'*-Dineopentyl-*N,N'*-bis(2-pyridylmethyl)-1,2-ethanediamine (dnbpn, 2). 1** (2.05 g, 5.00 mmol) and $NaBH_4$ (0.95 g, 25 mmol) were dissolved in 50 mL of THF. A 20 mL solution of I_2 (3.18 g, 12.5 mmol) in THF was added dropwise over 15 min at 0 °C. After the addition was complete, the resultant mixture was heated at 65 °C for 48 h. The reaction was cooled to 25 °C and 20 mL of methanol (MeOH) were added to quench the residual $NaBH_4$. The organic solvents were removed *in vacuo*. The residue was washed with 30 mL of Et_2O and extracted with three 50 mL portions of 1.0 M HCl. The acidic extracts were made basic (pH 10) through the addition of 2.0 M NaOH. The product was extracted from the basic solution by three 50 mL portions of CH_2Cl_2. After the organic layers were dried over Na_2SO_4 and filtered, the CH_2Cl_2 was removed to yield the product as a white solid (1.70 g, 89% yield). ^{1}H NMR ($CDCl_3$, 400 MHz): 8.47 (2H, d, *J* = 6.4 Hz), 7.60 (2H, t, *J* = 7.6 Hz), 7.48 (2H, t, *J* = 7.6 Hz), 7.11 (2H, d, *J* = 6.4 Hz), 3.75 (4H, s), 2.60 (4H, s), 2.27 (4H, s), 0.79 (18 H, s). ^{13}C NMR ($CDCl_3$, 100 MHz): 161.05, 148.72, 136.22, 122.60, 121.66, 67.97, 63.86, 33.06, 30.31, 28.12. HR-MS (ESI): Calcd MH^+: 383.3175; Found: 383.3092.

***cis*-(*N,N'*-Dineopentyl-*N,N'*-bis(2-pyridylmethyl)-1,2-ethanediamine) bis(trifluoromethanesulfonato)iron(II) ([Fe^{II}(dnbpn)$(OTf)_2$], 3)**. The dnbpn ligand (0.382 g, 1.00 mmol) and $Fe(OTf)_2$ (0.416 g, 1.00 mmol) were combined under N_2 and dissolved in 5 mL of MeCN and 5 mL of CH_2Cl_2. The mixture stirred under N_2 for 2 h, turning brown during the course of the reaction. After this time, 15 mL of Et_2O was added. Brown crystals of the product deposited from this solution; these were suitable for single crystal X-ray diffraction (0.618 g, 84%).

Solid-state magnetic susceptibility (295 K): μ_{eff} = 4.6 μB. Optical spectroscopy (MeCN, 295 K): 350 nm, 850 M^{-1} cm^{-1}. Elemental Analysis: Calcd for $C_{26}H_{38}FeF_6N_4O_6S_2 \cdot 2H_2O$: C, 40.42%; H, 5.48%; N, 7.25%; Found: C, 40.27%; H, 5.41%; N, 7.09%.

Reactivity

Three different reactivity protocols were used in order to facilitate comparison of the catalysis to previously reported results from ourselves and others.

The general procedure for the iron-catalyzed oxidation of hydrocarbons by H_2O_2 involved mixing 0.010 mmol of **3**, 10.0 mmol of the substrate, and 1.0 mmol of 1,2- dichlorobenzene in 9.0 mL of anaerobic MeCN. The 1,2-dichlorobenzene serves as an internal standard; it was found to be chemically inert under our reaction conditions. When the solids had completely dissolved, a degassed solution of 100 mM H_2O_2 in 1.0 mL of MeCN was added dropwise over 45 s. The starting concentrations of the iron catalyst, substrate, and terminal oxidant were therefore 1.0 mM, 1000 mM, and 10 mM, respectively. For select reactions, a lower concentration of substrate or a higher concentration of H_2O_2 was used. The reaction mixture was allowed to stir for 30 min at 298 K under N_2. At this point, a 2.0 mL aliquot of the reaction mixture was passed through a plug of silica gel in order to remove the metal species and residual terminal oxidant. This workup did not selectively remove any of the organic starting materials, organic products, or the internal standard from the reaction mixture, as confirmed by parallel NMR analysis and GC analysis of controls consisting of mixtures of the organic starting materials and products. The colorless filtrate was subsequently analyzed by GC to determine the identities and yields of each organic product. The organic products were identified by matching their GC retention times to those of authentic standards. All reported yields are the averages of at least three independent runs.

A modified procedure in which the catalyst and H_2O_2 were added in three portions was used for the oxidations of *cis*- and *trans*-1,2-dimethylcyclohexane, tertbutylcyclohexane, and 1,1-dimethylcyclohexane by H_2O_2. The alternative procedure was used in order to allow comparison of the results to prior work.[10,13] 0.025 mmol of **3**, 0.50 mmol of substrate, and 1.0 mmol of 1,2-dichlorobenzene were combined in 0.75 mL of MeCN. 0.60 mmol of H_2O_2 in 4.5 mL MeCN was added over 60 s. After 10 min, an additional 0.025 mmol of **3** and 0.60 mmol of H_2O_2 were added as a solution in 5.0 mL of MeCN. At 20 min, another 0.025 mmol of **3** and 0.60 mmol of H_2O_2 were added as a solution in 5.0 mL of MeCN. At 30 min, the reaction was quenched through the addition of excess Et_2O. Aliquots of the solution were passed through a plug of silica gel and analyzed by GC in the manner described above. All reactions were repeated at least thrice.

The procedure for the iron-catalyzed oxidation of hydrocarbons by O_2 used solutions containing 0.010 mmol of **3**, 5.0 mmol of substrate, and 1.0 mmol of 1,2-dichlorobenzene in 10 mL of MeCN. In some cases, a lower concentration of substrate was used to accommodate their limited solubility. A 200 mL balloon of dry O_2 was connected to the airtight vessel in order to start the reaction. After 30 min reaction, a 2.0 mL aliquot of the solution was passed through a plug of silica gel, and the filtrate was analyzed as described above. All reported values are the averages of at least three different reactions.

4.3 Results

Synthesis

The dnbpn ligand **2** can be prepared in two steps from the commonly used and readily synthesized bispicen compound (Scheme 4.1).[17,20-22] The overall yield is approximately 35%, with the addition of the pivaloyl groups being the less efficient of the two steps. The reduction of

intermediate **1** to **2** was relatively difficult. The reaction between **1** and BH_3•THF failed to reduce the carbonyls. The stronger reductants produced from a mixture of $NaBH_4$ and I_2 sufficed,[19,23,24] but the reduction required the reaction mixture to be heated at 65 °C for two days. One benefit of the synthetic route is that **2** can be isolated in high purity without chromatography.

The incorporation of iron(II) into the dnbpn ligand is straightforward. Upon combining **2** and $Fe(OTf)_2$ in an anaerobic 1:1 mixture of MeCN and CH_2Cl_2, the [Fe(dnbpn)$(OTf)_2$] product **3** can be crystallized directly from the reaction solution in high yield (>80%). The formation of **3** does not require elevated temperatures, and the anaerobic atmosphere may not be strictly necessary since solutions of the complex do not discolor upon prolonged exposure to air.

Given the conformational flexibility associated with the ethylenediamine linkage[22] and its potential to facilitate intramolecular oxidation at the expense of substrate oxidation,[25] we attempted to make an analog of dnbpn with a more rigid 1,2-cyclohexanediamine backbone.[26] When *N*,*N*'-bis(2-pyridylmethyl)-1,2-cyclohexanediamine[18] was substituted for bispicen in the synthetic route shown on Scheme 4.1, only one pivaloyl arm was installed onto the diamine, even when reaction times were extended beyond 12 h. This compound was subsequently reduced to *N*-neopentyl-*N*,*N*'-bis(2-pyridylmethyl)-1,2-cyclohexanediamine (**4**). An alternative route proceeding through *N*,*N*'-di(neopentyl)-1,2-cyclohexanediamine was likewise unsuccessful. Reaction of this intermediate with excess picolyl chloride resulted in only *N*,*N*'-di(neopentyl)-*N*-(2-pyridylmethyl)-1,2-cyclohexanediamine (**5**).

Compound **4** reacts with $Fe(OTf)_2$ to yield a 1:1 ligand/metal complex. Preliminary studies indicated that the complex with **4** was a poor catalyst for the oxidation of cyclohexane by H_2O_2; consequently, we did not pursue further studies. Compound **5** yielded a catalytically inactive 2:1

ligand/metal adduct, as assessed by a spectrophotometric titration. Given its inability to accelerate alkane oxidation, the complex with **5** was likewise not investigated further.

Structural Characterization

Complex **3** crystallizes readily upon adding Et_2O to the reaction mixture (Figure 4.1 and Table 4.1). Each asymmetric unit contains three unique molecules of composition [Fe(dnbpn)$(OTf)_2$]. The three Fe(II)-containing molecules strongly resemble each other, with only minor differences in their metrical parameters (Table 4.2). Each Fe(II) center is hexacoordinate, with the dnbpn ligand providing four donor atoms. The coordination geometry may be best described as a distorted octahedron. Each equiv. of **2** coordinates to a metal center in a *cis*-α conformation, with the two pyridine moieties *trans* to each other and the triflates *cis* to each other. This ligand conformation is commonly seen in first-row transition metal complexes with bispicen and its close derivatives.[20-22,27-29]

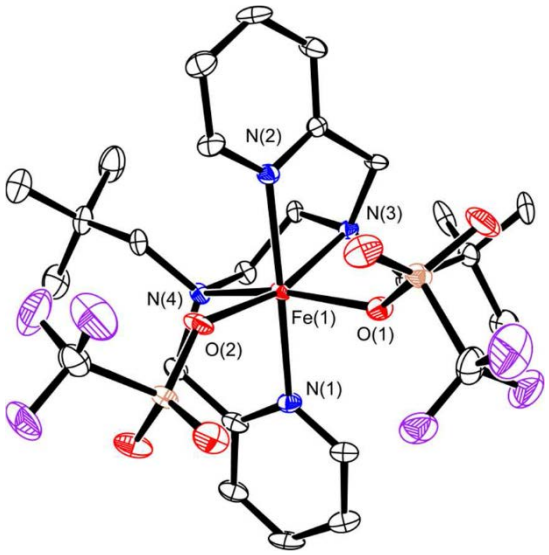

Figure 4.1. ORTEP representation of [Fe(dnbpn)$(OTf)_2$] (subunit A). All hydrogen atoms and the other two subunits have been removed for clarity. All thermal ellipsoids are drawn at 50% probability. The CCDC number of [Fe(dnbpn)$(OTf)_2$] is 968574.

Table 4.1. Selected Crystallographic Data for [Fe(dnbpn)$(OTf)_2$] (**3**).

parameter	[Fe(dnbpn)$(OTf)_2$]
formula	$C_{26}H_{38}F_6FeN_4O_6S_2$
MW	736.57
cryst. syst.	monoclinic
space group	$P2_1/c$ (#14)
a (Å)	30.947(15)
b (Å)	14.850(7)
c (Å)	23.242(11)
α (deg)	90
β (deg)	107.758(9)
γ (deg)	90
V (Å^3)	2915.0(5)
Z	12
crystal color	brown
T (K)	100
reflns collected	23306
unique reflns	12472
$R1$ (F, I > 2σ(I))[a]	0.0733
w$R2$ (F^2, all data)[a]	0.2276

[a] $R1 = \Sigma||F_o| - |F_c||/\Sigma|F_o|$; w$R2 = [\Sigma w(F_o^2 - F_c^2)^2/\Sigma w(F_o^2)^2]^{1/2}$.

The Fe-N bonds average ~2.21 Å, consistent with high-spin Fe(II) centers (Table 4.2). The spin-state assignment is corroborated by the 4.6 μB magnetic moment measured for solid samples of **3**. The Fe-N bonds for the amines and pyridines fall within narrow ranges: 2.246 ~ 2.274 Å for the amines and 2.141 ~ 2.168 Å for the pyridines. The six Fe-O bond lengths for the triflates

likewise show little variety, ranging from 2.109 to 2.126 Å. The Fe-O bonds are shorter than the Fe-N bonds, as would be anticipated from the negative charges on the triflates.

Table 4.2. Selected Bond Lengths for the Three [Fe(dnbpn)$(OTf)_2$] Molecules (Å)

subunit	A	B	C
Fe-N(1)	2.160(4)	2.141(4)	2.160(4)
Fe-N(2)	2.161(4)	2.161(4)	2.168(4)
Fe-N(3)	2.254(4)	2.250(4)	2.246(4)
Fe-N(4)	2.258(4)	2.259(4)	2.274(4)
Fe-O(1)	2.119(3)	2.122(3)	2.126(4)
Fe-O(2)	2.109(3)	2.111(3)	2.111(4)

The donor atoms relabeled from their CIF designations to facilitate comparison. N(1) and N(2) correspond to pyridine nitrogens; N(3) and N(4) correspond to amine nitrogens.

Catalysis of Hydrocarbon Oxidation by Hydrogen Peroxide

Complex **3** was tested as a catalyst for hydrocarbon oxidation by H_2O_2 and O_2. The ability of **3** to catalyze the oxidation of various aliphatic, allylic, and benzylic substrates by H_2O_2 is summarized on Table 4.3. In non-heme iron oxidative catalysis, the oxidation of cyclohexane by H_2O_2 is commonly used as a comparative standard.[30-34] By this standard, **3** is a poor catalyst relative to other reported non-heme iron complexes with tetradentate N-donor ligands, for it only turns over 0.5 times when 10 equiv. of H_2O_2 are added. A kinetic isotope effect (KIE) of 3.3 was measured from competition experiments between cyclohexane and cyclohexane-*d12* (C_6D_{12}). The ratio of cyclohexanol to cyclohexanone with this loading of terminal oxidant is 3:1, which is typical for a mononuclear non-heme iron catalyst. The activity does improve as the strength of the activated C-H bond weakens, and the allylic and benzylic bonds of cyclohexene and cumene are

most susceptible to oxidation among the investigated substrates. No alkene epoxidation is observed when cyclohexene is used as a substrate.

Table 4.3. Catalytic Oxidation of Hydrocarbons by H_2O_2.[a]

Substrate	$[H_2O_2]$ (mM)	Product(s)	Turnover Number (TON)
	10	cyclohexanol	0.3
		cyclohexanone	0.1
		overall	0.5
	100	cyclohexanol	1.0
		cyclohexanone	0.3
		overall	1.6
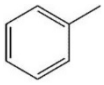	10	benzyl alcohol	0.05
		benzaldehyde	0.30
		overall	0.65
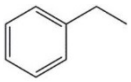	10	2-phenyl-2-ethanol	0.5
		acetophenone	0.4
		overall	1.3
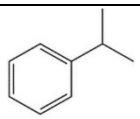	10	2-phenyl-2-propanol	2.9
		overall	2.9
[b] 	10	2-adamantanol(one)	0.2
		1-adamantanol	0.5
		overall	0.7
	10	2-cyclohexanol	4.5
		2-cyclohexanone	2.1
		overall	8.7

[a]Starting concentrations of **3** and the substrate were 1.0 mM and 1000 mM, respectively. The H_2O_2 was added in one portion at the beginning of the reaction. All reactions proceeded in MeCN at 298 K under N_2. The yields were measured by GC after 30 min. [b]Starting concentration of substrate was 10 mM, due to the limited solubility of adamantane in MeCN.

Table 4.4. Regioselectivity of Hydrocarbon Oxidation Catalyzed by **3**.[a]

Substrate	Products	TON
	*trans*-1,2-dimethylcyclohexanol	0.32
	cis-1,2-dimethylcyclohexanol	0.17
	cis-2,3-dimethylcyclohexanone	0.91
	cis-3,4-dimethylcyclohexanone	0.16
	*trans*-1,2-dimethylcyclohexanol	0.42
	cis-1,2-dimethylcyclohexanol	0.48
	trans-2,3-dimethylcyclohexanone	1.39
	trans-3,4-dimethylcyclohexanone	1.85
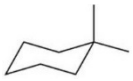	2,2-dimethylcyclohexanone	0.1
	3,3-dimethylcyclohexanone	0.5
	4,4-dimethylcyclohexanone	0.9
	3-*tert*-butylcyclohexanone	trace
	4-*tert*-butylcyclohexanone	1.2

[a]All reactions proceeded in MeCN at 298 K under N_2. The yields were measured by GC 30 min after the beginning of the reaction. Complex **3** and H_2O_2 were added in three portions as described in the Reactivity portion of the Experimental Section.

The tertiary and secondary carbons of adamantane are oxidized in a 5:2 ratio. Normally, non-heme iron catalysts direct the oxidation heavily towards the tertiary carbons, with typical tertiary:secondary ratios ranging from 15:1 to 30:1.[31,35] The ability of **3** to direct catalyzed oxidation towards less sterically congested secondary carbons was also tested using a protocol developed by Chen and White[10] and subsequently employed in two studies from our own laboratory.[13,36] The substrates *cis*-1,2-dimethylcyclohexane, *trans*-1,2-dimethylcyclohexane, 1,1-dimethylcyclohexane, and *tert*-butylcyclohexane were used to determine how steric repulsions between the catalyst and the substrate influenced the regioselectivity of the oxidation (Table 4.4).

Both 1,2-dimethylcyclohexanes are oxidized preferentially on the secondary carbons; this represents the first instance where the *cis* isomer has been oxidized predominantly on the secondary carbons in non-heme iron catalysis. The retention of configuration (RC), which was previously defined as [(1*R*,2*R* + 1*S*,2*S*) - (1*R*,2*S* + 1*S*,2*R*)] / (total amount of tertiary alcohol),[31] was found to be 82% for the cis isomer. The γ carbon of 1,1-dimethylcyclohexane is most reactive when **3** is used to catalyze its oxidation by H_2O_2, accounting for 60% of the organic products. Similarly, only the γ carbon of *tert*-butylcyclohexane is oxidized to a significant degree, with no observed oxidation of the carbons α to the *tert*-butyl group and only trace oxidation of the β carbons.

Catalysis of Hydrocarbon Oxidation by Dioxygen

We tested the ability of complex **3** to catalyze the oxidation of C-H bonds by O_2. The dnbpn complex was unable to promote the oxidation of aliphatic C-H bonds, even those on tertiary carbons. Cyclohexane and the two isomers of 1,2-dimethylcyclohexane failed to react when O_2 was present as the sole potential terminal oxidant. Allylic and benzylic C-H bonds, conversely, do react (Table 4.5). Using the reactivity of cyclohexene as a comparative standard, the oxidation by O_2 is noticeably slower than the oxidation by H_2O_2, with lower yields of both 2-cyclohexenol and 2-cyclohexenone at 30 min. The reactivity continues past 30 min, although the activity seems to decrease slightly over time (Figure 4.2). When 9,10-dihydroanthracene (DHA) is used as the substrate, anthrone is the major product, although there are substantial amounts of both anthracene and anthraquinone. A KIE of 4.5 was calculated from competition experiments between DHA and its tetradeuterated analog, DHA-*d4*.[16]

Table 4.5. Catalytic Oxidation of Hydrocarbons by O_2.[a]

Substrate	Times (min)	Products	TON
	30	2-cyclohexanol	1.8
		2-cyclohexanone	0.4
	120	2-cyclohexanol	4.5
		2-cyclohexanone	1.7
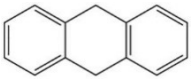	120	anthracene	22
		anthrone	30
		anthraquinone	12

[a]Reaction conditions: $[\text{cyclohexene}]_o$ = 500 mM; $[\text{DHA}]_o$ = 100 mM. $[\mathbf{3}]_o$ = 1.0 mM. All reactions were run in MeCN at 298 K. The concentration of O_2 was approximately 8 mM throughout the reaction.[37]

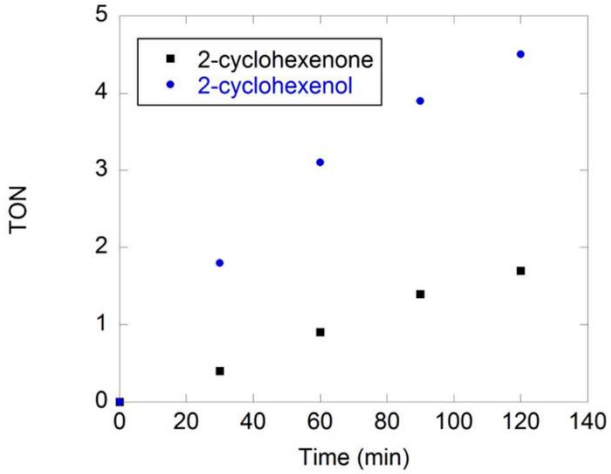

Figure 4.2. Oxidation of cyclohexene by O_2 catalyzed by **3**. The reaction conditions are identical to those described for Table 4.5. The errors in each TON are ±0.1.

Characterization of Intermediates

We attempted to locate and identify the metal-based oxidants relevant to the catalysis. Often, ferric hydroperoxide species and other high-valent iron oxidants can be detected when a terminal oxidant and a ferrous complex are combined in the absence of substrate.[13,35,38-41] When H_2O_2 and **3** were mixed in MeCN, no distinctive low-energy UV/Vis features were observed. Parallel analysis with mass spectrometry (MS) revealed that the dnbpn ligand in **3** is heavily

oxidized within 2 min from the start of the reaction. There are several *m*/*z* features that are consistent with methylene group oxidation and 2,2-dimethylpropanol, an anticipated product of neopentyl oxidation. Combining **3**, O_2, and a substrate with a weak C-H bond, such as cyclohexene, likewise does not result in a detectable intermediate; this approach had successfully produced a Fe(III)OOH species from our previously reported $[Fe(bbpc)(MeCN)_2]^{2+}$ complex.[9] Following a procedure described by Martinho, Blain, and Banse,[42] we also attempted to generate an Fe(III)OOH species by reacting **3** with O_2, $HClO_4$, and the electron donor $NaBPh_4$ but were likewise unsuccessful. As with the **3**/H_2O_2 mixture, only ligand decomposition is observed in the O_2 reactions.

Although the direct reaction between H_2O_2 and **3** failed to generate a detectable intermediate, the addition of a substrate with a weak C-H bond appeared to stabilize such a species. The combination of **3**, H_2O_2, and either cumene, ethylbenzene, or triphenylmethane resulted in a transient species with an UV/Vis feature at 690 nm (Figure 4.3). When 100 mM cumene was present, this feature had a peak ε of 170 M^{-1} cm^{-1} and half-life of 20 min at room temperature. With other substrates, the peak ε for the 690 nm band is lower: 160 M^{-1} cm^{-1} for ethylbenzene and 100 M^{-1} cm^{-1} for triphenylmethane. Parallel analysis of the cumene reaction with EPR showed two features with g = 4.28 and g = 1.99 (Figure 4.4). The g = 4.28 resonance is consistent with a rhombic, high-spin Fe(III) species. The g = 1.99 feature, conversely, is more consistent with an organic radical. MS analysis of the reaction mixture failed to find peaks that were unambiguously consistent with a higher-valent iron species. The MS, however, lacks many of the ligand decomposition *m*/*z* features observed in the absence of cumene.

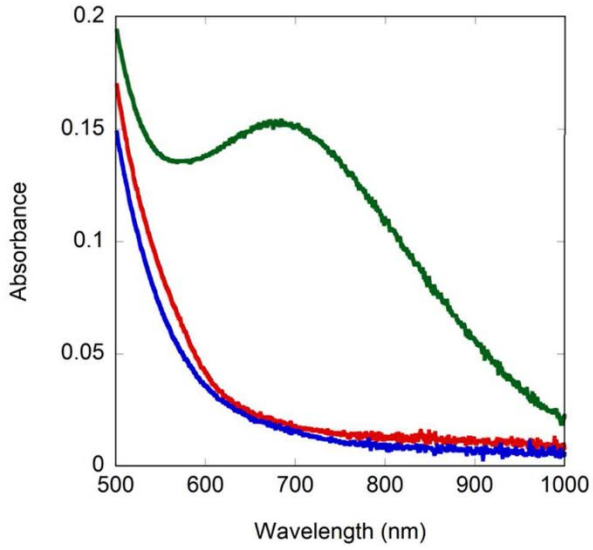

Figure 4.3. Comparative UV/vis plots of 1.0 mM **3** (red), 1.0 mM **3** plus 10 mM H_2O_2 (blue), and 1.0 mM **3** plus 10 mM H_2O_2 plus 100 mM cumene (green). All data were obtained from 294 K MeCN solutions. Both of the solutions containing H_2O_2 were scanned 120 s after the reagents were combined.

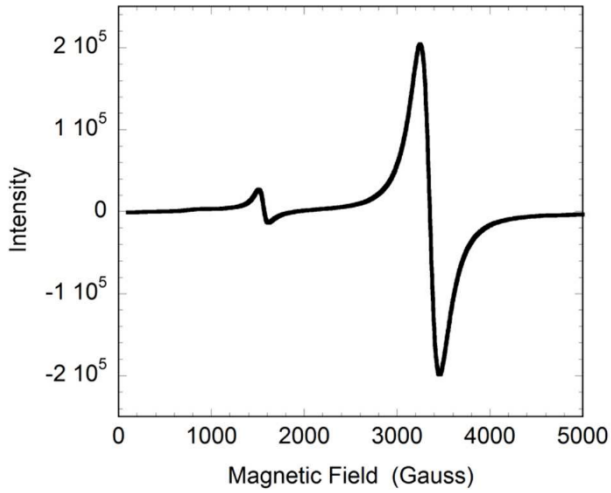

Figure 4.4. X-Band EPR spectrum of a 77 K solution of 1.0 mM **3**, 2 mM H_2O_2, and 50 mM cumene in MeCN. The sample was frozen for analysis 60 s after the reagents were mixed. g_1 = 4.28, g_2 = 1.99.

Resonance Raman spectroscopy detected features that are consistent with an iron species with an O-O bond (Figure 4.5). When 100 mM ethylbenzene is combined with 10 mM H_2O_2 and 2.0 mM **3** in MeCN, two vibrations at 637 cm^{-1} and 843 cm^{-1} are observed when the sample is exposed to 785 nm light but not when the sample was irradiated with 514 nm photons. Control

studies on samples without **3** indicated that these were not attributable to the excess H_2O_2, MeCN, or ethylbenzene. The MeCN and H_2O_2 do account for the features at 752 and 870 cm^{-1}, respectively; whereas, the ethylbenzene provides the features at 623 and 769 cm^{-1}. The resonance Raman spectrum of a sample prepared with 100 mM cumene in place of the ethylbenzene contains much weaker features, with a reproducible band at 844 cm^{-1}.

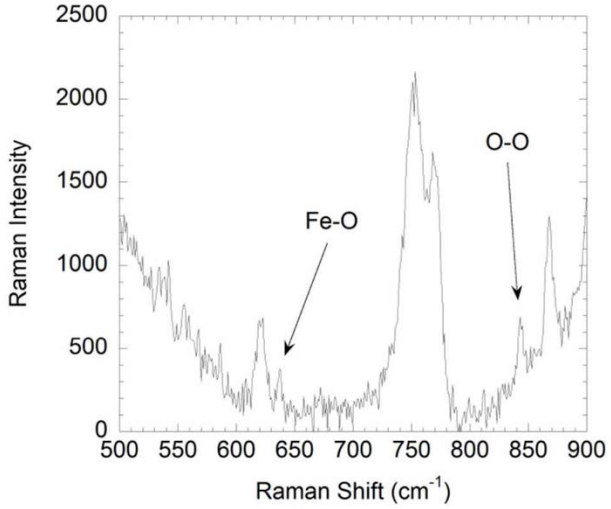

Figure 4.5. Resonance Raman spectroscopy of the intermediate generated from the reaction between 2.0 mM **3**, 10 mM H_2O_2, and 100 mM ethylbenzene in MeCN. The data were acquired 30 s after the reagents were mixed. The sample was irradiated with 785 nm photons. All assigned features were reproduced in three independently prepared samples.

4.4 Discussion

The dnbpn ligand **2** can be synthesized in two steps from the compound bispicen (Scheme 4.1).[17] The preparation of **2** is complicated by the low yield of the pivaloyl group installation and the resistance of these groups to subsequent reduction. Both **2** and its immediate precursor **1** can be isolated with relative ease. The ethylenediamine linkage between the picolyl groups is not ideal, as we previously found that ligands employing such backbones were conformationally dynamic.[22] The dynamism can potentially destabilize higher-valent oxidants by rendering them more susceptible to intramolecular decomposition processes.[25] We unsuccessfully attempted to prepare

analogs of **2** with a less flexible 1,2-cyclohexanediamine backbone.[26] Regardless of whether the neopentyl or picolyl arms were added first, we were able to install only three of the four desired functional groups on the amine nitrogens. The syntheses highlight a difficulty of installing highly bulky groups onto a ligand framework; at a certain point, repulsions between these groups appear to preclude further functionalization.

Crystals of **3** contain three symmetrically distinct molecules of [Fe(dnbpn)$(OTf)_2$]. The three molecules in each asymmetric unit strongly resemble each other; each has metrical parameters consistent with a high-spin Fe(II) center coordinated in a distorted octahedral geometry. To the best of our knowledge, **3** represents the first instances of neopentyl-substituted amines binding to an Fe(II) ion. Unlike the ferrous complexes with the likewise sterically encumbered bbpc, no large disparities in the Fe-N or Fe-O bonds are observed in any of the subunits in the crystal structures.[13] Instead, the Fe-N_{py}, Fe-N_{am}, and Fe-O bond lengths all fall within three narrow ranges (Table 4.2). Further comparison of the [Fe(dnbpn)$(OTf)_2$] and [Fe(bbpc)$(OTf)_2$] structures is complicated by the different ligand topologies. The dnbpn ligand is bound to Fe(II) in a *cis*-α fashion; whereas, the bbpc ligand coordinates in a *trans* mode in the triflate structure.[13]

Although complex **3** does not accelerate hydrocarbon oxidation by H_2O_2 to the same extent as other reported non-heme iron compounds,[13,30-34] the observed oxidation displays unusually high regioselectivity for the less sterically congested C-H bonds found on secondary carbons. We attribute the observed regioselectivity to the presence of the two neopentyl groups on the amines. These are generally perceived as being larger than methyl groups and benzyl groups[14,15] and would be anticipated to limit the access of more sterically congested C-H bonds to the active portion of the generated oxidants. To the best of our knowledge, complex **3** directs the catalyzed oxidation

to the secondary carbons of adamantane to a greater extent than any other reported mononuclear non-heme iron catalyst, besting the 3.3:1 ratio of tertiary to secondary oxidation reported for $[Fe(N4Py)(MeCN)]^{2+}$ and the 5:1 ratio reported for $[Fe(bbpc)(MeCN)_2]^{2+}$.[13,35] The diagnostic substrates *cis*- and *trans*-1,2-dimethylcyclohexane are also oxidized preferentially on the secondary carbons. As seen in Table 4.6, the dnbpn complex is the first non-heme iron catalyst that directs oxidation towards the secondary carbons of the cis isomer; with other non-heme iron catalysts the tertiary alcohols are the major products.[10,13,31] The ability to preferentially promote oxidation of the secondary carbons of the trans isomer is also strong, but inferior to that of the previously reported $[Fe(bbpc)(MeCN)_2]^{2+}$.[13] Although the 82% RC for the oxidation of *cis*-1,2-dimethylcyclohexane is relatively low for a non-heme iron catalyst, similar values have been reported for mononuclear non-heme iron catalysts with bulky N-donor ligands.[31] These smaller RC values are generally associated with longer-lived radical intermediates; however, the 82% retention of configuration is much higher than the sub-20% values that would be anticipated from a true free radical reaction.[31]

Table 4.6. Ratios of Tertiary (3°) to Secondary (2°) Carbon Oxidation Observed with Non-Heme Iron Catalysts.

Compound	3°:2° with *cis*-1,2-dimethylcyclohexane	3°:2° with *trans*-1,2-dimethylcyclohexane	Reference
$[Fe(bpmen)(OTf)_2]$	2.8:1	1:1.5	13
$[Fe(bpmcn)(MeCN)_2]^{2+}$	1.8:1	1:1.9	13
$[Fe(pdp)(MeCN)_2]^{2+}$	4.0:1	1:1.7	10
$[Fe(bbpc)(MeCN)_2]^{2+}$	1.4:1	1:4.8	13
$[Fe(dnbpn)(OTf)_2]$	1:1.7	1:3.6	This work

Ligand abbreviations: bpmen = *N*,*N*'-dimethyl-*N*,*N*'-bis(2-pyridylmethyl)-1,2-ethanediamine; bpmcn = *N*,*N*'-dimethyl-*N*,*N*'-bis(2-pyridylmethyl)-1,2-cyclohexanediamine; pdp = 2-([(*S*)-2-[(*S*)-1-(pyridin-2-ylmethyl)pyrrolidin-2-yl]pyrrolidin-1-yl]methyl)pyridine; bbpc = *N*,*N*' dibenzyl-*N*,*N*'-bis(2-pyridylmethyl)-1,2-cyclohexanediamine.

The ability of installed bulk on the substrate to impact the C-H activation catalyzed by **3** extends beyond the carbons immediately attached to the functional group. A *tert*-butyl group, for instance, effectively precludes oxidation on the carbons both α and β to itself (Table 4.4); oxidation on the β sites was observed for similar chemistry catalyzed by $[Fe(bbpc)(MeCN)_2]^{2+}$.[13] The oxidation observed on the carbons α to the methyl groups in 1,1-dimethylcyclohexane is likewise less extensive than that observed for reactions catalyzed by the bbpc complex.[13]

The neopentyl groups are not sufficient to direct catalyzed oxidation towards primary carbons over secondary carbons. When *n*-hexane is used as a substrate, oxidation is limited to the 2- and 3-positions, with fewer than 0.1 total turnovers.

Complex **3** also catalyzes the oxidation of certain substrates by O_2. This reactivity has been sporadically reported for other non-heme iron compounds.[4-9,43] Most of the previously characterized oxidation by O_2 has required either a sacrificial reductant[4] or the presence of an allylic or benzylic C-H bond on the hydrocarbon substrate.[5-8] The dnbpn complex falls into the latter category, for unlike the previously characterized $[Fe(bbpc)(MeCN)_2]^{2+}$,[9] **3** cannot catalyze the oxidation of substrates with aliphatic C-H bonds (Table 4.5). Although **3** is inferior to the bbpc complex as a catalyst for the oxidation of cyclohexene by O_2, it is a superior catalyst for the oxidation of DHA. The DHA reactivity is also unusual in that anthrone is the major product; previous iron-catalyzed oxidations of this substrate by O_2 have yielded mostly, and in some cases exclusively, anthracene.[6,7,9] The cyclohexene reactivity is notable for yielding exclusively oxygenated products; prior iron chemistry using the ligand 1,4,8,11-tetramethyl-1,4,8,11-tetraazacyclotetradecane, conversely, found substantial quantities of the dehydrogenated products 1,4-cyclohexadiene and benzene.[5] The lack of cyclohexene oxide in the product mixture has precedence in non-heme iron-catalyzed oxidation of cyclohexene by both O_2 and H_2O_2.[5,41] Overall,

complex **3** appears to promote hydrocarbon oxygenation over dehydrogenation to a greater extent than these previously described systems. A mechanistic explanation for this behavior is not readily apparent at this time.

Details regarding the mechanism(s) of substrate oxidation by O_2 and H_2O_2 are limited. The oxidation of DHA by O_2 has a KIE of 4.5, indicating that C-H bond cleavage is in the product-determining step. With the bbpc chemistry that inspired this work, a ferric hydroperoxide intermediate was observed, the formation of which depended upon C-H activation.[9] Based on these observations, we tentatively proposed that the initial metal-containing oxidant in the dioxygen chemistry of the bbpc complex was a ferric superoxo species;[9] Nam and co-workers proposed a similar oxidant in another non-heme iron system.[5] Despite substantial effort, a similar intermediate has not yet been observed in the reactions containing **3** and O_2 as the terminal oxidant.

We were also unable to generate a detectable amount of intermediate through the reaction between **3** and H_2O_2; instead, we observe rapid and extensive decomposition of the dnbpn ligand. MS analysis suggests that the methylene linkages of the neopentyl groups and perhaps the picolylic groups of **2** are oxidized within 2 min under these conditions. The data therefore indicate that the loss of catalytic activity cannot be attributed solely to steric repulsions between the substrate and catalyst; if this were the case, one would anticipate that any catalytically relevant intermediates would be stabilized. The neopentyl groups instead appear to destabilize the metal-based oxidants responsible for hydrocarbon oxidation, perhaps by accelerating ligand detachment and/or intramolecular oxidation. The ethylene linkage, which was installed when attempts to use a more rigid 1,2-cyclohexanediamine backbone failed, has also been associated with accelerated ligand decomposition.[25]

Paradoxically, the addition of cumene or another benzylic substrate appears to stabilize an intermediate, which we tentatively propose to be a high-spin Fe(III)OOH species on the basis of UV/Vis, EPR, and resonance Raman spectroscopy. The 690 nm band in the UV/Vis spectrum (Figure 4.3) has an energy consistent with a ligand-to-metal charge transfer band for a ferric hydroperoxide complex, although the low intensities relative to those of the bands seen for previously reported species suggest that this intermediate does not accumulate to more than a 20% yield at most.[13,41,42,44-47] The absorption band is inconsistent with either a cumenyl or cumeneperoxyl radical. The EPR contains a feature consistent with a high-spin Fe(III) center, although this is dwarfed by a feature with g = 1.99 (Figure 4.4). The Raman spectrum includes two features that can be assigned to Fe-O and O-O stretches at 637 cm^{-1} and 843 cm^{-1}, respectively (Figure 4.5). These have energies similar to previously characterized high-spin Fe(III)OOH species.[41,47] The intermediate does not accumulate to high enough concentrations to allow isotopic labeling studies. The intermediate prepared with cumene has a less intense feature with a nearly identical Raman shift of 844 cm^{-1}. If the intermediate were a ferric alkylperoxide, one would anticipate the O-O feature to shift to a lower, rather than a higher, value. Because the predicted shift would less than 5 cm^{-1}, however, we cannot completely preclude the possibility that the observed intermediate is an alkylperoxide species instead of a hydroperoxide complex.

Although the intermediate appears to be intrinsically unstable, the benzylic substrates appear to allow it to accumulate, perhaps by slowing the ligand oxidation. Hydrogen atom transfer from the cumene to a ligand radical would produce a relatively long-lived cumenyl radical, which may account for the g = 1.99 signal in the EPR spectrum (Figure 4.4). The alternative explanation that the added hydrocarbon stabilizes the intermediate by rendering the solvent more polar is implausible since substitution of 100 mM toluene, which has a stronger C-H bond,[48] does not

trigger the same effect. Given that the O_2 reactivity only proceeds in the presence of substrates with weak C-H bonds, this may explain why the reactivity using O_2 as the terminal oxidant is less diminished, relative to the bbpc system, than that using H_2O_2. Under these conditions, the oxidants formed from O_2 and **3** would persist longer in solution (Figure 4.2).

4.5 Conclusions

The installation of neopentyl groups onto the tetradentate ligand bispicen shifts the oxidation catalyzed by its iron(II) complex towards the less sterically congested C-H bonds on secondary carbons to a greater extent than was seen for a similar ligand with benzyl groups. The additional steric bulk, unfortunately, also appears to destabilize the reactive intermediates generated from **3**, resulting in reduced catalytic turnover. Counterintuitively, an intermediate can be stabilized through the addition of a substrate with a weak C-H bond. Preliminary results suggest that such substrates can slow the ligand oxidation. Complex **3** can also catalyze the oxidation of allylic and benzylic substrates by O_2. Since this chemistry is limited to substrates with weak C-H bonds, less of the O_2-driven activity is lost going from the benzyl groups of bbpc to the neopentyl groups of dnbpn. The O_2 reactivity catalyzed by **3** results in fewer dehydrogenated products than with other previously characterized non-heme iron catalysts.

Appendix

Addendum to Experimental Section

Syntheses of Compounds **4** *and* **5**

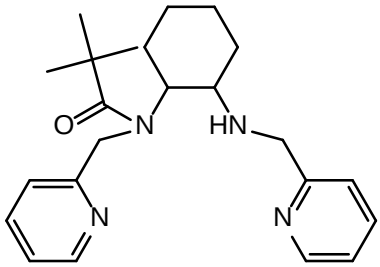

***N*-(2,2-Dimethylpropanamide)-*N,N'*-bis(2-pyridylmethyl)-1,2-cyclohexanediamine (A1).** (±)*trans*-*N,N'*-Bis(2-pyridinylmethyl)-1,2-cyclohexanediamine (2.96 g, 10.0 mmol) and NaOH (0.80 g, 20 mmol) were combined in 50 mL of H_2O. Pivaloyl chloride (12.5 g, 100 mmol) was slowly added to the solution, after which the reaction mixture was heated at 50 °C for 12 h. The reaction was cooled to room temperature (RT) at which point a 2.0 M NaOH solution was added until the pH reached 10. The product was extracted with three 50 mL portions of CH_2Cl_2. The extracts were combined and dried over Na_2SO_4. The solution was filtered, and the CH_2Cl_2 was removed through rotavaporation. The residue was washed with 30 mL of Et_2O to yield the product as a white solid (1.51 g, 40%). ^{1}H NMR ($CDCl_3$, 400 MHz): 8.50 (1H, d, *J* = 5.2 Hz), 8.10 (s, 1H), 7.62 (1H, t, *J* = 8.0 Hz), 7.48 (1H, t, *J* = 7.2 Hz), 7.35 (1H, d, *J* = 7.6 Hz), 7.25 (1H, d, *J* = 8.0 Hz), 7.13 (1H, t, *J* = 6.0 Hz), 6.97 (1H, t, *J* = 5.2 Hz), 4.60 (1H, d, *J* = 15.2 Hz), 4.42 (1H, d, *J* = 15.6 Hz), 4.12 (1H, s), 3.91 (1H, d, *J* = 14.8 Hz), 3.51 (1H, d, *J* = 14.8 Hz), 2.74 (1H, s), 2.21 (1H, d, J = 10.8 Hz), 1.84-1.64 (8H, m), 1.40 (9H, s). ^{13}C NMR ($CDCl_3$, 100 MHz): 178.97, 161.06, 159.07, 148.82, 148.62, 136.37, 136.28, 122.15, 121.47, 65.88, 62.27, 58.96, 52.62, 48.47, 39.71, 32.06, 31.36, 29.07, 25.62, 24.35, 15.30. HR-MS (ESI): Calcd [**A1**+H]$^+$, 381.2654; Found, 381.2646.

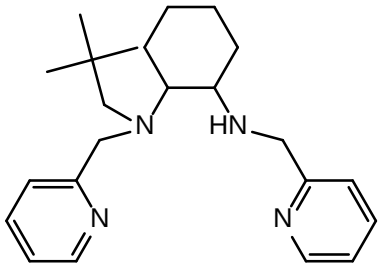

***N*-Neopentyl-*N*,*N*'-bis(2-pyridylmethyl)-1,2-cyclohexanediamine (4). A1** (1.90 g, 5.00 mmol) and $NaBH_4$ (0.95 g, 25 mmol) were dissolved in 50 mL of THF. A 20 mL solution of I_2 (3.18 g, 12.5 mmol) in THF was added dropwise to this solution over 15 min at 0 °C. After the addition was complete, the resultant mixture was heated at 65 °C for 48 h. The reaction was cooled to RT and 20 mL of MeOH were added to quench the residual $NaBH_4$. The organic solvents were removed *in vacuo*. The residue was washed with 30 mL of Et_2O and extracted with three 50 mL portions of 1.0 M HCl. The acidic extracts were made basic (pH 10) through the addition of 2.0 M NaOH, after which the product was extracted using three 50 mL portions of CH_2Cl_2. After the organic layers were dried over Na_2SO_4 and filtered, the CH_2Cl_2 was removed to yield the product as a white solid (1.47 g, 80% yield). ^{1}H NMR ($CDCl_3$, 400 MHz): 8.73 (1H, d, *J* = 5.6 Hz), 8.00-7.88 (3H, m), 7.54 (1H, t, *J* = 7.2 Hz), 7.31 (2H, t, *J* = 8.0 Hz), 6.97 (1H, *t*, *J* =5.2 Hz), 4.77 (1H, d, *J* = 15.2 Hz), 4.25 (1H, d, *J* = 14.8 Hz), 4.11 (2H, m), 3.96-3.76 (2H, m), 2.83 (1H, t, *J* = 7.2 Hz), 2.18 (1H, d, *J* = 12.8 Hz), 1.90-1.60 (6H, m), 1.56 (3H, s), 1.42 (9H, s). ^{13}C NMR ($CDCl_3$, 100 MHz): 161.55, 158.82, 148.55, 148.48, 139.29, 136.53, 123.73, 122.60, 122.15, 121.62, 65.88, 62.24, 59.46, 48.76, 39.63, 31.97, 31.31, 28.98, 25.59, 24.27, 15.30. HR-MS (ESI): Calcd [**4**+H]$^+$, 367.2862; Found, 367.2893.

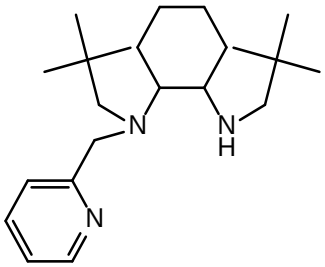

***N,N'*-Dineopentyl-*N*-(2-pyridylmethyl)-1,2-cyclohexanediamine (5).** *N*,*N*'-Dineopentyl-1,2-cyclohexanediamine (0.508 g, 2.01 mmol), 2-picolyl chloride hydrochloride (0.820 g , 5.00 mmol), potassium carbonate (0.552 g, 3.99 mmol) and potassium iodide (0.332 g, 2.00 mmol) were mixed in 50 mL of MeCN. The mixture was stirred at 40 °C for 48 h, at which point the reaction was cooled to RT. The solvents were removed under reduced pressure, leaving a red residue. The residue was dissolved in 50 mL of CH_2Cl_2, washed with one 50 mL portion of 1.0 M KOH. The CH_2Cl_2 solution containing the red residue was passed through a plug of basic alumina. The solvent was removed under reduced pressure to yield the product as a red oil (0.223 g, 32%). ^{1}H NMR (CD_3OD, 400 MHz): 8.45 (1H, d, *J* = 4.8 Hz), 7.78 (1H, t, *J* = 7.6 Hz), 7.51 (1H, s), 7.30 (1H, m), 3.95 (1H, d, *J* = 14.0 Hz), 3.61(1H, m), 2.45 (4H, m), 2.33 (1H, d, *J* = 10.4 Hz), 2.06 (2H, m), 1.82 (1H, m), 1.70 (1H, m), 1.40 (2H, s), 1.35-1.13 (4H, m), 0.99 (9H, s), 0.76 (9H, s). ^{13}C NMR (CD_3OD, 100 MHz): 162.45, 149.52, 138.51, 126.27, 123.84, 60.56, 59.66, 58.47, 33.74, 32.21, 31.04, 29.21, 28.68, 26.99, 25.79, 25.23, 24.58, 10.52. HR-MS (ESI): Calcd [**5**+H]$^+$, 346.3222; Found, 346.3199.

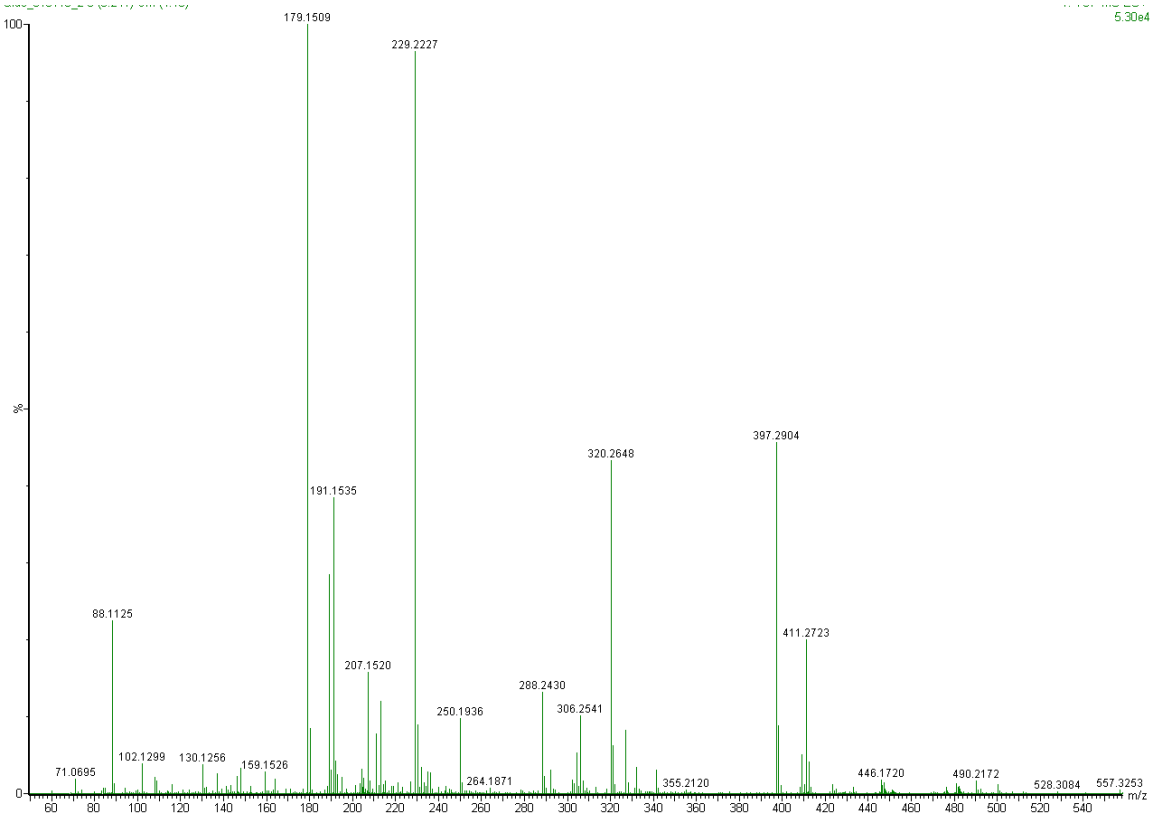

Figure 4.A1. HR-MS of reaction between 1.0 mM [Fe(dnbpn)(OTf)$_2$] and 10 mM H_2O_2 in MeCN at 294 K. The data were collected 2 min after the start of the reaction. The feature with *m*/*z* = 88.1125 corresponds to 2,2-dimethylpropanol (calculated *m*/*z* = 88.0888). The peak with *m*/*z* = 397.2904 can be assigned to a singly oxygenated dnbpn ligand (calculated *m*/*z* for $[C_{24}H_{37}N_4O]^+$ = 397.2967). The *m*/*z* = 411 feature can be assigned to a dnbpn ligand that has been doubly oxygenated (calculated *m*/*z* for $[C_{24}H_{35}N_4O_2]^+$ = 411.2760). The latter oxidation product(s) may potentially include compound **1**.

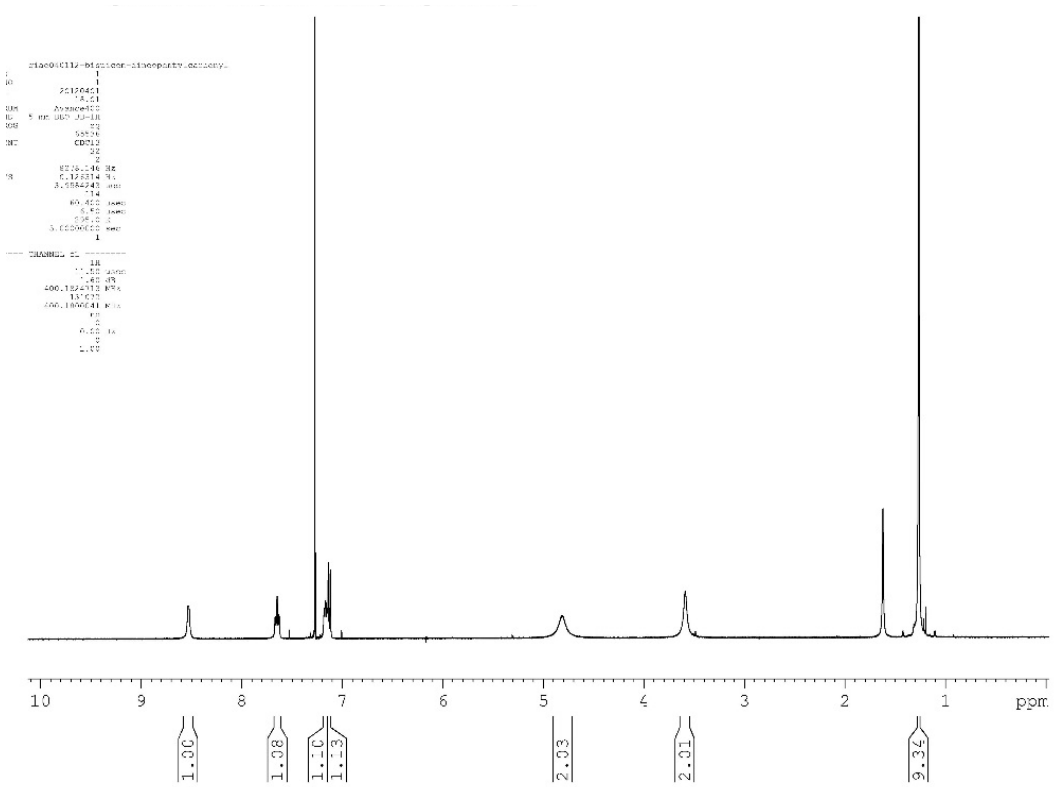

Figure 4.A2. ^{1}H NMR spectrum of compound **1**.

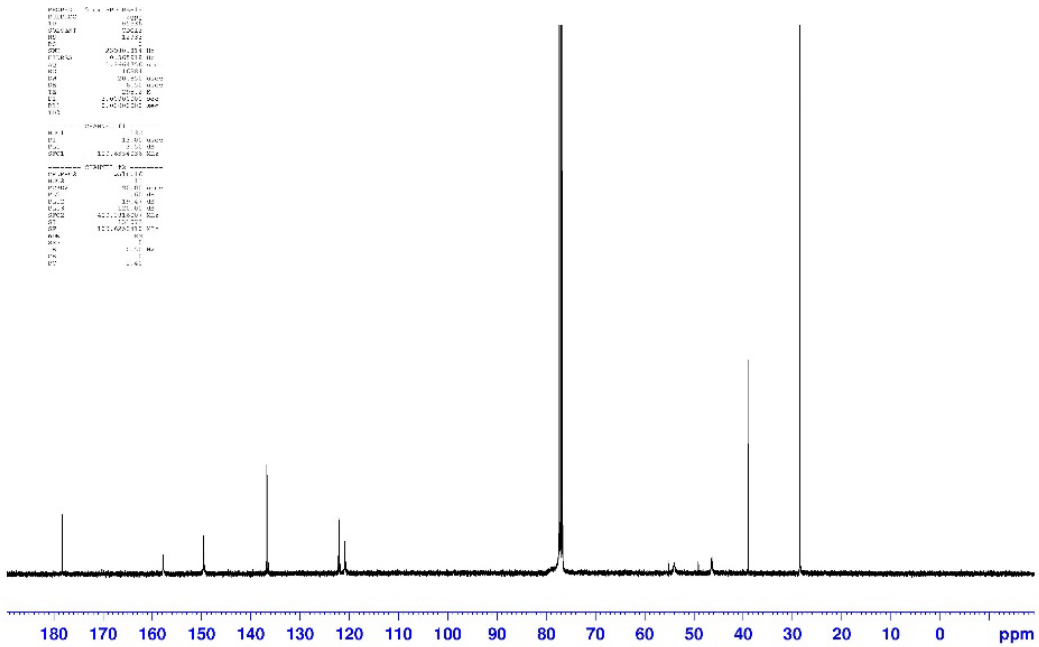

Figure 4.A3. ^{13}C NMR spectrum of compound **1.**

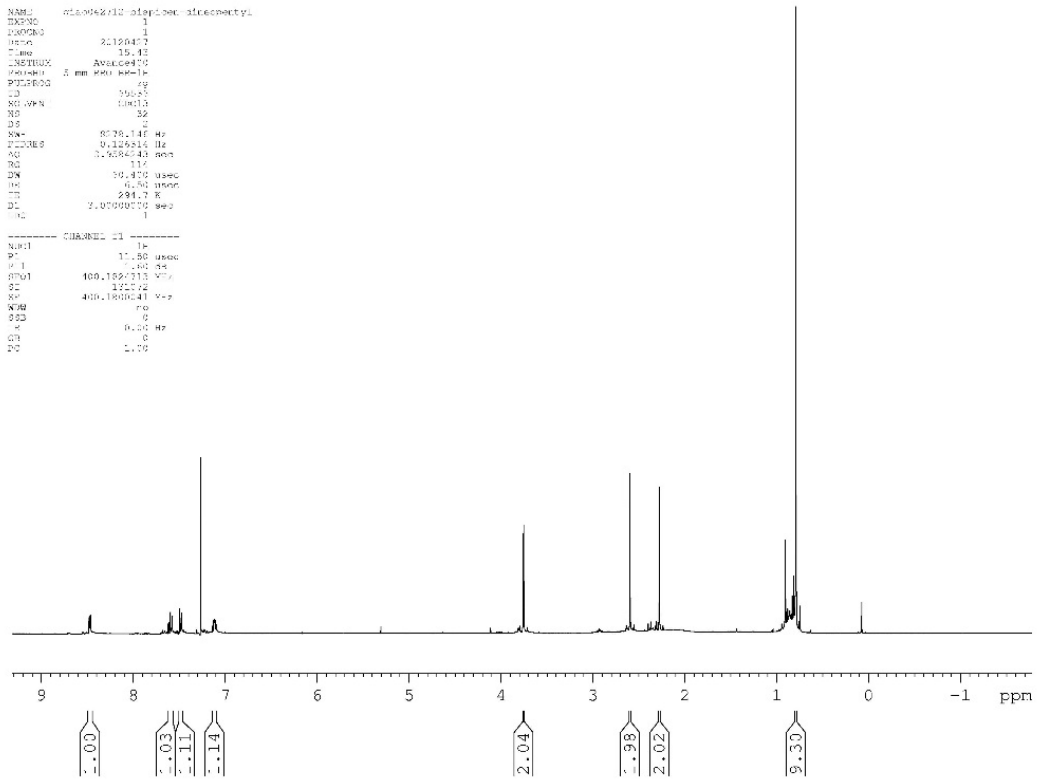

Figure 4.A4. ^{1}H NMR spectrum of dnbpn ligand (**2**).

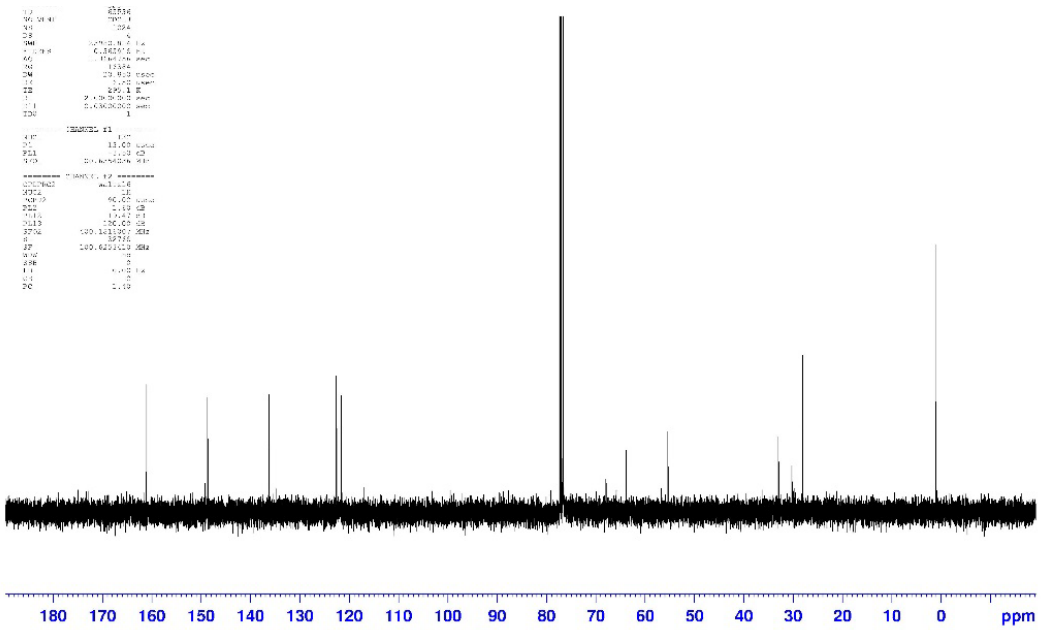

Figure 4.A5. ^{13}C NMR spectrum of compound **2**. The features at 0 ppm and 55 ppm correspond to tetramethylsilane (TMS) and CH_2Cl_2, respectively.

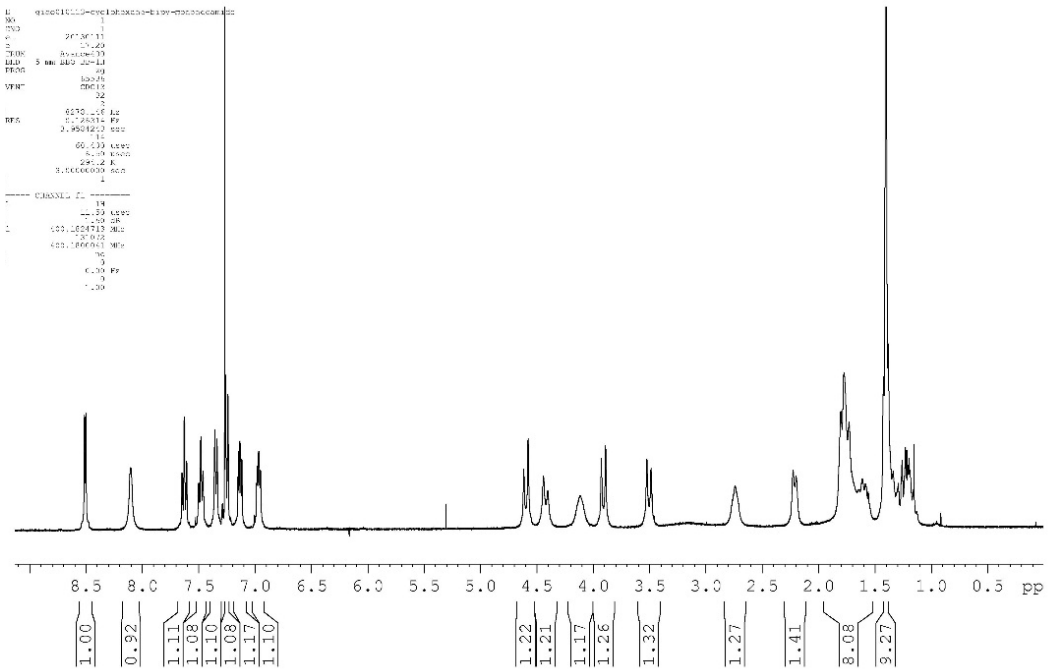

Figure 4.A6. ^{1}H NMR spectrum of compound **A1**.

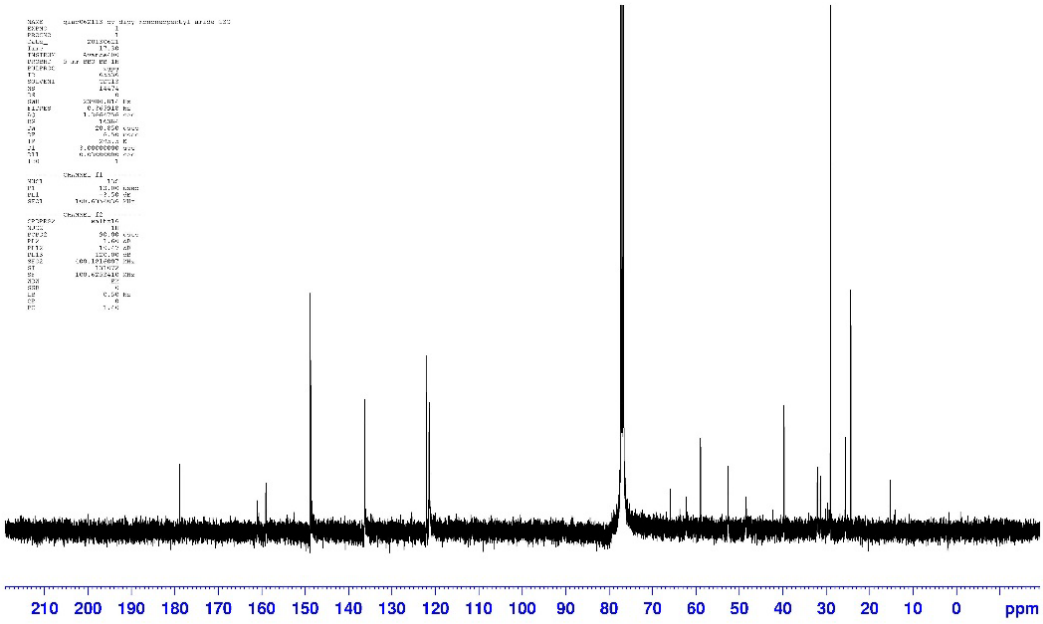

Figure 4.A7. ^{13}C NMR spectrum of compound **A1.**

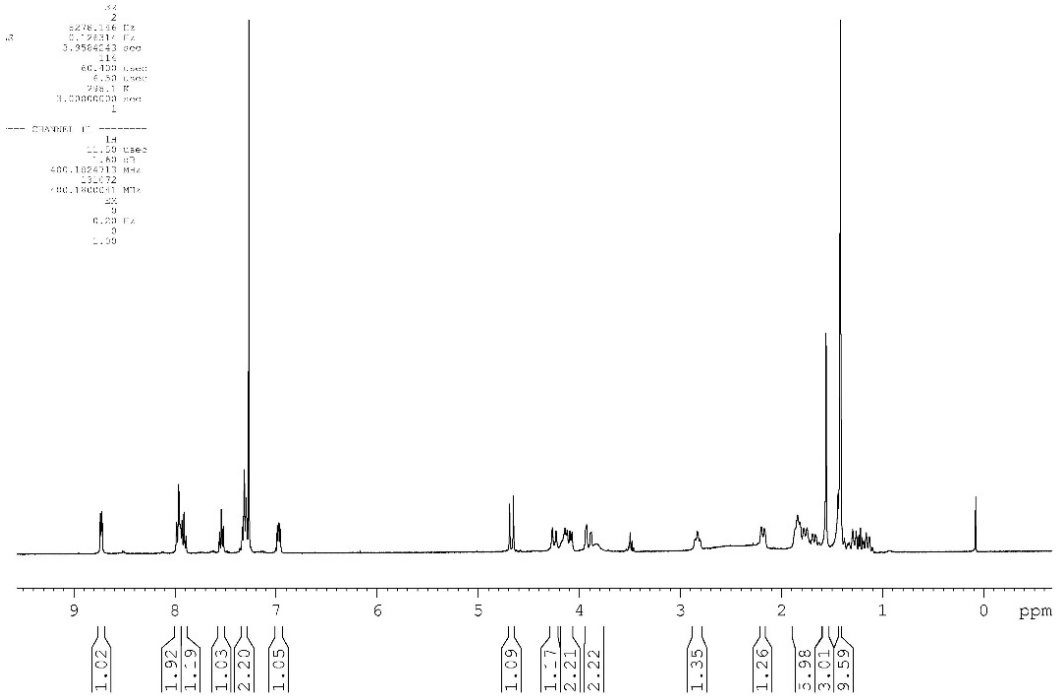

Figure 4.A8. ^{1}H NMR spectrum of compound **4**.

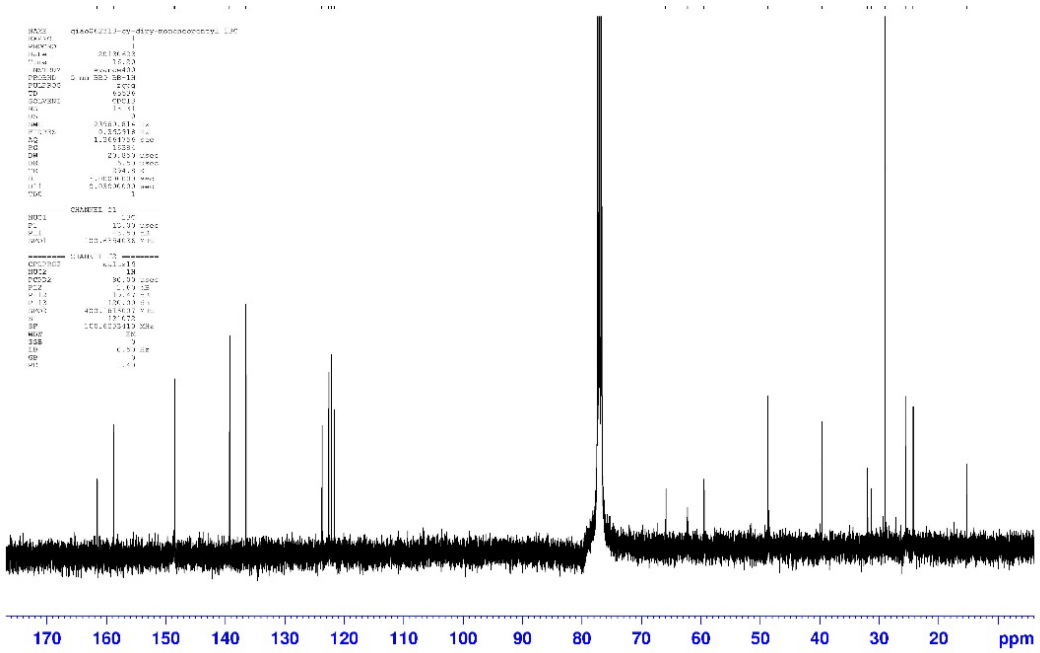

Figure 4.A9. ^{13}C NMR spectrum of compound **4.**

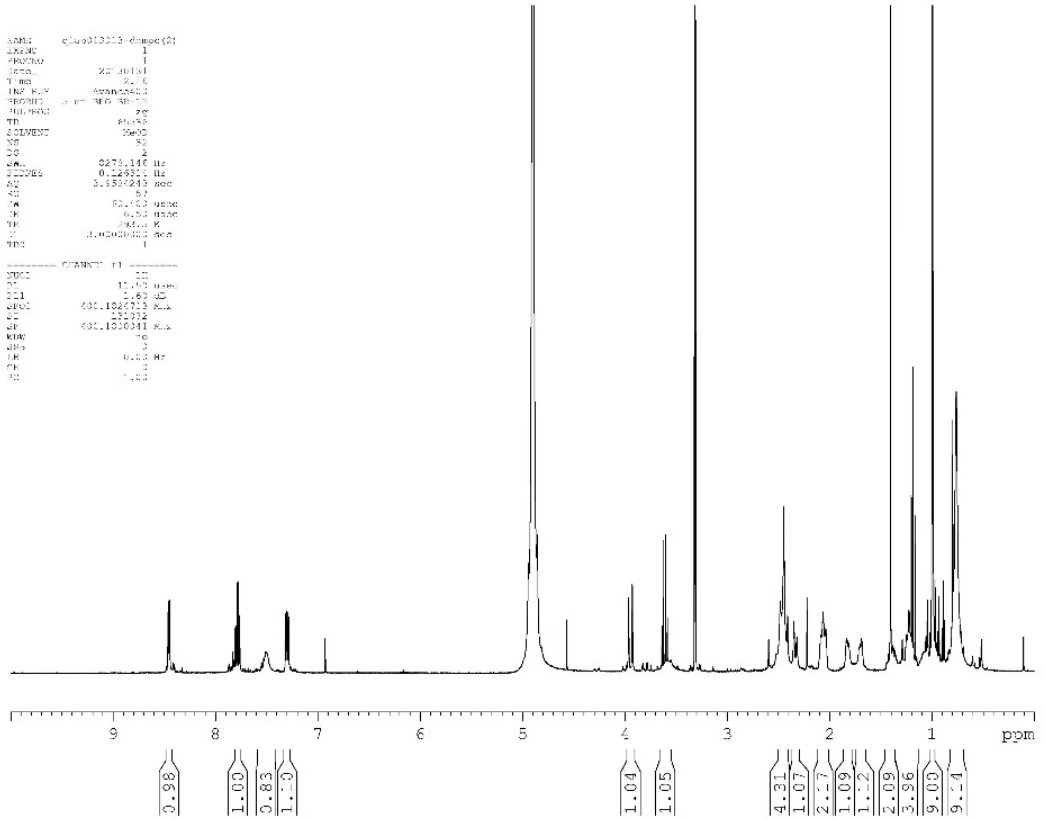

Figure 4.A10. ^{1}H NMR spectrum of compound **5**.

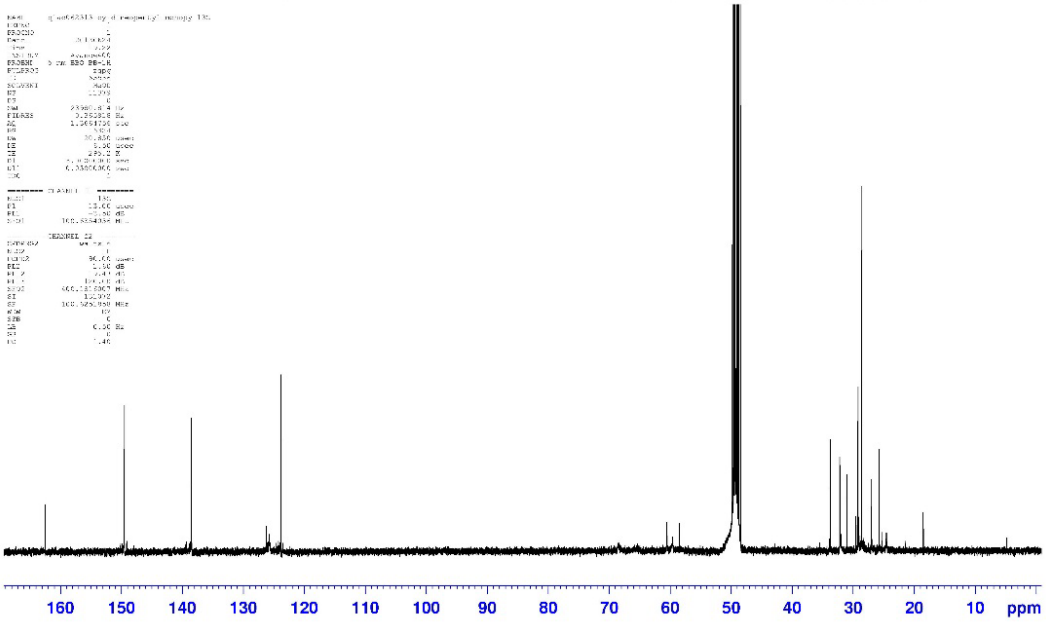

Figure 4.A11. ^{13}C NMR spectrum of compound **5.**

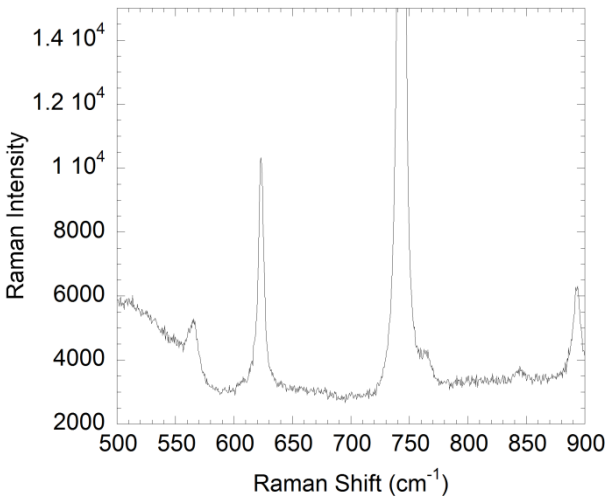

Figure 4.A12. Resonance Raman spectroscopy of the intermediate generated from the reaction between 2.0 mM **3**, 10 mM H_2O_2, and 100 mM cumene in MeCN. The data were acquired 30 s after the start of the reaction with 785 nm irradiation. A control experiment with cumene, but no **3**, contained features at 381, 462, 581, 623, 744, and 893 cm^{-1}. The 844 cm^{-1} feature was reproduced with two other independently prepared samples.

References

(1) Costas, M.; Mehn, M. P.; Jensen, M. P.; Que, L., Jr. *Chem. Rev.* **2004**, *104*, 939-986.

(2) Nam, W. *Acc. Chem. Res.* **2007**, *40*, 522-531.

(3) Kim, S. O.; Sastri, C. V.; Seo, M. S.; Kim, J.; Nam, W. *J. Am. Chem. Soc.* **2005**, *127*, 4178-4179.

(4) Jaafar, H.; Vileno, B.; Thibon, A.; Mandon, D. *Dalton Trans.* **2011**, *40*, 92-106.

(5) Lee, Y.-M.; Hong, S.; Morimoto, Y.; Shin, W.; Fukuzumi, S.; Nam, W. *J. Am. Chem. Soc.* **2010**, *132*, 10668-10670.

(6) Gupta, R.; Borovik, A. S. *J. Am. Chem. Soc.* **2003**, *125*, 13234-13242.

(7) Mukherjee, J.; Lucas, R. L.; Zart, M. K.; Powell, D. R.; Day, V. W.; Borovik, A. S. *Inorg. Chem.* **2008**, *47*, 5780-5786.

(8) Furukawa, S.; Hitomi, Y.; Shishido, T.; Tanaka, T. *Inorg. Chim. Acta* **2011**, *378*, 19-23.

(9) He, Y.; Goldsmith, C. R. *Chem. Commun.* **2012**, *48*, 10532-10534.

(10) Chen, M. S.; White, M. C. *Science* **2010**, *327*, 566-571.

(11) Chen, M. S.; White, M. C. *Science* **2007**, *318*, 783-787.

(12) Gómez, L.; Canta, M.; Font, D.; Prat, I.; Ribas, X.; Costas, M. *J. Org. Chem.* **2013**, *78*, 1421-1433.

(13) He, Y.; Gorden, J. D.; Goldsmith, C. R. *Inorg. Chem.* **2011**, *50*, 12651-12660. Correction: *Inorg. Chem.* **2012**, *51*, 7431.

(14) Rheingold, A. L.; Zakharov, L. N.; Trofimenko, S. *Inorg. Chem.* **2003**, *42*, 827-833.

(15) Calabrese, J. C.; Trofimenko, S. *Inorg. Chem.* **1992**, *31*, 4810-4814.

(16) Goldsmith, C. R.; Jonas, R. T.; Stack, T. D. P. *J. Am. Chem. Soc.* **2002**, *124*, 83-96.

(17) Toftlund, H.; Pedersen, E.; Yde-Andersen, S. *Acta. Chem. Scand. A* **1984**, *38*, 693-697.

(18) Fenton, R. R.; Vagg, R. S.; Jones, P.; Williams, P. A. *Inorg. Chim. Acta* **1987**, *128*, 219-229.

(19) Duguet, N.; Donaldson, A.; Leckie, S. M.; Douglas, J.; Shapland, P.; Brown, T. B.; Churchill, G.; Slawin, A. M. Z.; Smith, A. D. *Tetrahedron: Asymmetry* **2010**, *21*, 582-600.

(20) Glerup, J.; Goodson, P. A.; Hazell, A.; Hazell, R.; Hodgson, D. J.; McKenzie, C. J.; Michelsen, K.; Rychlewska, U.; Toftlund, H. *Inorg. Chem.* **1994**, *33*, 4105-4111.

(21) Coates, C. M.; Fiedler, S. R.; McCullough, T. L.; Albrecht-Schmitt, T. E.; Shores, M. P.; Goldsmith, C. R. *Inorg. Chem.* **2010**, *49*, 1481-1486.

(22) Coates, C. M.; Hagan, K.; Mitchell, C. A.; Gorden, J. D.; Goldsmith, C. R. *Dalton Trans.* **2011**, *40*, 4048-4058.

(23) McKennon, M. J.; Meyers, A. I.; Drauz, K.; Schwarm, M. *J. Org. Chem.* **1993**, *58*, 3568-3571.

(24) Periasamy, M.; Thirumalaikumar, M. *J. Organomet. Chem.* **2000**, *609*, 137-151.

(25) Goldsmith, C. R.; Coates, C. M.; Hagan, K.; Mitchell, C. A. *J. Mol. Catal. A* **2011**, *335*, 24-30.

(26) Costas, M.; Que, L., Jr. *Angew. Chem., Int. Ed.* **2002**, *41*, 2179-2181.

(27) Chen, K.; Costas, M.; Kim, J.; Tipton, A. K.; Que, L., Jr. *J. Am. Chem. Soc.* **2002**, *124*, 3026-3035.

(28) Goodson, P. A.; Hodgson, D. J. *Inorg. Chem.* **1989**, *28*, 3606-3608.

(29) Hureau, C.; Blondin, G.; Charlot, M.-F.; Philouze, C.; Nierlich, M.; Cesario, M.; Anxolabéhère-Mallart, E. *Inorg. Chem.* **2005**, *44*, 3669-3683.

(30) Britovsek, G. J. P.; England, J.; White, A. J. P. *Inorg. Chem.* **2005**, *44*, 8125-8134.

(31) Chen, K.; Que, L., Jr. *J. Am. Chem. Soc.* **2001**, *123*, 6327-6337.

(32) England, J.; Britovsek, G. J. P.; Rabadia, N.; White, A. J. P. *Inorg. Chem.* **2007**, *46*, 3752-3767.

(33) Gómez, L.; Garcia-Bosch, I.; Company, A.; Benet-Buchholz, J.; Polo, A.; Sala, X.; Ribas, X.; Costas, M. *Angew. Chem., Int. Ed.* **2009**, *48*, 5720-5723.

(34) Tanase, S.; Marques-Gallego, P.; Browne, W. R.; Hage, R.; Bouwman, E.; Feringa, B. L.; Reedijk, J. *Dalton Trans.* **2008**, 2026-2033.

(35) Roelfes, G.; Lubben, M.; Hage, R.; Que, L., Jr.; Feringa, B. L. *Chem.− Eur. J.* **2000**, *6*, 2152-2159.

(36) Zhang, Q.; Goldsmith, C. R. *Inorg. Chim. Acta* **2013**, *406*, 301-306.

(37) Achord, J. M.; Hussey, C. L. *Anal. Chem.* **1980**, *52*, 601-602.

(38) Roelfes, G.; Lubben, M.; Chen, K.; Ho, R. Y. N.; Meetsma, A.; Genseberger, S.; Hermant, R. M.; Hage, R.; Mandal, S. K.; Young, V. G., Jr.; Zang, Y.; Kooijman, H.; Spek, A. L.; Que, L., Jr.; Feringa, B. L. *Inorg. Chem.* **1999**, *38*, 1929-1936.

(39) Shearer, J.; Scarrow, R. C.; Kovacs, J. A. *J. Am. Chem. Soc.* **2002**, *124*, 11709-11717.

(40) Li, F.; Meier, K. K.; Cranswick, M. A.; Chakrabarti, M.; Van Heuvelen, K. M.; Münck, E.; Que, L., Jr. *J. Am. Chem. Soc.* **2011**, *133*, 7256-7259.

(41) Wada, A.; Ogo, S.; Nagatomo, S.; Kitagawa, T.; Watanabe, Y.; Jitsukawa, K.; Masuda, H. *Inorg. Chem.* **2002**, *41*, 616-618.

(42) Martinho, M.; Blain, G.; Banse, F. *Dalton Trans.* **2010**, *39*, 1630-1634.

(43) Mukherjee, A.; Martinho, M.; Bominaar, E. L.; Münck, E.; Que, L., Jr. *Angew. Chem., Int. Ed.* **2009**, *48*, 1780-1783.

(44) Ho, R. Y. N.; Roelfes, G.; Hermant, R.; Hage, R.; Feringa, B. L.; Que, L., Jr. *Chem. Commun.* **1999**, 2161-2162.

(45) Hong, S.; Lee, Y.-M.; Shin, W.; Fukuzumi, S.; Nam, W. *J. Am. Chem. Soc.* **2009**, *131*, 13910-13911.

(46) Mialane, P.; Nivorojkine, A.; Pratviel, G.; Azéma, L.; Slany, M.; Godde, F.; Simaan, A.; Banse, F.; Kargar-Grisel, T.; Bouchoux, G.; Sainton, J.; Horner, O.; Guilhem, J.; Tchertanova, L.; Meunier, B.; Girerd, J.-J. *Inorg. Chem.* **1999**, *38*, 1085-1092.

(47) Roelfes, G.; Vrajmasu, V.; Chen, K.; Ho, R. Y. N.; Rohde, J.-U.; Zondervan, C.; la Crois, R. M.; Schudde, E. P.; Lutz, M.; Spek, A. L.; Hage, R.; Feringa, B. L.; Münck, E.; Que, L., Jr. *Inorg. Chem.* **2003**, *42*, 2639-2653.

(48) Berkowitz, J.; Ellison, G. B.; Gutman, D. *J. Phys. Chem.* **1994**, *98*, 2744-2765.

Chapter 5

Kinetic Analysis of the Formation and Decay of a Non-Heme Ferric Hydroperoxide Species Susceptible to O-O Bond Homolysis

5.1 Introduction

C-H bonds, particularly those on aliphatic carbons, are difficult to modify chemically. The key difficulty in activating these functional groups is that the harsh oxidants and reaction conditions generally needed for such chemical transformations tend to over-oxidize hydrocarbon substrates. This has prompted much research into developing synthetic options that work under milder conditions.[1-3] Among these are processes that rely on non-heme iron catalysts, which have been designed to mimic metalloenzymes capable of catalyzing alkane oxidation under ambient conditions.[4-6] The general consensus is that the terminal oxidant reacts with the iron to convert it to a higher-valent species, which is ultimately responsible for C-H activation. Ferric hydroperoxide and ferryl species are commonly proposed as intermediates in this chemistry and have been amply observed in both enzymatic and small molecule systems.[7-15]

One difficulty is the identification of the metal-based oxidant responsible for C-H activation. Whether ferric hydroperoxide species can directly activate C-H bonds, in particular, is debated.[16,17] Complicating matters is that the O-O bonds in these species can potentially break either homolytically or heterolytically; this may give rise to fundamentally different sorts of reactivity.[11] Que has found that strong evidence against the direct oxidation of alkene and alkane substrates by a Fe(III)-OOH species susceptible to heterolytic O-O cleavage.[6,11]

In order to further probe this problem, we have investigated the formation and decay of a relatively well-established ferric hydroperoxide species **2** through the use of stopped-flow kinetics. This intermediate can be generated from either H_2O_2 or O_2 (Scheme 5.1).[7,18] We have determined the influence of several additives, notably acid, water, and substrate, on the formation and decomposition of this intermediate.

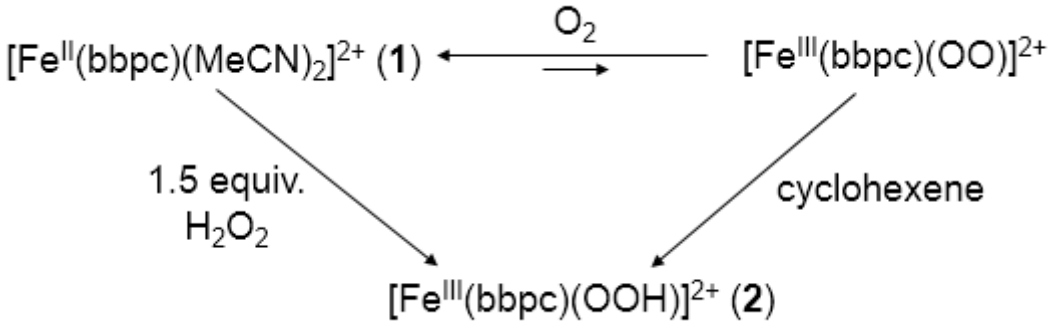

Scheme 5.1. Conversion of $[Fe(bbpc)(MeCN)_2]^{2+}$ (**1**) to $[Fe(bbpc)(OOH)]^{2+}$ (**2**).

5.2 Experimental Section

Materials

Except where noted otherwise, all chemicals were purchased from Sigma-Aldrich and used as received. Dry dioxygen (O_2) was purchased from Airgas. Anhydrous acetonitrile (MeCN) was purchased from Acros Organics. Hydrogen peroxide (H_2O_2, 50% wt) was bought from Fisher, and the concentration was calibrated by titration of $KMnO_4$ in acidic aqueous solution.[19] *N*,*N*'-di(phenylmethyl)-*N*,*N*'-bis(2-pyridinylmethyl)-1,2-cyclohexanediamine (bbpc) and its ferrous complex $[Fe(bbpc)(MeCN)_2](SbF_6)_2$ (**1**) were synthesized as described previously.[18]

Instrumentation

A Hi-Tech SF-51 Stopped-Flow Spectrophotometer was used for the described stopped-flow kinetic studies. The reactions were monitored at either 690 nm or 535 nm. These wavelengths were chosen since they displayed the greatest changes in absorbance during the reactions corresponding to the formation and decay of $[Fe(bbpc)(OOH)]^{2+}$ (**2**). A Hi-Tech C-400 circulator was used to control and maintain the temperature. The program Olis 4300 was used for data acquisition. GraphPad Prism 6 software was used for data analysis. A Varian Cary 50 UV-Vis

spectrophotometer was used to collect routine optical data; software from the WinUV Analysis Suite was used to process and analyze these data.

Reactivity

(1) Oxidation of **1** by H_2O_2

For each stopped-flow kinetic experiment, 0.20 mL aliquots from two syringes, one filled with filled with **1** in MeCN (**A**) and one filled with H_2O_2 in MeCN (**B**), were simultaneously injected into the instrument. Additives, if present, were introduced via syringe **B**. The solution was allowed to mix for 0.1 ms before the data acquisition began. The spectrophotometer was set to 690 nm, which corresponds to the peak absorbance of a strong ligand-to-metal charge transfer (LMCT) feature associated with **2**. For most experiments, the initial concentration of **1** after mixing was 0.50 mM. The concentration of **1** was controlled and varied by diluting a 1.0 mM stock solution with pure MeCN. Except where stated otherwise, the initial concentration of H_2O_2 after mixing was 5.0 mM; the temperature was set at 298 K.

(2) Oxidation of **1** by O_2

The reactions involving the oxidation of **1** by O_2 proceeded in a manner analogous to those involving H_2O_2. For each experiment, 0.20 mL aliquots from two syringes, one containing an aerobic solution of **1** (**A**) and one containing an aerobic solution of cyclohexene (**B**), were simultaneously injected into the stopped-flow instrument. The solution was allowed to mix for 0.1 ms prior to the start of data acquisition. Additives, if any, were introduced via syringe **B**. The aerobic solutions were prepared by bubbling pure O_2 through MeCN solutions of **1** and cyclohexene for 20 min at room temperature, resulting in stock solutions containing 8.1 mM O_2.[20] The concentration of O_2 was controlled and varied via dilution with solutions made with degassed anhydrous MeCN. The stopped-flow spectrometer was set to 535 nm to monitor the changes in

absorbance since intermediate **2** does not form cleanly when generated from O_2 and cyclohexene. The previously observed side reactivity prompted us to limit the analysis to an initial rates analysis of the formation of **2**.[7]

Data Analysis

Kinetic data were modeled using the GraphPad Prism 6 software. All reactions were repeated at least three times in order to confirm their reproducibility and to assess the precision of the measurements. All first-order or pseudo-first-order processes were allowed to proceed for at least five half-lives. All calculated activation parameters were obtained from measurements taken at four temperatures. Data points were taken from each temperature, and the entire experiment was repeated two additional times with fresh stock solutions in order to confirm the reproducibility of the obtained values of $\Delta H^{\neq}$ and $\Delta S^{\neq}$. Whenever a rate or a rate constant was correlated to the concentration of a reagent, at least four different concentrations of that reagent were investigated.

5.3 Results and Discussion

Reactivity: H_2O_2

A ferric hydroperoxide species can be generated from the reaction between 1.0 equiv. $[Fe(bbpc)(MeCN)_2](SbF_6)_2$ (**1**) and 1.5 equiv. H_2O_2 in MeCN (**1** + $1.5H_2O_2$ = **2** + 2MeCN + H_2O).[7,18] This species was assigned as $[Fe(bbpc)(OOH)]^{2+}$ (**2**) on the basis of its UV-Vis, EPR, and resonance Raman spectra.[7,18] We find that the formation of **2** is first order with respect to the concentration of **1** using an initial rate analysis (Figure 5.1), and it is first order with respect to the concentration of H_2O_2 due to the linear relationship between k_{obs} and $[H_2O_2]$ (Figure 5.2). The formation of **2** therefore follows the following rate law described by Equation 1:

Eq. 1: $$d[\mathbf{2}]/dt = k_2[\mathbf{1}][H_2O_2].$$

Although the reaction stoichiometry suggests that 1 equiv. of H_2O_2 will lead to the one-electron oxidation of two Fe(II) centers, the rate-determining step (RDS) involves only one equiv. of Fe(II) and is inconsistent with the formation of a binuclear iron species. However, the data cannot preclude the formation of such a species subsequent to the RDS but prior to the formation of **2**.

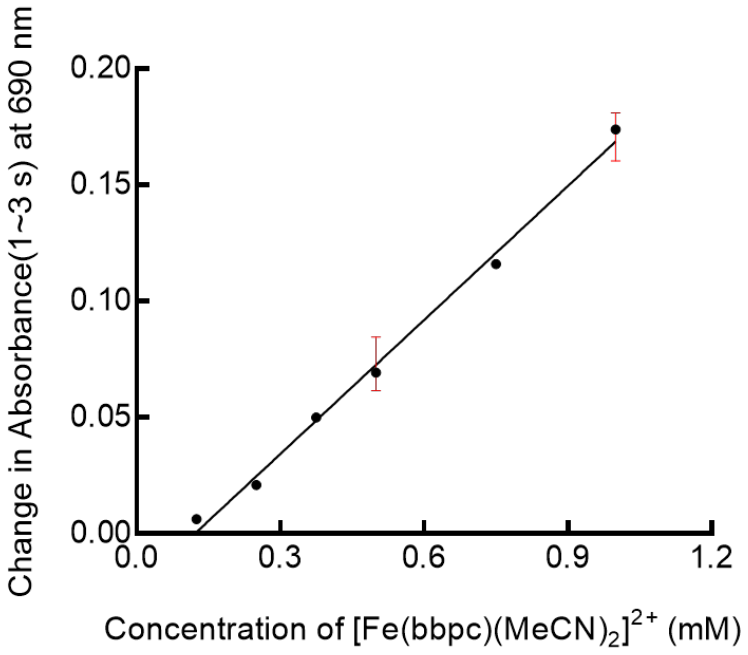

Figure 5.1. Initial rate analysis for the formation of **2** from **1** and H_2O_2. The focus is on the dependence of initial rate of the reaction on [**1**]; the initial concentration of H_2O_2 was kept at 5.0 mM for all of the above measurements. The change in the absorbance at 690 nm was monitored from 1.0 to 3.0 s; this change is directly proportional to the change in the concentration of **2**, which has a strong ligand-to-metal charge transfer band at this wavelength. The linear fit equation is $y = 0.1922x - 0.02344$ ($R^2 = 0.9841$). The data were also fit to a polynomial fit in order to test the possibility that the reaction is second-order with respect to **1**. The best polynomial fit was $y = 0.0456x^2 + 0.1405x - 0.01306$ ($R^2 = 0.9876$). Given the near-negligible improvement in the fit, we concluded that the linear fit was more likely to be physically accurate.

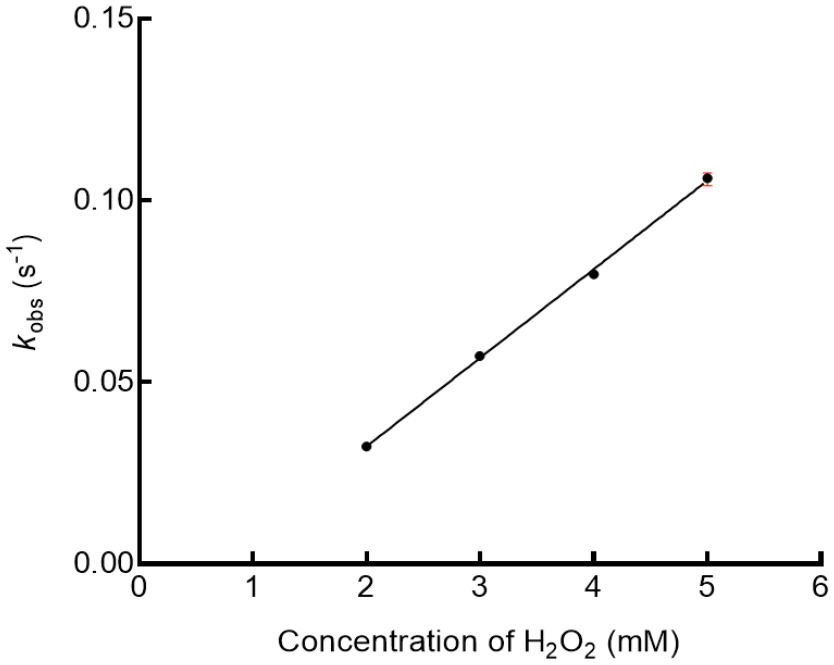

Figure 5.2. Relationship between the k_{obs} for the formation of **2** from **1** and H_2O_2 and the initial concentration of H_2O_2. The initial concentrations of **1** were 0.50 mM for all of the above reactions. The values of k_{obs} were obtained from A→B→C fits to the kinetic traces. At higher concentrations, k_{obs} scales linearly with [H_2O_2], suggesting that the formation of **2** is first-order with respect to this reagent. The fit corresponds to the equation $y = 0.02438x - 0.016454$ ($R^2 = 0.9983$).

The formation of **2** from 0.50 mM **1** and 5.0 mM H_2O_2 and its subsequent decay were studied in MeCN from 294 K to 324 K. The second-order rate constants at these temperatures were measured and used to prepare an Eyring plot (Figure 5.3). $\Delta H^{\neq}$ and $\Delta S^{\neq}$ were calculated to be 51 (± 2) kJ mol^{-1} and -50 (± 3) J mol^{-1} K^{-1}, respectively. The negative entropy of activation is indicative of an associative process and corroborates the bimolecular rate law (Eq. 1).

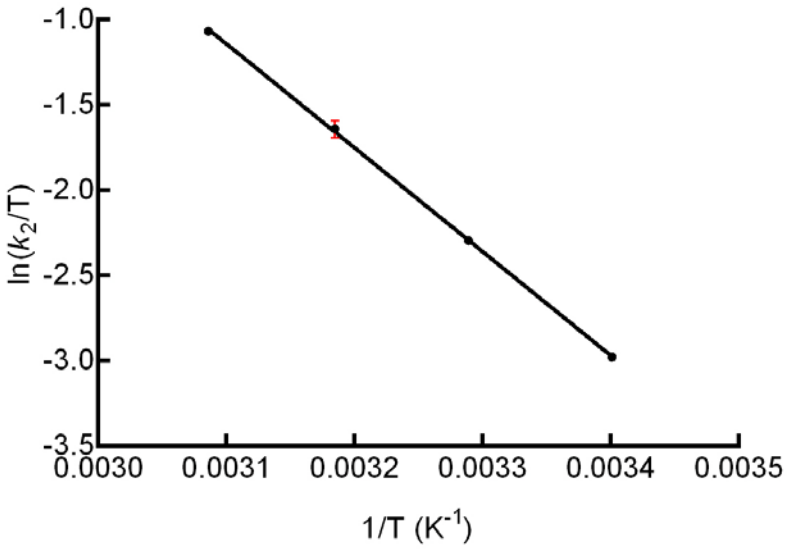

Figure 5.3. Eyring plot for the formation of **2** from a reaction between 0.50 mM **1** and 5.0 mM H_2O_2 in MeCN at temperatures ranging from 294 K to 324 K. The second order rate constant from the average of three independent experiments is plotted. The fit corresponds to the equation $y = -6085.2x + 17.723$ ($R^2 = 0.9987$).

Various concentrations of H_2O and the oxidizable substrates, cyclohexane (C_6H_{12}) and cyclohexene (C_6H_{10}), were added, but none of these additives influenced the rate of formation of **2** from **1** and H_2O_2 to a significant degree (Figure 5.4). Water might have been expected to inhibit the formation of **2** by acting as a competing ligand, but the data instead suggest that H_2O cannot effectively compete with H_2O_2 for binding sites on the iron. Conversely, the k_{obs} for the formation of **2** from 0.50 mM **1** and 5.0 mM H_2O_2 increases slightly (~10%) as the concentration of water increases from 5.0 mM to 50 mM (Figure 5.4).

Aliquots of $HClO_4$ were also added to determine if the presence of an acid influenced the rate of formation. A noticeable decrease in the k_{obs} is observed past 5 equiv. of $HClO_4$ (Figure 5.4). The result is not surprising given that H_2O_2 is harder to reduce under acidic conditions in aqueous media; making this reduction potential less favorable would likewise render the oxidation of **1** less favorable both thermodynamically and kinetically.

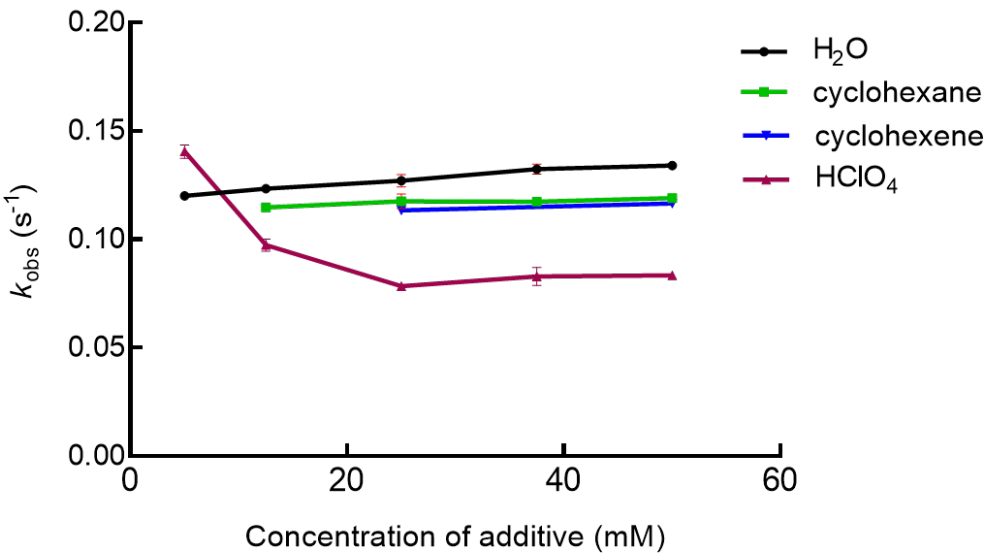

Figure 5.4. Influence of additives of the k_{obs} for the formation of **2** from 0.50 mM **1** and 5.0 mM H_2O_2 in MeCN at 298 K. The data from three independent series of experiments are plotted.

The decomposition of **2** formed from H_2O_2 and **1** can be followed by the loss of the 690 nm UV-Vis band associated with **2** and fit to a simple B→C step. Excess H_2O_2 hastens the disappearance of **2** (Figure 5.5). Similar observations have been made in other mononuclear non-heme iron systems; those have been used to explain the lessened oxidative efficiency for hydrocarbon oxidation catalysis with higher loadings of terminal oxidant.[21] At the higher concentrations of H_2O_2, the relationship between [H_2O_2] and the observed rate constant for the decay appears to be linear, suggesting that the H_2O_2 is reacting directly with **2**. Although H_2O_2 could potentially be a substrate, with O-H bond dissociation energies of approximately 88 kcal mol^{-1},[22] the inability of C_6H_{12} or C_6H_{10} to hasten the decomposition of **2** (*vide infra*) suggest that the excess H_2O_2 reacts with **2** in other means, perhaps through the formation of a more reactive species.

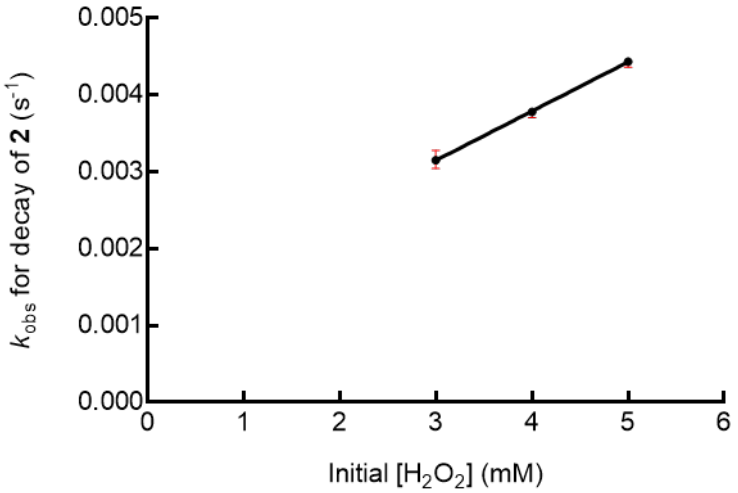

Figure 5.5. Relationship between the k_{obs} for the decomposition of **2** and the concentration of H_2O_2 originally present in solution. All reactions were performed in MeCN at 298 K. The data from three independent series of experiments are plotted. The fit corresponds to the equation $y = 0.00064x + 0.00123$ ($R^2 = 0.9821$).

The addition of C_6H_{12}, which is oxidized to cyclohexanol and cyclohexanone under these conditions,[18] fails to significantly alter the rate of decomposition of **2** (Figure 5.6). A 10% increase in the rate of decay is observed as the concentration of C_6H_{12} is increased from 5.0 mM to 50 mM; this may be consistent with a change in the solvent polarity, rather than a direct reaction between **2** and C_6H_{12}. The addition of C_6H_{10}, which has more readily oxidized allylic C-H bonds that may be anticipated to increase k_{obs} if substrate oxidation were involved in the RDS, likewise fails to increase the rate of the ferric hydroperoxide's disappearance (Figure 5.6). This supports earlier observations made by ourselves that suggested that **2** does not directly react with C-H bonds.[7] The hydrocarbon oxidation instead appears to correspond to a step subsequent to the RDS of the Fe(III)-OOH compound's decay. The addition of H_2O or acid fails to accelerate the disappearance of **2**, consistent with a decay process involving homolysis, rather than heterolysis, of the O-O bond.[9,11]

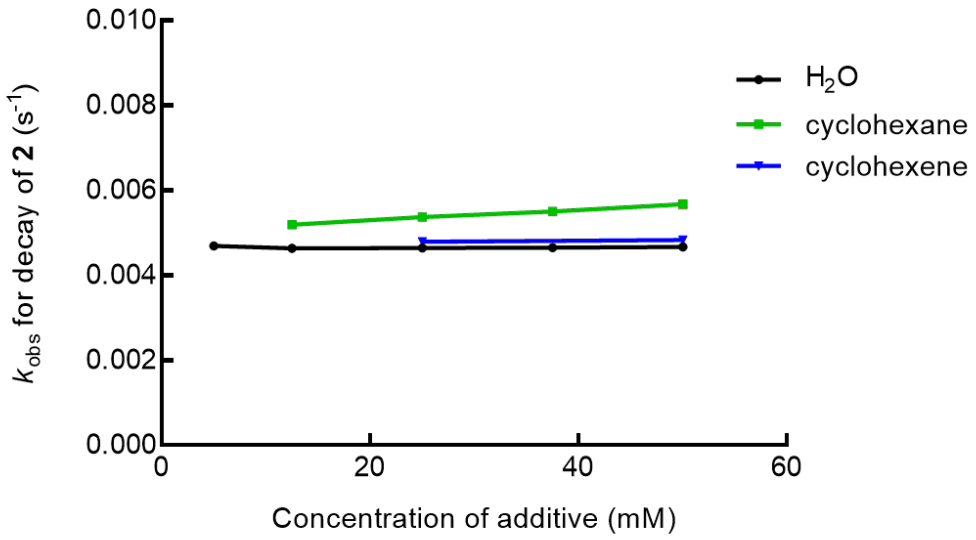

Figure 5.6. Influence of additives on the k_{obs} for the decomposition of **2** formed from 0.50 mM **1** and 5.0 mM H_2O_2 in MeCN at 298 K. The data from three independent series of experiments are plotted for each additive. The k_{obs} for the decomposition of **2** without any additives was found to be 0.0044 s^{-1}; this value is equal within error to the *y* intercept for each plot.

The O-O bond likely cleaves in the RDS of the decomposition reaction. The temperature dependence of the decay portion of the reaction between 0.50 mM **1** and 5.0 mM H_2O_2 yields the following kinetic parameters: $\Delta H^{\neq}$ = 54 (± 1) kJ mol^{-1}, $\Delta S^{\neq}$ = -68 (± 1) J mol^{-1} K^{-1} (Figure 5.7). The $\Delta H^{\neq}$ is more similar to those of non-heme Fe(III)-OOH species that undergo homolytic O-O cleavage than those that undergo O-O heterolysis.[11] Prior results from our laboratory suggested that the cleavage of the O-O bond is reversible.[7] The reversibility of the O-O cleavage may indicate that the hydroxyl radical that would be generated from the homolytic cleavage of the hydroperoxide ligand remains associated with the iron-containing product, which would be isoelectronic with a ferryl species (Scheme 5.2). The close association of the hydroxyl radical with the ferryl species would be a possible explanation for the regioselectivity of the alkane oxidation catalyzed by **1**, which shows a stronger than usual preference for oxidizing C-H bonds on

secondary carbons over those on tertiary carbons.[18] This regioselectivity is inconsistent with the agency of a freely diffusing hydroxyl radical.[6]

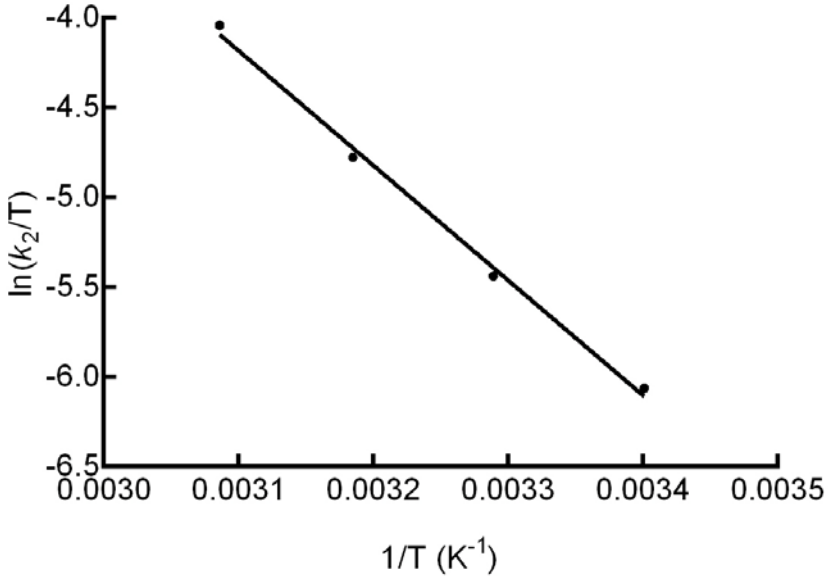

Figure 5.7. Eyring plot for the decomposition of **2** from a reaction between 0.50 mM **1** and 5.0 mM H_2O_2 in MeCN at temperatures ranging from 294 K to 324 K. The second order rate constant from the average of three independent experiments is plotted. The fit corresponds to the equation $y = -6429.4x + 15.621$ ($R^2 = 0.9957$).

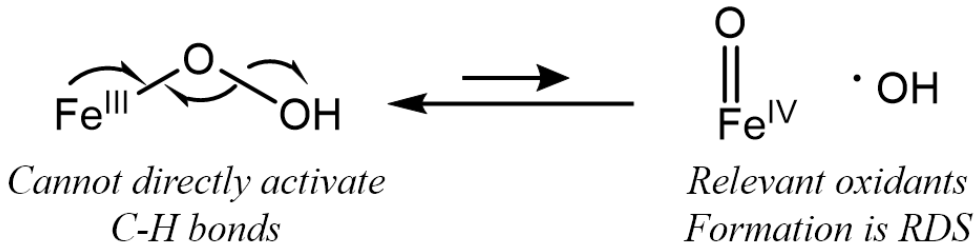

Scheme 5.2

Reactivity: O_2

The formation of **2** from mixtures of **1**, O_2, and cyclohexene was also investigated. Prior work had found that the rate of the formation of **2** was first-order with respect to the concentration of cyclohexene, or an analogous allylic or benzylic substrate.[7] Based on this observation plus the

detection of organic radicals in these mixtures, we proposed that the formation of **2** proceeds through a ferric superoxo species, which abstracts a hydrogen atom from the hydrocarbon to yield the ferric hydroperoxide respect to **1** (Figure 5.8). At higher concentrations of O_2, the observed rate constants scale with $[O_2]$. With lower concentrations of O_2, the pseudo-first-order approximation is not valid (Figure 5.9) because the formation of ferric hydroperoxide from O_2 is not clean. The rate law can be described by Equation 2:

Eq. 2: $$d[\mathbf{2}]/dt = k_3[\mathbf{1}][O_2][\text{substrate}].$$

This rate law suggests that both the oxidation of **1** by O_2 and the initial oxidation of cyclohexene proceed through mononuclear, rather than a binuclear, iron species; otherwise, the rate law would be second-order in iron. The rate law is consistent with our previously hypothesized mechanism, in which a ferric superoxide species abstracts a hydrogen atom from an allylic substrate in the RDS to yield **2** (Scheme 5.1).[7]

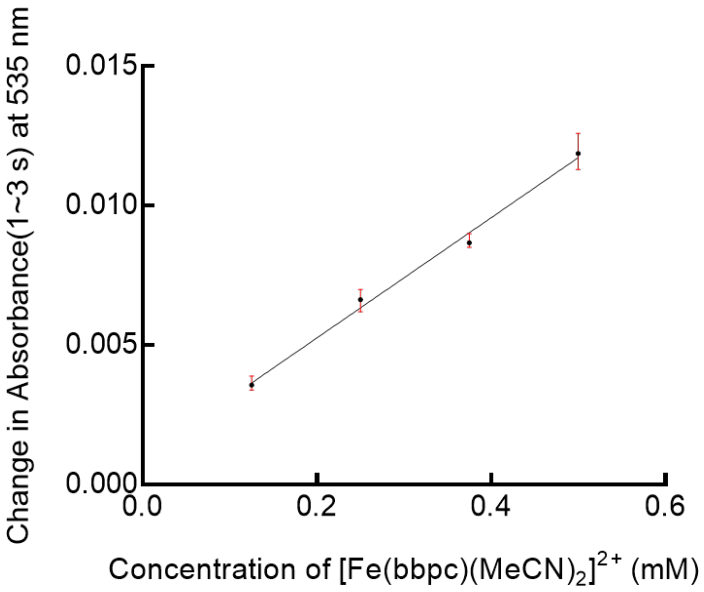

Figure 5.8. Initial rate analysis for the formation of **2** from **1** and O_2. The focus was on the dependence of initial rate of the reaction on [**1**]; the initial concentration of O_2 and cyclohexene were kept at 8.1 mM and 100 mM, respectively. The change in the absorbance at 535 nm was monitored from 1.0 to 3.0 s scales with the formation of **2** and was consequently plotted as a function of [**1**]. The fit corresponds to the equation $y = 0.02155x + 0.00095$ ($R^2 = 0.9794$).

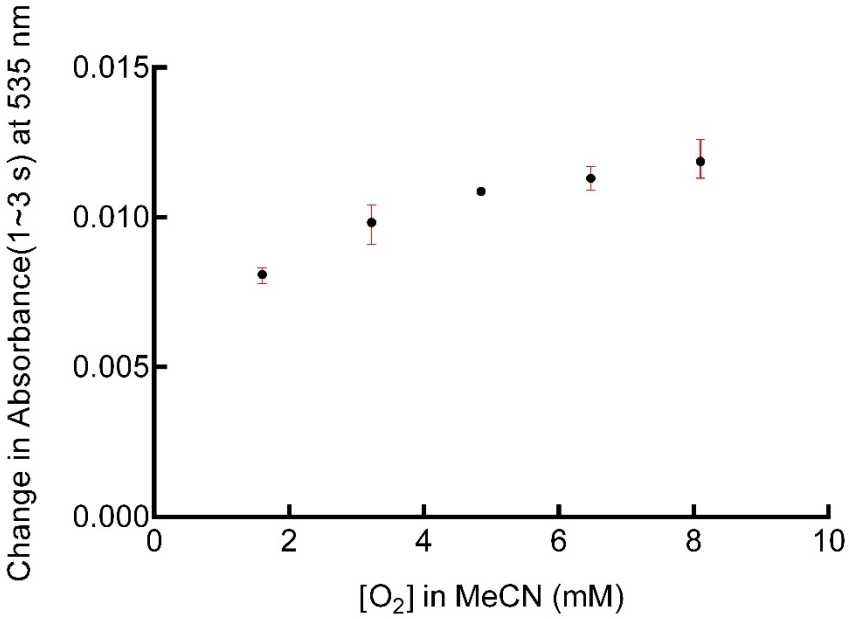

Figure 5.9. Initial rate analysis for the formation of **2** from **1** and various [O_2]. The focus was on the dependence of initial rate of the reaction on [O_2]; the initial concentration of **1** and cyclohexene were kept at 0.50 mM and 100 mM, respectively. The change in the absorbance at 535 nm was monitored from 1.0 to 3.0 s scales with the formation of **2**.

5.4 Conclusions

We have determined that the Fe(III)-OOH species with the bbpc ligand decomposes through homolysis of the O-O bond. As with related species that undergo O-O heterolysis, the ferric hydroperoxide species itself does not appear to be the relevant oxidant for C-H activation. The previously observed regioselectivity of the alkane oxidation and the reversibility of the O-O bond cleavage are inconsistent with freely diffusing radicals, suggesting that any generated hydroxyl radicals instead remain associated with the higher-valent iron by-product. We have also determined the rate law associated with the formation of **2** from O_2; this rate law is consistent with the previously proposed intermediacy of a mononuclear ferric superoxo species.

Appendix

Analysis of the reaction between MeCN and H_2O_2

The reaction between RCN and H_2O_2 yields $RC(=O)NH_2$, H_2O, and O_2.[23] For MeCN, MeC(=NH)OOH is formed in the first step. Despite the speed of the reaction, the equilibrium constant *K* is 2.0×10^{-4} at 20 °C.[24] The ^1H NMR of a control reaction between 100 mM MeCN and 100 mM H_2O_2 in $CDCl_3$ failed to detect the product signal associated with the product RC(=NH)OOH. This suggested that the concentration of H_2O_2 in MeCN is equal within error to the added H_2O_2.

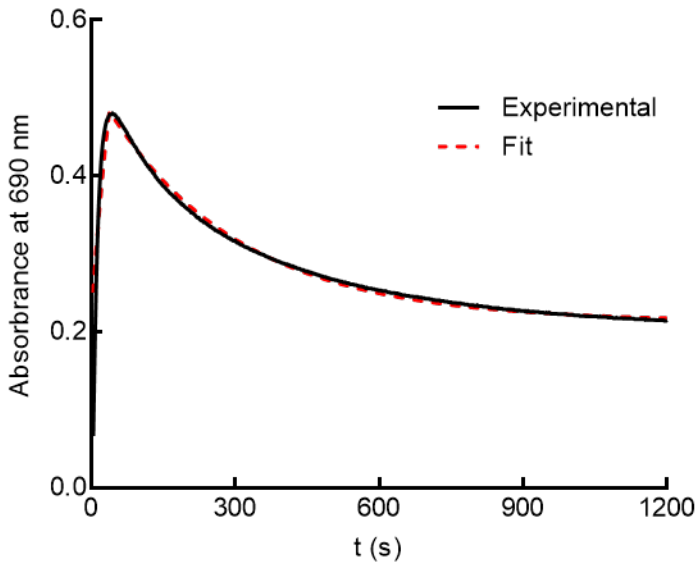

Figure 5.A1. Sample kinetic trace for a reaction between 0.50 mM **1** and 5.0 mM H_2O_2 in MeCN at 298 K. The absorbance were measured at 690 nm, which corresponds to the peak absorbance of a ligand-to-metal charge transfer band for **2**. The data have been fit to an A→B→C model, where the A→B portion corresponds to the formation of **2** (B) from **1** (A) and the B→C portion corresponds to the decomposition of **2**. Each step is first order with respect to either A or B.

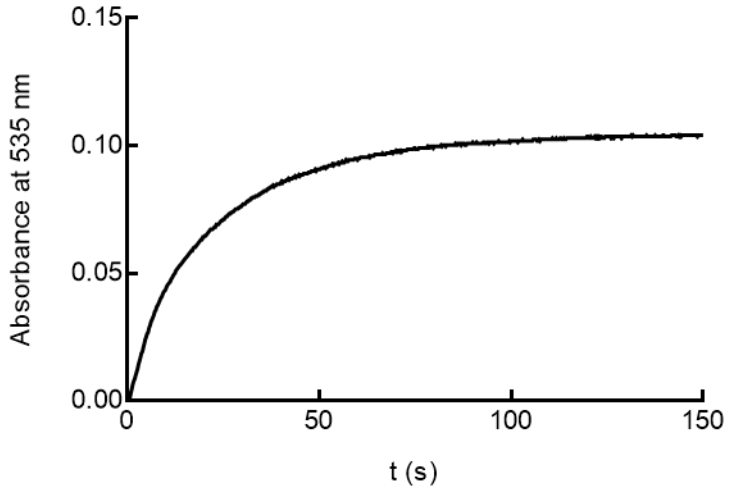

Figure 5.A2. Sample kinetic trace for a reaction between 0.50 mM **1** and 8.1 mM O_2, and 100 mM cyclohexene in MeCN at 298 K. The absorbance were measured at 535 nm.

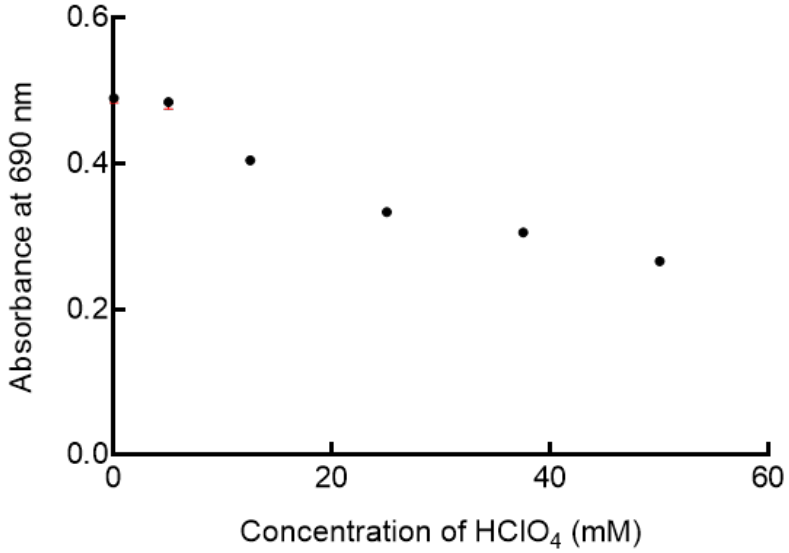

Figure 5.A3. Absorbance measured at 690 nm at 600 s for the reaction between 0.50 mM **1** and 5.0 mM H_2O_2 in MeCN at 298 K with various concentration of $HClO_4$. The intensity of the absorbance is correlated to the concentration of **2**. The decrease in the peak absorbance can be attributed to the slower rate of formation of **2**. When $HClO_4$ is added 30 s after the start of the reaction, the absorbance does not decrease and the intensity of the 690 nm feature persists for a longer period of time.[18]

References

(1) Gunay A.; Theopold, K. H. *Chem. Rev.* **2010**, *110*, 1060-1081.

(2) Brückl, T.; Baxter, R. D.; Ishihara Y.; Baran, P. S. *Acc. Chem. Res.* **2012**, *45*, 826-839.

(3) Shilov, A. E.; Shul'pin, G. B. *Chem. Rev.* **1997**, *97*, 2879-2932.

(4) Costas, M.; Mehn, M. P.; Jensen, M. P.; Que, L., Jr. *Chem. Rev.* **2004**, *104*, 939-986.

(5) Que, L., Jr.; Ho, R. Y. N. *Chem. Rev.* **1996**, *96*, 2607-2624.

(6) Chen, K.; Que, L., Jr. *J. Am. Chem. Soc.* **2001**, *123*, 6327-6337.

(7) He, Y.; Goldsmith, C. R. *Chem. Commun.* **2012**, *48*, 10532-10534.

(8) Lee, Y.-M.; Hong, S.; Morimoto, Y.; Shin, W.; Fukuzumi S.; Nam, W. *J. Am. Chem. Soc.* **2010**, *132*, 10668-10670.

(9) Li, F.; Meier, K. K.; Cranswick, M. A.; Chakrabarti, M.; Van Heuvelen, K. M.; Münck, E.; *J. Am. Chem. Soc.* **2011**, *133*, 7256-7259.

(10) Nam, E.; Alokolaro, P. E.; Swartz, R. D.; Gleaves, M. C.; Pikul, J.; Kovacs, J. A. *Inorg. Chem.* **2011**, *50*, 1592-1602.

(11) Oloo, W. N.; Fielding A. J.; Que, L., Jr. *J. Am. Chem. Soc.* **2013**, *135*, 6438-6441.

(12) Rohde, J.-U.; In, J.-H.; Lim, M. H.; Brennessel, W. W.; Bukowski, M. R.; Stubna, A.; Münck, E.; Nam W.; Que, L., Jr. *Science* **2003**, *299*, 1037-1039.

(13) Wada, A.; Ogo, S.; Nagatomo, S.; Kitagawa, T.; Watanabe, Y.; Jitsukawa, K.; Masuda, H. *Inorg. Chem.* **2002**, *41*, 616-618.

(14) Ho, R. Y. N.; Roelfes, G.; Hermant, R.; Hage, R.; Feringa B. L.; Que, L., Jr. *Chem. Commun.* **1999**, 2161-2162.

(15) Martinho, M.; Blain G.; Banse, F. *Dalton Trans.* **2010**, *39*, 1630-1634.

(16) Chen, K.; Costas, M.; Kim, J.; Tipton A. K.; Que, L., Jr. *J. Am. Chem. Soc.* **2002**, *124*, 3026-3035.

(17) Decker, A.; Chow, M. S.; Kemsley, J. N.; Lehnert N.; Solomon, E. I. *J. Am. Chem. Soc.* **2006**, *128*, 4719-4733.

(18) He, Y.; Gorden, J. D.; Goldsmith, C. R. *Inorg. Chem.* **2011**, *50*, 12651-12660. Correction: *Inorg. Chem.* **2012**, *51*, 7431.

(19) Klassen, N. V.; Marchington, D.; McGowan, H. C. E. *Anal. Chem.* **1994**, *66*, 2921-2925.

(20) Sawyer, D. T.; Chiericato, G.; Angelis, C. T.; Nanni, E. J.; Tsuchiya, T. *Anal. Chem.* **1982**, *54*, 1720-1724.

(21) Britovsek, G. J. P.; England, J.; White, A. J. P. *Inorg. Chem.* **2005**, *44*, 8125-8134.

(22) Litorja, M.; Ruscic, B. *J. Electron Spectrosc.* **1998**, *97*, 131-146.

(23) Brauer, H.-D.; Eilers, B.; Lange, A. *J. Chem. Soc., Perkin Trans. 2* **2002**, 1288-1295.

(24) Laus, G. *J. Chem. Soc., Perkin Trans. 2* **2001**, 864-868.

Appendix

Crystal Structure of the Perchloric Acid Salt of the Macrocyclic Ligand 1,8-Bis(2-pyridylmethyl)-1,4,8,11-tetraazacyclotetradecane

The title compound, $C_{22}H_{34}Cl_2N_6O_8$, is the perchloric acid salt of a hexadentate cyclam derivative that has been used in recent studies involving spin-crossover behavior and coordination chemistry. The crystallized organic molecule is doubly protonated, with each proton shared between a pyridine ring and one of the secondary amines from the macrocycle. The asymmetric unit contains a perchlorate anion and half of the dication, which are linked through an additional hydrogen bond.

Comment

Due to their ability to form thermodynamically and kinetically stable complexes with a wide range of metal ions, tetraazamacrocycles have been of great interest to coordination chemists. Because of the high aqueous stability of their chelates, these macrocycles are common components in inorganic pharmaceuticals and imaging agents.[1,2] Varying either the size of the organic ring or the identity and number of the substituents on the N-donors allows one to tune the ligand's coordinative preferences and size selectivity for metal ions.[3] The protonation state of the macrocycle modulates its ability to bind to metals, and different molecular architectures can result as the pH of the solution is varied.[4]

With respect to 1,4,8,11-tetraazacyclotetradecane (cyclam), the chemistry of disubstituted derivatives has been relatively unexplored. Compared to the synthetic techniques used to prepare tetrasubstituted cyclams, the methodology capable of synthesizing disubstituted derivatives has

been optimized only recently.[5] The potentially hexadentate 1,8-bis(2-pyridylmethyl)-1,4,8,11-tetraazacyclotetradecane (**1**) has been found to coordinate Cu(II) and Ni(II) in significantly different fashions, with the pendant pyridine rings positioned *cis* relative to each other in the Ni(II) structure[6] and *trans* to each other in the Jahn-Teller distorted Cu(II) structure.[7] A recently reported Fe(II) structure resembles that of the Ni(II) complex and was the first example of a spin-crossover complex with a substituted tetraazamacrocycle.[8] Compound **1** has also been used as a precursor to cyclam derivatives with two different sorts of pendant arms.[5,9] This has proven useful in solubilizing the ligand in water.[9]

In our investigation of polydentate N-donor ligands, we have prepared the perchloric acid salt of **1,** [**1**H_2](ClO_4)$_2$. The cyclam derivative is doubly protonated and co-crystallizes with two equiv. of perchlorate anions. The crystal structure provides insight into the speciation chemistry of **1**, specifically detailing where ligand protonation occurs.

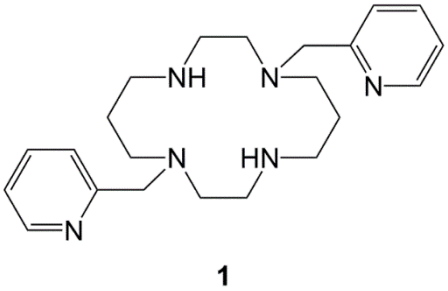

1

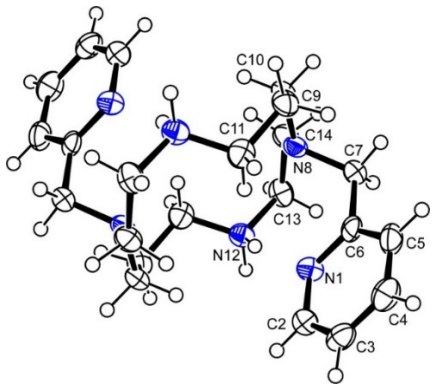

Figure A1. ORTEP representation of the **1**H_2^{2+} dication showing the numbering scheme. All thermal ellipsoids are drawn at 50% probability.

The [**1**H_2]$(ClO_4)_2$ salt results from an unsuccessful metal complexation reaction. A single crystal with dimensions of 0.09 × 0.05 × 0.03 mm^3 was mounted on a glass fiber and optically aligned on a Bruker APEX CCD X-ray diffractometer using a digital camera. Initial intensity measurements were performed using graphite monochromated Mo *K*α radiation from a sealed tube and monocapillary collimator. SMART[10] was used for preliminary determination of the cell constants and data collection control. The intensities of reflections of a sphere were collected by a combination of three sets of exposures (frames). Each set had a different φ angle for the crystal and each exposure covered a range of 0.3° in ω. A total of 1800 frames were collected with an exposure time per frame of 30 s.

Determinations of integrated intensities and global refinement were performed with the Bruker SAINT (v 6.02) software package using a narrow-frame integration algorithm. These data were treated with a semi-empirical absorption correction by SADABS.[11] The program suite SHELXTL (v 6.12) was used for space group determination (XPREP), direct methods structure solution (XS), and least-squares refinement (XL).[12] The final refinements included anisotropic displacement parameters for all atoms. Secondary extinction was not noted.

The $|E^2 - 1|$ statistic is near the expected value for a centrosymmetric crystal, which suggests space group *P2/n* or *P2₁/n*, rather than *Pn*. The program XPREP suggested *P2/n*, and the SHELXS input files were set up and merged in this space group. SHELX appeared to find an appropriate solution; however, closer inspection at the suggested atomic positions revealed non-positive definites (NPD) for atoms N(1) and N(8), showing this to be only a pseudo-solution. The space group *Pn* was also investigated resulting in NPD for atoms N(1), C(6), and C(7) when refined anisotropically. Other strategies, such as trying other semivariants, Patterson methods, or modeling these NPD atoms, did not result in a suitable solution in either space group. The most reasonable

solution for [**1**H_2](ClO_4)$_2$ was the monoclinic space group *P2$_1$/n* (unit cell dimensions: *a* = 10.0747(7) Å, *b* = 12.6663(9) Å, *c* = 11.4804(8) Å, β = 112.6560(10)°) with half a molecule in the asymmetric unit. The other half is generated by the inversion center of the space group (Figure 1). Although the final refinement of [**1**H_2](ClO_4)$_2$ has a significantly high Final R index ([I>2sigma(I)] R1 = 0.1050), ADDSYM, NEWSYM and TwinRotMat of the PLATON software[13], were used to search for missed symmetry and twinning. Neither case was detected here. The perchlorate ion was modeled over two positions with approximate part occupancies of 0.611(1) and 0.389(1) and restrained to a regular tetrahedron using SADI.

The secondary amines from the **1**H_2^{2+} dication hydrogen bond to perchlorate anions from neighboring asymmetric units, as indicated by the short distances between N12 and the O atoms in the disordered perchlorates (Figure 2, Table 1). There is also extensive hydrogen bonding within the **1**H_2^{2+} dication. In the crystal structure, the pyridine ring is oriented towards the secondary amine. The distance between N1 and N12 is 2.86 Å, consistent with a proton shared between these two functionalities (Table 1). The tertiary amine (N8) does not appear to participate in either intermolecular or intramolecular hydrogen bonding. This is initially surprising since the amine functionalities are more basic than the pyridines. In the doubly protonated forms of cyclam and a closely related derivative, the two protons are localized within the macrocycle.[14,15] The pattern of hydrogen bonding observed in **1**H_2^{2+} better separates the bound protons, however, minimizing the coulombic repulsion between them and stabilizing the overall structure. Hydrogen bonding between cyclam N-donors and functional groups on pendant arms has previously been noted.[16]

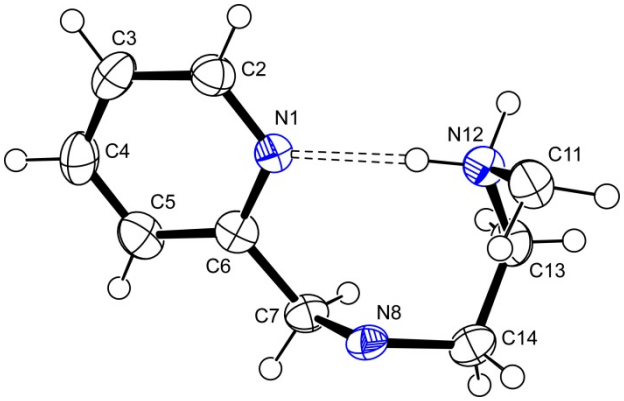

Figure A2. ORTEP representation of a portion of the $\mathbf{1}H_2^{2+}$ dication, highlighting the hydrogen bond interaction between the pyridine ring and the secondary amine. The other proton on N12 hydrogen bonds to a ClO_4^- anion in an adjacent asymmetric unit. All thermal ellipsoids are drawn at 50% probability.

Table A1. Hydrogen Bond Geometry.

D-H···A	D-H (Å)	H···A (Å)	D···A (Å)	D-H···A (°)	Symmetry Codes
N12-H12A···O2a	0.90(2)	2.00(2)	2.871(2)	162.8(2)	[*x*+1/2, -*y*+3/2, *z*+1/2]
N12-H12A···O1B	0.90(2)	2.01(2)	2.882(2)	161.8(2)	[*x*+1/2, -*y*+3/2, *z*+1/2]
N12-H12A···O2B	0.90(2)	2.49(2)	3.209(2)	137.1(2)	[*x*+1/2, -*y*+3/2, *z*+1/2]
N12-H12A···O4a	0.90(2)	2.63(2)	3.351(2)	137.5(2)	[*x*+1/2, -*y*+3/2, *z*+1/2]
N12-H12B···N1	0.90(2)	2.00(2)	2.861(2)	159.0(2)	

Experimental Section

The macrocyclic ligand 1,8-bis(2-pyridylmethyl)-1,4,8,11-tetraazacyclotetradecane (**1**) was prepared as previously described.[5] The crystals were grown from a reaction between manganese(II) perchlorate hydrate and **1** in acetonitrile (MeCN). $Mn(ClO_4)_2$ (254 mg, 1.00 mmol) and the cyclam derivative (350 mg, 1.00 mmol) were dissolved in 10 mL of MeCN. After the reaction was stirred for 12 h at 22 °C, 10 mL of diethyl ether was added. Over the next 7 days, approximately 100 mg of white crystals of $[\mathbf{1}H_2](ClO_4)_2$ precipitated from solution.

CAUTION: Perchlorate salts of organic compounds are potentially explosive and should be handled carefully. The dangers associated with these compounds can be reduced by using minimal amounts of these materials and using appropriate safety equipment, such as blast shields.

Crystal data

$[C_{22}H_{36}N_6][ClO_4]_2$	$Z = 2$
$M_r = 583.47$	$F(000) = 616$
Monoclinic, $P2_1/n$	$D_x = 1.433$ Mg m^{-3}
Hall symbol: -P 2yn	Mo $K\alpha$ radiation, $\lambda = 0.71073$ Å
$a = 10.0747(7)$ Å	Cell parameters from 3355 reflections
$b = 12.6663(9)$ Å	$\theta = 2.7–23.6°$
$c = 11.4804(8)$ Å	$\mu = 0.73$ mm^{-1}
$\beta = 112.6560(10)°$	$T = 183$ K
$V = 1351.96(16)$ Å^3	Colorless, fragment
	0.09 × 0.05 × 0.03 mm

Data collection

Bruker APEXII CCD area-detector diffractometer	3355 independent reflections
Radiation source: fine-focus sealed tube	2874 reflections with $I > 2\sigma(I)$
Graphite	$R_{int} = 0.1050$
phi and ω scans	$\theta_{max} = 28.3°$, $\theta_{min} = 2.29°$
Absorption correction: multi-scan (*SADABS*; Sheldrick, 2008)	$h = -13\rightarrow13$
$T_{min} = 0.982$, $T_{max} = 0.991$	$k = -16\rightarrow16$
13855 measured reflections	$l = -15\rightarrow15$

Refinement

Refinement on F^2	Primary atom site location: structure-invariant direct methods
Least-squares matrix: full	Secondary atom site location: difference Fourier map
$R[F^2 > 2\sigma(F^2)] = 0.105$	Hydrogen site location: inferred from neighboring sites
$wR(F^2) = 0.181$	H atoms treated by a mixture of independent and constrained refinement
$S = 1.315$	
3355 reflections	$(\Delta/\sigma)_{max} = 0.005$
233 parameters	$\Delta\rho_{max} = 0.396$ e Å^{-3}
42 restraints	$\Delta\rho_{min} = -0.514$ e Å^{-3}

Data collection: SMART;[10] cell refinement: SAINT;[17] data reduction: SAINT; program(s) used to solve structure: SHELXS97;[18] program(s) used to refine structure: SHELXL97;[18] molecular graphics: XP[19] and Ortep-3 for Windows;[20] software used to prepare material for publication: WinGX publication routines.[21]

References

(1) Caravan, P.; Ellison, J. J.; McMurry, T. J.; Lauffer, R. B. *Chem. Rev.* **1999**, *99*, 2293-2352.

(2) Delgado, R.; Felix, V.; Lima, L. M. P.; Price, D. W. *Dalton Trans.* **2007**, 734-2745.

(3) Hancock, R. D. *Pure Appl. Chem.* **1986**, *58*, 1445-1452.

(4) Meyer, M.; Dahaoui-Gindrey, V.; Lecomte, C.; Guilard, R. *Coord. Chem. Rev.* **1998,** *178-180*, 1313-1405.

(5) Royal, G.; Dahaoui-Gindrey, V.; Dahaoui, S.; Tabard, A.; Guilard, R.; Pullumbi, P.; Lecomte, C. *Eur. J. Org. Chem.* **1998**, 1971-1975.

(6) Batsanov, A. S.; Goeta, A. E.; Howard, J. A. K.; Maffeo, D.; Puschmann, H.; Williams, J. A. G. *Polyhedron* **2001**, *20*, 981-986.

(7) Goeta, A. E.; Howard, J. A. K.; Maffeo, D.; Puschmann, H.; Williams, J. A. G.; Yufit, D. S. *J. Chem. Soc., Dalton Trans.* **2000**, 1873-1880.

(8) El Hajj, F.; Sebki, G.; Patinec, V.; Marchivie, M.; Triki, S.; Handel, H.; Yefsah, S.; Tripier, R.; Gomez-Garcia, C. J.; Coronado, E. *Inorg. Chem.* **2009**, *48*, 10416-10423.

(9) Morfin, J.-F.; Tripier, R.; Le, B. M.; Handel, H. *Polyhedron* **2009**, *28*, 3691-3698.

(10) Bruker SMART. Version 5.611., Bruker AXS Inc., Madison, WI, **2000**.

(11) Sheldrick, G. M. *Acta Crystallogr.* **1995**, *A*51, 33.

(12) Sheldrick, G. M. SHELXTL PC, Version 6.12., Siemens Analytical X-ray Instruments Inc., Madison, WI, **2001**.

(13) Spek, A. L. PLATON. Utrecht University, the Netherlands, **2002**.

(14) Alfonso, I.; Astorga, C.; Rebolledo, F.; Gotor, V.; Garcia-Granda, S.; Tesouro, A. *J. Chem. Soc., Perkin Trans. 2* **2000**, 899-904.

(15) Kim, N.-H.; Ha, K. *Acta Crystallogr.* **2009,** *E65*, o2504.

(16) Lima, L. M. P.; Delgado, R.; Drew, M. G. B.; Brandao, P.; Felix, V. *Dalton Trans.* **2008**, 6593-6608.

(17) Bruker Saint-Plus. Version 6.02., Bruker AXS Inc., Madison, WI, **1999**.

ttingen, Germany, **1997.**

(19) Sheldrick, G. M. XP and SHELXTL, Bruker AXS Inc., Madison, WI, **1997**.

(20) Farrugia, L, J. *J. Appl. Crystallogr.* **1997**, *30*, 565.

(21) Farrugia, L, J. *J. Appl. Crystallogr.* **1999**, *32*, 837-838.